HYDROGELS FROM BIOMIMETIC RESOURCES: SYNTHESIS, CHARACTERIZATION AND APPLICATIONS

A THESIS SUBMITTED TO

SAVITRIBAI PHULE PUNE UNIVERSITY

FOR AWARD OF DEGREE OF

DOCTOR OF PHILOSOPHY (Ph.D.)

IN

CHEMISTRY

SUBMITTED BY

ARUN TORRIS A. T.

UNDER THE GUIDANCE OF

Dr. MANOHAR V. BADIGER

RESEARCH CENTRE

POLYMER SCIENCE & ENGINEERING DIVISION

CSIR – NATIONAL CHEMICAL LABORATORY

PUNE – 411008

OCTOBER 2019

Declaration by the Candidate

I declare that the thesis entitled "**Hydrogels from Biomimetic Resources: Synthesis, Characterization and Applications**" submitted by me for the degree of Doctor of Philosophy is the record of work carried out by me during the period from **16-04-2013** to **11-10-2019** under the guidance of **Dr Manohar V. Badiger** and has not formed the basis for the award of any degree, diploma, associateship, fellowship, titles in this or any other University or other institution of Higher learning.

I further declare that the material obtained from other sources has been duly acknowledged in the thesis.

Date :

Place : Pune

Arun Torris A. T.
(Research Student)
CSIR-National Chemical Laboratory
Pune-411 008

Acknowledgement

I would like to express my deepest gratitude to my thesis supervisor, Dr Manohar V. Badiger, for his incredible patience, vision, encouragement and advice which were instrumental in the successful completion of this piece of work. I am indebted to him for the liberty to carry out independent research in his lab at CSIR – National Chemical Laboratory (CSIR-NCL). I am grateful to him for the introduction to the fascinating world of hydrogels and its chemistry.

I would like to acknowledge the support received from NCL Director's office to pursue a doctoral program in NCL along with other official activities and for extending all available infrastructures necessary for my doctoral program.

I am thankful to the doctoral committee members Dr Prakash Wadgaonkar, Dr Suresh Bhat, Dr Jayakannan (IISER Pune) and Dr Vaishali Shinde (SPPU), for investing their valuable time which rendered fruitful discussions and constructive criticism of the thesis work.

I am grateful towards the inputs and guidance received from Dr Ashish Lele, Dr K Guruswamy, Dr P R Rajamohanan, Dr Sreekumar Kurungot and Dr G V N Rathna which helped to resolve the bottlenecks experienced during the research activities.

Inspiring conversations and stimulating discussions with the Indo-French Research Project (CEFIPRA-IFCPAR) collaborators Dr Dominique Hourdet, Dr Costantino Creton and Dr Guylaine Ducouret from ESPCI UPMC University Paris was acknowledged which contributed significantly towards improvising the understanding of fundamental concepts during my early stages of the doctoral program.

I wish to accord special gratitude and heartfelt thanks to my senior colleague and lab mate Mr Suresha P R for all his extended help and support ever since my first day in CSIR-NCL.

My senior lab mates Dr Nivika Gupta, Dr Hemanth Nair, Dr Santhosh Hire, Dr Ujwal Kohle, Dr Satish Biradar and Dr Sameera Kandekar, was acknowledged for their constant support, invaluable discussions and motivation.

Words are not enough to elaborate the deeds of my best friend and critique Dr Sreekuttan Unni (*Pintru*), whose motivation, criticism, inspiration and friendship have been a constant jolt to my days in NCL.

I am very grateful for the attachment of my roommates Dr Reji N K, Dr Vijayadas, Dr Sreekuttan Unni, Dr C P Jijil, Dr Rajesh Thattarathody, Dr Harikrishan and Dr Bipinal for making my life in NCL more wonderful and homely.

In addition, I would like to thank my lab mates Dr Aarti Shedge, Dr Vivek Kodgire, Dr Nivika Gupta, Dr Anumon V D, Dr Manjusha Patwadkar, Dr Rajeshwari Gour, Dr Neha Tiwari, Ashwini Wali, Yogesh Marathe, Sanoop Nair, Rajimol K P, Ajay Khairnar, Dr Rupavani, Bhagyashri Thorat, Naresh Killi, Pratiksh Patel, Amarnath Singham, Tripurari Rao, Sravanya Konchada and Siva Kakku for their support and co-operation.

Working with collaborators, Dr Bihag Anothumakkool, Vidyanand Vijayakumar, Meena Ghosh, Siddheshwar Bhange, Sajna Veeliyath, Nikhil Chandran and Dr Suvendu Karak, I got various opportunities to appreciate the depth and wealth of other allied research domains in chemistry and material sciences. Fortunately, all these opportunities provided a platform to share the understanding of various scientific aspects among researchers of multiple fields and end up in co-authored research publications.

I also wish to thank the staff members of NCL Student Academic Office, PSE Office, PG section of SPPU, Mrs Puranik, Mrs Kolhe, Mr Pavithran, Mr Iyer, Mr U V Dhavale, Mr Mahajan, Mr Bharati, Mr Harshal, Mr Shaikh, Mr Shivaji Sondkar for their extended help and support.

I would like to thank my friends Dr Prajitha K P, Dr Leena George, Dr Indravadan Parmar, Dr Anumon V D, Dr Sharath Kandambeth, Dr Renji Reghu, Dr Venugopal Edakkal, Dr Vinisha Valsaraj Dr Kiran Sukumaran, Dr Manoj Sharma, Aakash Sharma, Prashanth Patil for inculcating healthy scientific discussions and provoking various thought processes, during my doctoral tenure in NCL.

I would like to acknowledge the support received from my senior technical group members Suresha P R, Dr Deepa Dhoble, Dr Smitha Mule, Dr Neelima Bulakh, Dr Kalpana Trimukhe, Sangeetha Hambir and Poorvi Purohith for advice and suggestions helpful during divisional activities.

I am also grateful to senior scientific staffs in Sree Chitra Tirunal Institute for Medical Science and Technology (SCTIMST) Dr Kalliyana Krishnan, Dr Lissy Krishnan, Dr Roy Joseph and Dr P Ramesh who had provided me with the first-hand exposure to the *world of biomaterials* during my tenure at Biomedical Technology Wing in SCTIMST.

I acknowledge Science and Engineering Research Board (SERB) of the Department of Science and Technology (DST) New Delhi for the research grant, which helped us to procure necessary testing facilities, chemicals and consumables to pursue my doctoral studies.

I wish to express my gratitude to the Chair of PSE division Dr Ashish Lele, Dr Manohar Badiger and Director NCL Prof Ashwini Nangia for approving *major equipment funds* for establishing state-of-the-art 3D X-ray micro-computed tomography (micro-CT) facility in CSIR-NCL, which was very instrumental in the research works undertaken in my PhD thesis.

It gives me great pleasure to express my gratitude to my parents for their blessings, love, care and support from the beginning of the journey to the end. Words are not enough to wife to express my deepest heartfelt gratitude to my wife and son for their faith, patience, sacrifices and have been the source of my inspiration and will remain throughout my life. Without their continuous support and tireless efforts, this journey would never have been so successful.

Arun

Table of Contents

Abstract

Hydrogels from Biomimetic Resources: Synthesis, Characterization and Applications

The objective of the thesis was to undertake design and synthesis of mechanically robust hydrogels from biomimetic resources such as polysaccharides, by employing the double network (DN) strategy. Hydrogels are water-swollen three-dimensional network of hydrophilic polymers crosslinked by chemical or physical interactions. Hydrogels show numerous applications, particularly in medical and pharmaceutical fields, such as ophthalmological devices, biosensors, bio-membranes, substitutes for organs such as artificial skin, carriers of drug delivery devices, etc. The major strategy employed in regenerative medicine for reconstructing organs is the replacement of degraded organ part(s) with natural extracellular matrix (ECM), which is a complex and dynamic three-dimensional structure surrounding cells in an organ. Biocompatible and hydrophilic hydrogels can provide many of the normal signals and interactions to cells by the ECM in tissues. This unique property of hydrogels as synthetic ECM analogs is primarily due to their ability to retain large amounts of water along with their soft and rubbery consistence which closely resembles the living tissues. Two major drawbacks of hydrogels generally encountered in biomedical applications are their low mechanical strength and toxic degradation bye products. Therefore, major focus is now given on developing mechanically strong and tough hydrogels from biomimetic resources such as polysaccharides with non-toxic bye products.

In this context, three polysaccharides were selected for the preparation of biomimetic hydrogels, which are carboxymethyl xyloglucan (CMX), carboxymethyl cellulose (CMC) and alginate (Alg). Michael-type addition reaction between the primary hydroxyl group in the polymer backbone and divinyl sulphone (DVS) was utilized to crosslink CMX and CMC polysaccharides. These crosslinked structures were swollen in water to form transparent hydrogels. Alginate hydrogels were prepared by the physical crosslinking method, where divalent cations such as Ca^{2+} were used to form an ionic bond between the polymer chains.

CMX was used to design neural interface by *in-situ* crosslinking of CMX with DVS by Michael-addition reaction, inside the hollow carbon nano-fibers (CNF). Neural interfaces are "*communication bridges*" between the artificial electronic prosthesis and the central nervous system of the physically challenged personnel. Resultant microelectrodes do possess dual characteristics of electrical as well as conductivity by virtue of the inherent properties of CMX and CNF. The concentration of CMX plays a crucial role in the formation of a homogeneous hydrogel network inside the hollow core of CNF. Electrochemical studies show that these microelectrodes possess higher charge density and active surface area than pristine CNF, which enhances and promotes ion conducting channels that are ideal for developing neural interfaces. Cytotoxicity studies revealed the biocompatible characteristics of these microelectrodes and their cyto compatible nature. The results indicate the potential of these microelectrodes for their applications in designing new generation neural interfaces.

CMX, CMC and Alg were used for the preparation of mechanically robust double network (DN) hydrogels, along with another synthetic polymer, namely Poly (hydroxyethyl acrylate) (PHEA) and/or Poly (hydroxyethyl acrylate-co-stearyl methacrylate (PHEA-co-SM), by a sequential process. Initially, hydrogels were prepared using CMX, CMC and Alg, called the first network. These hydrogels were washed and immersed in aqueous solution of hydroxyethyl acrylate (HEA) and/or stearyl methacrylate (SM) containing 0.1 Wt. % photoinitiator for seven days. Equilibrium swollen hydrogels were exposed to UV radiation to affect the free-radical photo-polymerization of HEA and/or SM to form a second hydrogel network of PHEA and/or PHEA-co-SM, inside the first network. Gelation, swelling and mechanical and/or rheological properties of these DN hydrogels were studied.

Microgels (MGs) were prepared by the co-polymerization of SM and HEA using oil-in-water (O/W) emulsion method, where concentration of HEA was 5, 10 and 15 mol % as that of SM. Average size and range of these MGs were measured with micro-CT. Curcumin as a model drug is loaded onto these MGs and embedded inside DN hydrogels prepared from CMX and PHEA. Release of curcumin in PBS (pH 7.4 and 37^0C) from these MGs embedded in the DN hydrogels showed release pattern dependent on the concentration of HEA. These drug loaded DN hydrogels showed

promise for applications in developing rate pre-programmed release systems for addressing chronic wound healing process.

During the preparation of CMC DN hydrogels, concentration of SM (co-monomer in second network) was varied from 2, 4 and 6 mol % of HEA, to study the effect of hydrophobic co-monomer (SM) in the network structure of DN hydrogels. Hydrophobic co-monomer (SM) is incorporated into the second network by micelle-assisted free-radical co-polymerization method and the role of SM in energy dissipation mechanism of these DN hydrogels were studied by cyclic strain, step strain and stress relaxation measurements. Compressive strength of the CMC DN hydrogel was 280 times more than that of CMC hydrogel and with increase in SM concentration DN hydrogels showed better recovery after deformation. Microstructure of porous xerogels prepared from CMC DN hydrogels was studied in detail by micro-CT (Micro-computed Tomography), to explore more information about their porosity and pore-characteristics. Cell viability studies showed the advantage of DN hydrogels over it single network counterparts, where biocompatibility of DN hydrogels was enhanced due to a better response of cells towards hydrogel network structure with faster relaxation rates and also due to the presence of bioactive polysaccharide units in them.

During the preparation of Alg DN hydrogels, the concentration of SM (co-monomer in the second network) was increased up to 10 Wt. % of HEA, to impart self-healing property to the hydrogel network. Thermo-reversible behaviour of Alg hydrogel (first network) was studied by rheometry as a function of temperature. Step strain rheological measurements explored self-healing characteristics of the Alg DN hydrogels. These DN hydrogels were also examined to study the *in-situ* bio-mineralization of HAP, confined in the DN hydrogel network.

DN strategy was proven to be a unique route for designing polysaccharide based hydrogels with exceptional mechanical behaviour. These hydrogels exhibited great potential in drug delivery, regenerative medicine, implant design etc.

List of Schemes

List of Tables

List of Figures

Abbreviations and Symbols

Alg	Alginate
API	Active pharmaceutical ingredients
CDDS	Controlled drug delivery systems
CUR	Curcumin
CMC	Carboxymethyl cellulose
CMX	Carboxymethyl xyloglucan
CMT	Carboxymethyl tamarind
CNT	Carbon nano tube
CNF	Carbon nano fiber
DDS	Drug delivery systems
DLS	Dynamic light scattering
DMEM	Dulbecco's modified eagle medium
DMA	Dynamic mechanical analyser
DMSO	Dimethyl sulfoxide
DN	Double network
DPBS	Dulbecco's phosphate buffer solution
DVS	Divinyl sulphone
EAA	Electrochemically active area
ECM	Extracellular matrix

FTIR	Fourier transform infra red spectroscopy
G′	Storage modulus
G”	Loss modulus
GC	Glassy carbon
HA	Hyaluronic acid
HMPP	Hydroxyl methyl propiophenone
kPa	Kilo pascal
ME	Micro electrode
Micro-CT	Micro-computed tomography
MPa	Mega Pascal
MR	Microgel reinforced
MTT	3-(4,5-Dimethylthiazol-2-yl)-2,5-Diphenyltetrazolium Bromide
NC	Nanocomposite
NMR	Nuclear magnetic resonance
ORR	Oxygen reduction reaction
Pa	Pascal
PAAm	Poly (acrylamide)
PAMPS	Poly (2-acrylamido-2-methylpropanesulfonic acid)
PEDOT	Poly (3,4-ethylenedioxythiophene)
PEG	Polyethylene glycol
PEO	Poly ethylene oxide

PGA	Poly glycolic acid
PGDI	Poly (dodecyl glyceryl itaconate)
PHEA	Poly (2, hydroxyl ethyl acrylate)
PHEMA	Poly (2, hydroxyl ethyl methacrylate)
PSAPS	Poly (3-sulfopropyl acrylate potassium salt)
PSS	Poly (styrene sulfonate)
PVA	Poly (vinyl alcohol)
RDE	Rotating disk electrode
RPM	Rotations per minute
SDS	Sodium dodecyl sulphate
SEM	Scanning electron microscopy
SN	Single network
TKP	Tamarind kernel powder
UTM	Universal testing machine
XG	Xyloglucan

Introduction
&
Literature Survey

Chapter – I

In the first chapter, a short introduction about biomaterials, hydrogels and their applications, micro-computed tomography are given. It was followed by detailed literature survey on double network (DN) hydrogels in terms of their structure, methods of preparation, proposed structure model, toughening mechanisms, role of individual networks in DN hydrogels, their applications in tissue engineering, drug delivery, antifouling, sensors and actuators.

1.1 Biomaterials

One of the major accepted definitions of biomaterials is coined by D F Williams[1], which says "*A biomaterial is a substance that has been engineered to take a form which, alone or as part of a complex system, is used to direct, by control of interactions with components of living systems, the course of any therapeutic or diagnostic procedure, in human or veterinary medicine*"[1]. Today's optimal meaning of biomaterials originates from two perspectives; first one is concerned with the evolution of materials science and the second one is from the evolution of health care technologies[1]. Biomaterials, which are conventionally termed as materials used in medical devices, exists since the beginning of human civilization but regularly evolves over a period of time. Today, biomaterials available are very rich in information and also incorporate biologically active components originated from nature. In the future, biomaterials could play a key role in medicine and could find numerous non-medical applications through biologically inspired design[2]. The vast domain space of biomaterials includes metals, alloys, ceramics, glasses, thermosets, thermoplastics, elastomers, textiles, etc.

The designs of new biomaterials are mostly inspired from structure–function analysis of the extracellular materials (ECM) that cells use to organize themselves into tissues[2]. There has been a great progress in mimicking ECM molecules and in using synthetic peptides to mimic key epitopes, to facilitate cell adhesion. Among the wide array of polymers used in such design are hydrogels. They are unique due to their three-dimensional hydrated network which mimics the micro-environment of ECM, thereby facilitating cell adhesion and proliferation[3].

1.2 Hydrogels

Hydrogels are three-dimensional networks, comprising of hydrophilic polymer chains, which are cross-linked to form matrices with high water content. Their remarkable physico-chemical characteristics, biological properties and similarity to native ECM enables them to be promising materials for biomedical applications[4]. One of the major classifications of hydrogels are based on their source of origin; i.e., synthetic and natural. Hydrogels from synthetic sources possess controllable degradation, generally higher mechanical properties, but lack biological moieties. However, naturally-derived hydrogels are more appealing for biological applications due to their cell

signaling and cell-interactive properties and biodegradability[5-7]. But they are well-known for their lower mechanical properties and poor control over degradability[8]. Therefore designing hydrogels based on the combination of both natural and synthetic polymers have attracted significant attention for various biological applications[9]. Among the efforts to design mechanically robust hydrogels, new concepts were emerged in the recent years, such as nanocomposite (NC) hydrogels[10], slide-ring hydrogels[11], tetra-PEG hydrogels[12] and double network (DN) hydrogels[13]. In this thesis the focus is towards the design and synthesis of mechanically robust hydrogels derived from the combination of both natural and synthetic polymers, employing the concept of DN hydrogels for their preparation.

1.2.1 Hydrogels from biomimetic resources

Hydrogels derived from natural origin generally possess advantage over synthetic counterparts where biocompatibility is concerned since they offer better chemical and morphological cues to cells. Few of the natural polymers used for designing hydrogels with biomimetic characteristics are hyaluronic acid (HA), fibrin, alginate (Alg), cellulose, collagen, chitosan, etc. HA is known for its applications in tissue engineering due to its high visco-elasticity and space filling characteristics. These rheological characteristics make them ideal for ophthalmic surgery and in osteoarthritis treatment[14]. Fibrin is well known for its ability to control bleeding and tissue adhesion during surgery. It also showed better performance as skin grafts and fosters wound healing by delivering necessary growth factors[14]. Collagen composites are known for their ability to restore appropriate shape and pliability of scarred vocal folds and foster its regeneration[14]. Chitosan can undergo thermal and pH triggered gelation and hence can be utilized in a minimally invasive manner. It can also be enzymatically degraded *in vivo* by lysozyme and chitosanase enzyme[15].

1.2.2 Biomedical applications of hydrogels

As discussed earlier, the structural similarity of hydrogels to that of the extracellular matrix (ECM) and other characteristics makes them ideal for soft-tissue applications such as neural bioelectronics, wound dressings, tissue grafts, cardiac repair, skin graft, cancer therapy, etc. Devices used in conventional approach towards bioelectronics are metals which are significantly stiffer than the target neural tissues. They are commonly associated with a chronic inflammatory response which reduces implant

efficacy and lifetime. Therefore hydrogel systems have emerged as ideal candidate to enhance biointegration and long-term performance of bioelectronic devices[16]. Hydrogels are also known to enhance the bio-availability of drugs, reduce drug side-effects and their network structure could be tuned to attain desired therapeutic dosage[17].

1.3 3D X-ray micro-CT imaging of hydrogels

Biomedical imaging techniques are essential for the characterization of engineered tissues and biomaterials. Recent advances have extended the application of sophisticated 2D and 3D imaging technologies to reveal and visualize complex biological events at biomaterial–tissue interfaces. The ability to probe such interactions is essentially valuable to quantify molecular, cellular, and tissue level interactions with biomaterial surfaces and porous structures in vitro and in vivo. X-ray micro-computed tomography (micro-CT) is one such technique. It is a non-invasive X-ray imaging technique that provides precise three-dimensional imaging of micro-architectures and allows quantification of volumetric parameters in hydrogels and devices[18-19].

Micro-CT imaging technique provides precise quantification of both soft and hard tissue[20] regeneration[21] in various scaffold materials including polymers[22-23], ceramics, metals, etc[19]. *In vivo* bone regeneration as well as mineralization inside HA hydrogel scaffolds containing growth factors were studied by Patterson et al with the aid of micro-CT 3D imaging technique[24]. Kolambkar et al[25] has reported micro-CT based study of an alginate based growth factor delivery system that consists of an electrospun nanofiber mesh tube for guiding bone regeneration in large osseous defects. Result shows consistent bridging of defect ends, accelerated by growth factors, resulting in the functional restoration of regenerated bone.

1.4 Double network hydrogels

Double network (DN) hydrogels are new class of hydrogels, reported first by Jian Ping Gong[13] (2003), which contains two independent polymer networks. First network, poly(2-acrylamido-2-methylpropanesulfonic acid) (PAMPS) mainly comprised of a densely cross-linked polyelectrolyte whereas the second network,

poly(acrylamide) (PAAm) contained a non-ionic polymer with lower cross-link density or without any cross-links (**Fig. 1.1**)[13].

PAMPS-PAAm based DN hydrogel exhibited a tensile strength of 17.2 MPa, whereas their single network (SN) hydrogels prepared from PAMPS and PAAm could sustain stress of 0.4 and 0.8 MPa, respectively. Similarly, these DN hydrogels showed fracture strain of 92%, while SN hydrogels prepared from PAMPS and PAAm failed at 41 and 84% strain, respectively. This remarkable difference in the mechanical strength of these hydrogels compared to their SN hydrogels arises from three major attributes: i) combination of rigid, brittle first network and soft as well as ductile second network, ii) molar concentration of second network is 20 – 30 times that of first network, and iii) the first network is heavily cross-linked, whereas the second network is loosely cross-linked.

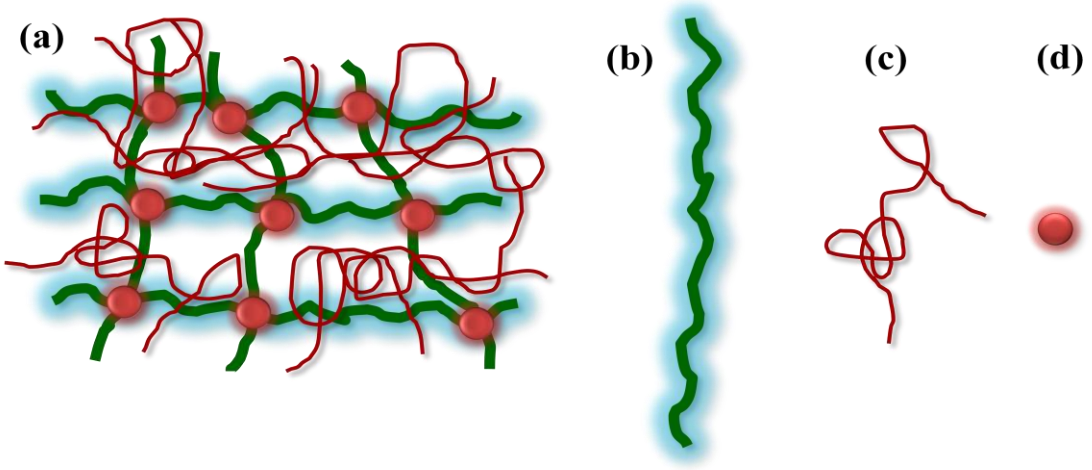

Figure 1.1: (a) Schematic representation of DN hydrogel comprising of two different polymers (b & c) where the first network is tightly bound by (d) cross-linker

1.4.1 True chemical structure of PAMPS–PAAm DN hydrogels

Nakajima et al have prepared PAMPS-PAAm DN hydrogels with and without cross-links in the second network of PAAm, to study the role of cross-links in the second network. Results showed that c-DN gels prepared without cross-links in the second network is actually connected to the first network by copolymerizing with the residual cross-linker of the first network. This results in the formation of inter-network cross-

linking (INC) points in DN network, connecting two networks with each other (**Fig. 1.2**).

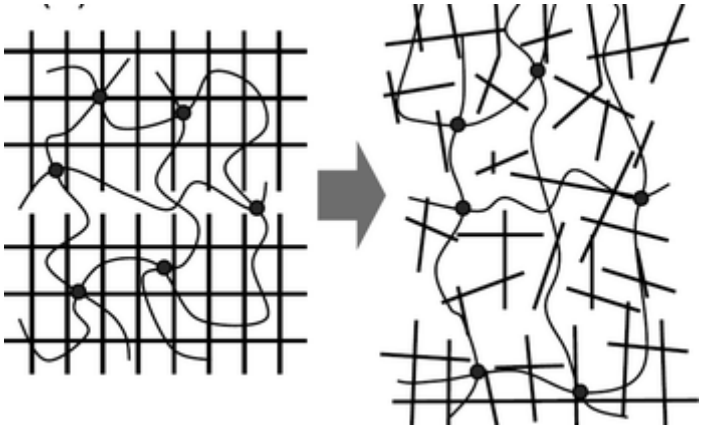

Figure 1.2: Schematic representation of chemical structure in PAMPS–PAAm DN hydrogel, where applied force is transferred through INC[26]

As shown in **fig. 1.2**, solid mesh denotes PAMPS network, curved lines represent PAAm chains, and filled circles denote cross-linking points of PAAm and/or INC. The force applied to DN hydrogel is transferred to the first network and to the second one through this interconnected structure. Cross-linking points acts as anchors and hence applied force can be transferred to PAMPS network from a crack by elongation of PAAm network. Shestakova et al[27] reported the origin of toughening mechanism in PAMPS-PAAm DN hydrogels from detailed ^{1}H HRMAS NMR spectroscopy studies. Studies points towards the existence of strong hydrogen-bond interactions originated from N-H groups in PAMPS, as H-bond donor and C=O group of PAAm, as H-bond acceptor.

1.4.2 Proposed structure model for PAMPS–PAAm DN hydrogels

Yang-Ho Na et al[28] has studied the dynamic aspect of PAMPS–PAAm DN hydrogels by DLS measurements. The results showed the presence of slow modes beside the hydrogel mode (fast mode) increase the strength of DN hydrogels at lower cross-linking density of second network. Dynamic of slow mode is similar to the translational motion of PAAm polymers in semi-dilute media.

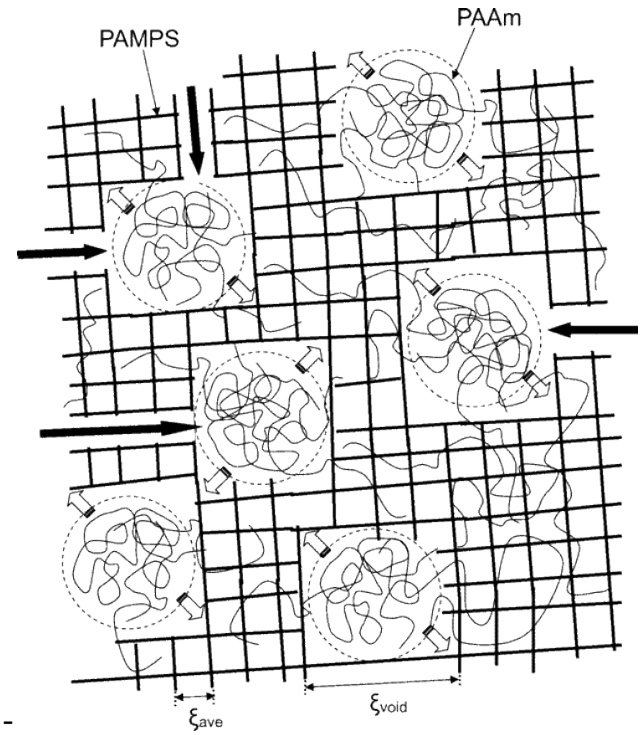

Figure 1.3: Proposed structure model of PAMPS–PAAm DN hydrogel, where PAAm occupies 'voids' in the PAMPS network[28]

As shown in **fig. 1.3**, large 'voids' exists in the tightly cross-linked network of PAMPS due to specific radical polymerization mechanism, which results in a rigid and inhomogeneous network. Loosely cross-linked PAAm chains interpenetrates PAMS network and also occupies or fills these large 'voids', partially gets entangled with PAMPS network and acts as 'molecular crack stopper'. PAAm chains in the 'voids' could efficiently absorb crack energy either by viscous dissipation or by large deformation of their own. Thus, PAAm plays a key role to attain higher fracture energy in PAMPS–PAAm DN hydrogels by restricting the growth of cracks to macroscopic level. A molecular mechanism is proposed by Tirumala et al[29] addresses the toughness enhancement in PAMPS-PAAm DN hydrogels by in-situ neutron scattering measurements. It was proposed that efficient stress transfer between the two networks is responsible for the formation of cracks with regular spacing.

1.4.3 Preparation methods of DN hydrogels

DN hydrogels were prepared by different routes. The details have been given by Cheng et al[30]. DN hydrogels possess exceptional mechanical properties compared to

their inter-penetrating network (IPN) counterpart. IPNs are prepared by the linear combinations of two different cross-linked polymer networks and one pot methods are generally used for their preparation. Polymers used for their preparation can be ionic or neutral. Semi-IPNs (sIPN) are prepared by cross-linking only one polymer network where the second polymer remains entangled inside the network of first polymer. In contrast, most of the DN hydrogels are prepared by a two step process and the molar concentration of second polymer is approximately 10 to 30 times higher than that of the first one. Some of the major strategies to prepare DN hydrogels are discussed in the following:

1.4.3.1 Two-step swelling process

For the first time PAMPS–PAAm DN hydrogelsl[13] were synthesized via a two-step polymerization method. As shown in **fig. 1.4**, the first step is to use strong polyelectrolytes to form a covalently cross-linked, rigid and brittle, first network via UV photo-polymerization. Then, the first polyelectrolyte hydrogel is immersed and swollen in a precursor solution containing neutral second-network monomers, initiators, and cross-linkers. Duo to the high swelling nature of first network, the 2nd network reactants slowly diffuse into the first network, resulting in a large volume expansion of the 1st network. The polymerization occurs in the first network to form a loosely cross-linked, soft and ductile, neutral, 2nd network within the 1st network, resulting into DN hydrogels.

This method has been widely used to prepare most of the DN hydrogels with both networks being chemically cross-linked. On the other hand, since this method involves swelling, diffusion, and two polymerization processes, it requires a large excess of the 2nd network reactants (i.e. the 2nd network monomers are 20‑50 times more than the 1st monomers) to efficiently initiate the second polymerization and to form strong network entanglement with the 1st network. The typical two-step method usually takes 1‑2 days to complete the DN hydrogels. This method is the most widely used method for preparation of DN hydrogels.

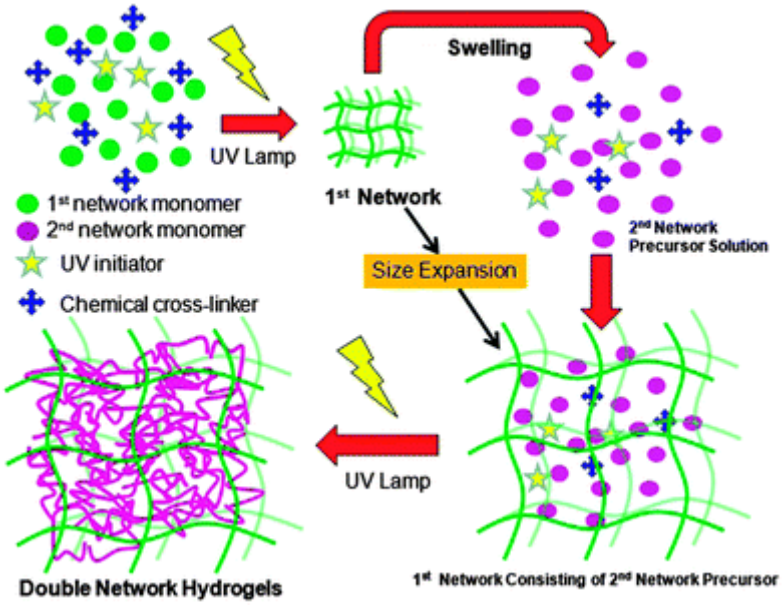

Figure 1.4: Schematic representation of two-step process for the preparation of DN hydrogel[30]

1.4.3.2 Molecular stent process

For the two-step process used to prepare most of the chemically linked DN hydrogels, the swelling ability of the 1st network formed by strong polyelectrolytes is extremely important for the subsequent 2nd polymerization process to prepare tough DN hydrogels. However, when the neutral polymers are used to form the 1st network, the poor swelling ability of the 1st network makes the two-step process difficult to prepare tough DN hydrogels. To overcome this limitation, Nakajima et al[31] developed a ‘‘molecular stent’’ method to synthesize tough DN hydrogels with both networks formed by neutral polymers[32]. **Fig. 1.5** shows a schematics to prepare DN hydrogel network containing ‘‘molecular stent’’. Briefly, similar to the two-step process, the first, neutral network with well-defined network structure is synthesized first. Then, linear, strong polyelectrolytes (molecular stent) are introduced into the neutral first-network to form a semi-IPN hydrogel. During this process, the overall osmotic pressure of the semi-IPN hydrogel is increased to stretch the first-network chains to the extended conformation, resulting in a highly swollen structure similar to the strong polyelectrolyte hydrogels.

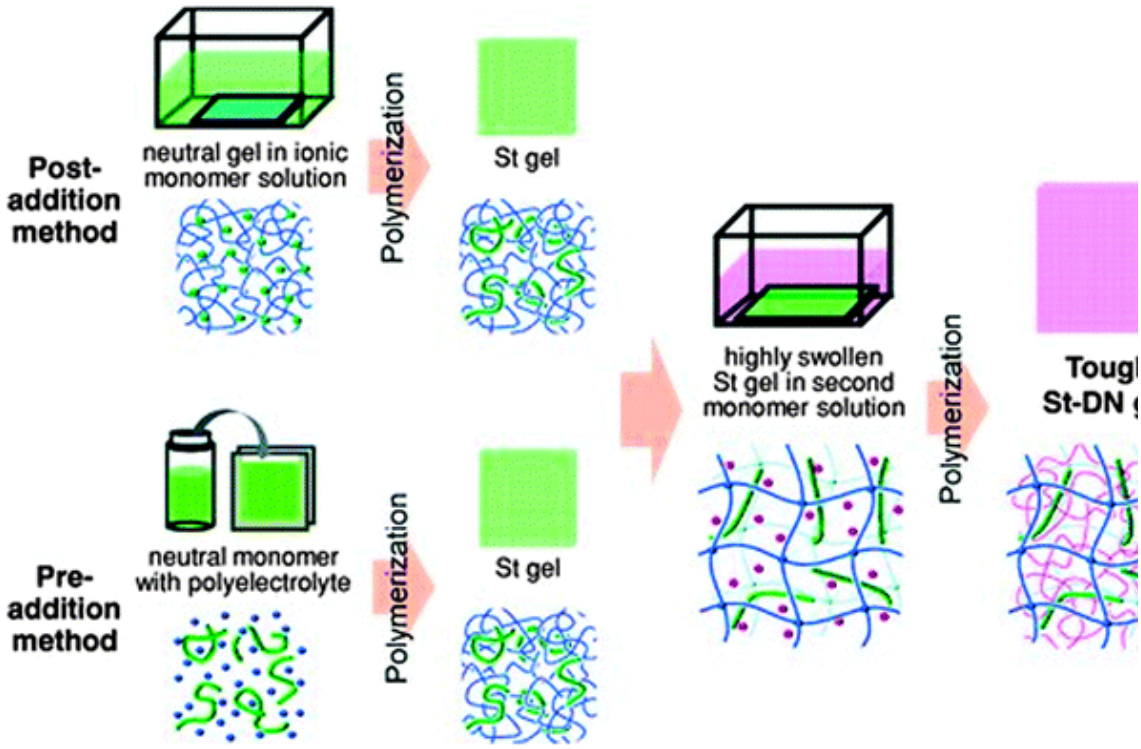

Figure 1.5: Schematic representation of molecular stent process for the preparation of DN hydrogel[30]

1.4.3.3 One pot process

The two-step and molecular stent processes have offered great flexibility in the preparation of tough DN hydrogels. However, both methods involve multiple steps for hydrogel synthesis and thus encounter some limitations: (i) the multi-step synthesis process of DN hydrogels is tedious and time-consuming, which often involves swelling, diffusion, and two polymerization processes that demand 2–7 days to complete the DN hydrogels; (ii) conventional multi-step methods are not easy to prepare complex shaped hydrogels to meet broad or specific applications and (iii) both the methods are developed for obtaining chemically cross-linked DN hydrogels. However, the fracture of chemically linked networks, particularly the first network, causes irreversible and permanent bond breaks, making the hydrogels very difficult to be repaired and recover from damage. To overcome these limitations, Chen et al.[33] (**fig 1.6**) recently developed a new, simple, one-pot method to synthesize a new type of hybrid physically–chemically cross-linked agar–polyacrylamide (agar–PAAm) DN hydrogels, consisting of two interpenetrating networks of a hydrogen-bond linked agar network and a covalently cross-linked PAAm network.

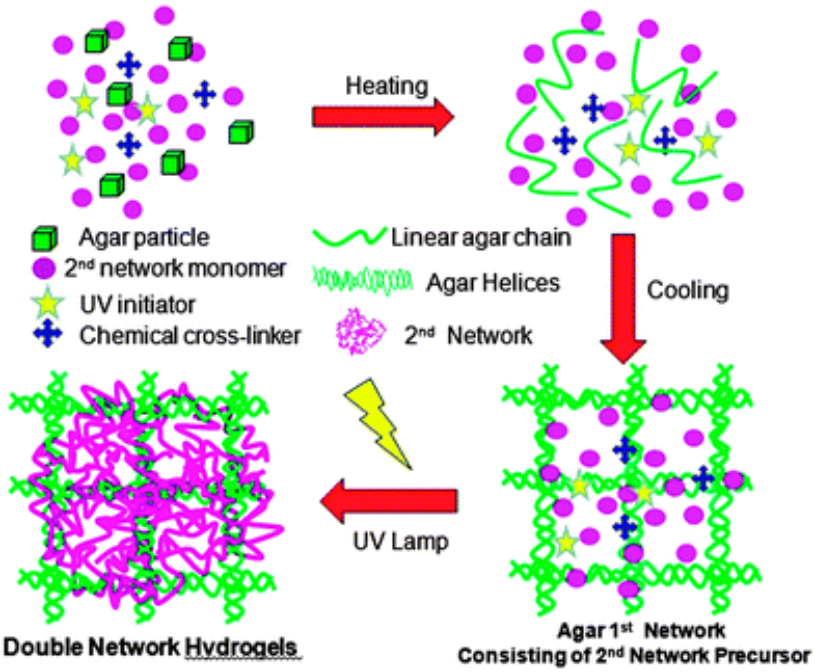

Figure 1.6: Schematic representation of one-pot process for the preparation of DN hydrogel[30]

© Royal Society of Chemistry

1.4.3.4 Other processes

The three-dimensional (3D) printing technique has been used to produce DN hydrogels[34]. The printing of hydrogel-like materials often involves the injection of a hydrogel precursor solution into a defined mold, followed by gelation reaction initiated by light, chemicals, or thermal stimulus. Bakarich et al[35] have developed a simultaneous extrusion printing and photo-polymerization method for rapidly engineering tough ionic–covalent entanglement (ICE) hydrogels with complex shapes on a large scale. This UV-extrusion printing method offers exciting features for quick fabrication of functional and tough hydrogels with very complex 3D geometries. The 3D printing technique is a very powerful tool for the fabrication of multi-component hydrogel structures and devices for applications in artificial muscles and tissue scaffolds.

Most of the synthetic hydrogels prepared by two-step and molecular stent methods lack shape-flexibility, and only simple shapes such as a sheet or a disc can be formed. In both methods, the shape of DN hydrogels is determined by the first network acting

as a ‘‘skeleton’’, but upon swelling of the first network in the second network solution, the original ‘‘skeleton’’ shapes of the hydrogels are difficult to be preserved. To overcome this problem, Nakajima et al[36] proposed a new ‘‘internal mold’’ method to synthesize free-shaped and tough DN hydrogels by introducing physically crosslinked poly(vinyl alcohol) (PVA) as an internal mold into the PAMPS–PAAm hydrogel system. Firstly, the PVA hydrogels with complex shapes were synthesized by the freeze-thaw method and used as internal molds, because they are very flexible and relatively strong as to form any complicated shape. Then, the PAMPS network was polymerized inside the PVA hydrogels, without inducing shape deformation. Last, the PAAm network was synthesized in the presence of the PVA–PAMPS DN hydrogels (PVA–PAMPS DN hydrogels), leading to the free-shaped PVA–PAMPS–PAAm triple-network hydrogels (PVA-DN hydrogels).

1.4.4 Structure of DN hydrogel network

The combination of different hydrogel preparation processes created a wide variety of network structures in DN hydrogels and is primarily responsible for its toughening mechanism[30]. The remarkable enhancement of mechanical properties of DN hydrogels cannot be simply explained by the classical theories for soft polymeric systems such as Lake–Thomas theory and de Genes theory. Different network structures reported in DN hydrogel systems are detailed in the following.

1.4.4.1 Chemically cross-linked networks

Most of the DN hydrogels synthesized by two-step and molecular stent processes are chemically linked in both networks; thus these chemically linked DN hydrogels appear to have similar network structures and mechanical behaviors[30]. The two or multiple-step polymerization of different network polymers lead to heterogeneous network structures, as evidenced by DLS measurements and explained by the void model[28,37-39]. The 1st network is inhomogeneous with many voids due to the specific radical polymerization mechanism. When the 2nd network chains are formed in the 1st network, they not only interpenetrate in the 1st network, but also fill some of the voids to entangle with the 1st network, increasing the in-homogeneity of both network structures. Both polymer-filled voids and polymer entanglement with voids can effectively absorb and dissipate elastic energy around the cracks either by viscous dissipation or by large deformation of the polymer chains, preventing stress

accumulation and crack propagation to a macroscopic level. In some cases, the fracture of the rigid and brittle 1st network also involves chain scission of polymers for energy dissipation. Thus, the in-homogeneity appears to be positively correlated with the mechanical properties of DN hydrogels. Additionally, due to the chemically cross-linked nature, once the fracture of polymer networks reaches irreversible damage caused by permanent bond breakage at high strain, DN hydrogels will lose most of their mechanical properties after loading, leading to the difficulty to recover from damage. From a network structure point of view, the introduction and optimization of in-homogeneity of network structures, instead of eliminating network in-homogeneity, is one way to improve the toughness of DN hydrogels[30].

1.4.4.2 Physically and chemically cross-linked networks

Physically and chemically linked DN hydrogels are generally termed as hybrid DN hydrogels and only a few of them with a combination of non-covalent and covalent linkers were developed recently[35,40-41]. In the hybrid DN hydrogels, the 1st network is always constructed by physically cross-linked hydrogels, while the 2nd network is chemically linked. The association forces between both networks and within the physical network are non-covalent bonds such as hydrophobic interactions, van der Waals (VDW) interactions, hydrogen bonds, and electrostatic association, depending on the intrinsic physicochemical properties of both polymers.

Suo et al[40,42] developed hybrid DN hydrogels by combining alginate hydrogel cross-linked by Ca^{2+} ions and the covalently cross-linked PAAm network (namely, Ca^{2+}–alginate–PAAm hybrid hydrogels). The Ca^{2+}–alginate–PAAm hybrid hydrogels exhibit excellent extensibility (>20 times their initial length) and high fracture energy (~9000 J m^{-2}), close to natural rubber (~10 000 J m^{-2})[43], but they are soft with a tensile strength of ~160 kPa. Notably, the hydrogels also showed notch-insensitive (the notched hydrogel can be stretched up to 17 times its original length) and recoverable properties (~74% work from the first loading).

1.4.4.3 Lamellar bilayer network

Conventional chemically cross-linked DN hydrogels have almost negligible recovery and fatigue resistance, once the covalent bonds break permanently at high strains. Hybrid physically–chemically crosslinked DN hydrogels possess a better recovery

ability, but they usually need external stimuli to trigger the recovery property[30]. Haque et al[44-47] developed a new type of lamellar bilayer DN hydrogels consisting of rigid, hydrophobic poly(dodecyl glyceryl itaconate) (PDGI) lamellar bilayers and a ductile, hydrophilic PAAm matrix, both of which alternatively and periodically stack on top of each other to form multiple sandwich-like bilayers. Specifically, DGI surfactants were self-assembled into a lamellar DGI bilayer under a shear flow. Upon polymerization, PDGI bilayers were entrapped in the PAAm matrix, forming a PDGI bilayer-PAAm structure.

The PDGI–PAAm bilayer hydrogels demonstrated their structural reversibility under cyclic compression–release deformation tests. Such structural reversibility does not require any external stimuli. Moreover, the PDGI–PAAm bilayer hydrogels exhibited much better mechanical properties than either PDGI–PAAm hydrogels without the bilayer or PAAm SN hydrogels. More importantly, hysteresis loops also revealed multiple self-recovery and fatigue resistance of the PDGI–PAAm DN hydrogels on several tens of successive loadings.

1.4.4.4 Micro or nano-composite network

Inspired by carbon reinforced nano-composite hydrogels, microscopic hydrogel spheres can be used to improve the mechanical properties of conventional hydrogels where they act as multifunctional crosslink nodes[30]. Hu et al[48] developed novel microgel reinforced (MR) hydrogels with two phase composite structures, where the disperse phase is the rigid DN microgels and the continuous phase is the soft PAAm matrix. At the optimal formulation, the MR hydrogels showed high mechanical strength and toughness, comparable to conventional DN hydrogels. A prominent hysteresis and softening phenomena were also found for MR hydrogels, as with conventional DN hydrogels, but not for the sMR hydrogels (PAAm single-network hydrogel), indicating that the irreversible structural change that is related to the rupture of covalent bonds occurred in MR hydrogels. Additionally, in contrast to the sMR hydrogels, the MR hydrogels increased the reinforcement efficiency (the ratio of fracture stress of MR to that of the PAAm hydrogel) up to 6 times. The results indicated that the toughening mechanism of MR hydrogels could be similar to that of conventional DN hydrogels.

Panhuis et al[49] proposed to use gellan gum–gelatin ICE hydrogel microspheres to reinforce genipin cross-linked gelatin hydrogels. The genipin cross-linked gelatin hydrogels without adding microspheres were relatively soft and ductile (compressive failure stress of 0.41 MPa, compressive strain to failure of 69%, compressive secant modulus of 0.074 MPa, and compressive strain energy to failure of 39 kJ m^{-3}).

Nanoparticles can also be incorporated into DN hydrogels to generate tough hydrogels. Fu and coworkers[50-51] used silica particles and attapulgite (ATP) nanorods as macro-crosslinkers to copolymerize with conventional PAMPS–PAAm DN hydrogels. Both silica–PAMPS–PAAm and ATP–PAMPS–PAAm DN hydrogels were able to achieve a compressive strain of up to 98% and a stress of 65–70 MPa without fracturing, which were much higher than those of PAMPS–PAAm DN hydrogels. The covalent bond formation and physical adsorption between nanoparticles and polymer networks are suggested to account for the high mechanical strength and toughness.

1.4.5 Toughening mechanism in DN hydrogels

As discussed in sections 2 and 3, major unique structural characteristics of DN hydrogels are i) rigid and brittle first network along with soft and ductile second network, ii) very high molar concentration of 2nd network, iii) tightly cross-linked 1st network and loosely cross-linked 2nd network and iv) effective polymer chain density ratio and critical polymer strand density ratio[30]. For better understanding of the touching mechanism and structure-property relationships in DN hydrogel networks, the influence of 1st and 2nd network structures as well as network interactions on mechanical properties are explained in the foregoing.

1.4.5.1 Role of first network

The first network of DN hydrogels is often tightly cross-linked by strong polyelectrolytes, such as PAMPS and poly(3-sulfopropyl acrylate potassium salt) (PSAPS). Although tightly cross-linked, owing to the polyelectrolyte nature, the first network highly swells in water, allowing it to absorb a large amount of the second network monomers, making the molar ratio of the second network to the first network larger than 20–30. Due to high cross-link density in the first network, it is rigid and brittle and helps in dissipating energy upon deformation via fracturing. Some attempts

have been made to use neutral polymers along with molecular stents, weak polyelectrolytes, or physically linked polymers to form the first network via different synthesis methods, Many studies have shown that the high toughness of DN hydrogels is mainly derived from the fracture of the first network upon deformation, because relatively large damage zones formed in the first network allow for more accumulated damage before macroscopic crack propagation occurs throughout the whole network[28-29,32,38,52-54]. Considering the toughening mechanism from a network structure point of view, the in-homogeneity of the first network is thought to be critical for the mechanical properties of DN hydrogels.

1.4.5.2 Role of second network

In most cases, the second network of DN hydrogels is chemically loosely linked by random copolymerization of monomers and cross-linkers. To achieve high toughness, the second network is often designed with soft and ductile polymers of high molecular weight[55], including neutral polyacrylamide[13,33], PEG[56], polydimethylacrylamide[57] and zwitterionic poly N-(carboxymethyl)-N,N0-dimethyl-2-(methacryloyloxy) ethanaminium[58]. Due to the loosely cross-linked second network, only a very small amount of crosslinker (0–0.03 mol% of monomer) is needed to form the second network. In general, the molar ratios of the first network to the second network monomers, cross-linker concentrations of both networks, and molecular weight of the second network are three important parameters that affect the network structures and the mechanical properties of DN hydrogels. An increase of the second network cross-linking often causes the break of mechanical balance between the two networks and lead to the decrease of fracture stress and fracture energy of DN hydrogels[59]. In contrast, an increase of the second network concentrations generally improves the mechanical strength of the hydrogels, because of the more and stronger chain entanglement being formed within the second network and between the two networks[60].

1.4.5.3 Role of network entanglement and interaction

Strong chain entanglement between the two networks of DN hydrogels is the origin of high toughness and strength of DN hydrogels[59-60]. Such chain entanglement between two networks strongly depends on the density ratio of elastically effective polymer chains of two networks. The propagation of the micro-cracks in the brittle first

network is prevented by the ductile second network. The second network transfers the stress back to the first network, causing further internal fracture of the brittle first network. This stress-loading transfer between the two networks is determined by inter-network topological entanglement. The extent of network interactions between two networks indicates the nature and strength of different molecular interactions and association between two networks. If two networks are cross-linked by covalent bonds, the strength of the DN hydrogels generally increases as the entanglement between the networks increases.

1.4.5.4 Fracture process inside network

The failure of a material generally involves two sequential processes of the initial fracture formation and the following fracture propagation[55]. Depending on the network structures and network interactions, the fracture process and associated energy dissipation mechanisms are likely to be different between hybrid physically/chemically linked hydrogels and chemically linked hydrogels. For hybrid-linked DN hydrogels, the internal fracture of hybrid DN hydrogels exhibits large differences as compared to the conventional DN hydrogels[61]. Physical association and their interaction with chemically linked networks vary significantly, leading to a very diverse internal fracture process. The unzipping of the ionically cross-linked 1st network can effectively dissipate energy, resulting in large hysteresis. The toughening mechanisms in hybrid hydrogels are considered as synergistic effects of crack bridging by the network of covalent cross-links and hysteresis by unzipping of the network of ionic cross-links.

1.4.6 Applications of DN hydrogels

The enhanced mechanical property of DN hydrogels in contrast to conventional IPNs has enabled them to find applications in challenging scenarios where IPN counterparts have failed. These challenging areas of research include tissue engineering, drug delivery, antifouling, sensors, actuators, etc.

1.4.6.1 Tissue engineering

Tissue engineering mainly aims to restore, maintain, and improve tissue functions by developing and reconstructing biocompatible and functional substitutes or tissues via implantation of isolated cells, delivery of tissue inducing substances, and culture of

cells on the extracellular matrix[62]. Hydrogels are the most appropriate biomaterials to mimic several features of the natural extracellular matrix for cell encapsulation, proliferation, and signaling, as well as stimulation of matrix production by cells, due to their highly hydrated, mechanically supportive and 3D porous structures[63]. Recent studies have shown that cells are exquisitely sensitive to changes in the mechanical properties[64], surface characteristics and network structures of supportive substrates. Despite some controversial data and poorly understood mechanisms of cell–hydrogel interactions, a number of DN hydrogels with tunable physicochemical properties have been developed to study the effect of hydrogel networks and stiffness on various cell functions in a 3D environment.

Weng et al[65] found that HA–PDAAm (hyaluronan– N,N-dimethylacrylamide) DN hydrogels did not show any noticeable effects of DAAm monomer concentrations (0 mol L^{-1} or 3 mol L^{-1}) and crosslinker concentrations (0.01–2 mol% of DAAm) on cell growth even after 2 months of co-culturing with fibroblasts. Zhao et al[66] have found that in St-PDMAAm–PDMAAm DN hydrogels, use of proteoglycans (PGs) as a molecular stent leads to the strong adhesion of human coronary artery endothelial cells (HCAECs) to the hydrogels, but such cell adhesion was not eliminated in the absence of PGs in the hydrogels. This fact indicates that PGs in the DN hydrogels enhance cell adhesion and may also promote cell proliferation to some extent.

The DN hydrogels are considered as the most promising materials for cartilage regeneration, because they serve not only as a tissue scaffold with high mechanical strength and sufficient stability, but also as a carrier for loading stem cells and growth factors, both of which aim to facilitate retention of encapsulated biomolecules in the defect sites and to form a functional repair tissue. Yasuda et al[67] has systematically studied different biological responses and implantation of PAMPS–PDMAAm DN hydrogels for tissue and cartilage repair. They found that the mechanical properties of the PAMPS–PDMAAm DN hydrogel implanted in the subcutaneous tissue did not deteriorate over 6 weeks after implantation. Further pellet implantation tests demonstrated that PAMPS–PDMAAmDN hydrogel only induced a mild cell infiltration around para-vertebral muscle during the 1st week, and the degree of inflammation remained at a similar degree to that of the negative control (high density polyethylene pellet) at the 4th and 6th week[68]. More importantly, when PAMPS–

PDMAAm DN hydrogel was implanted into the bone defects, after 4 weeks of surgery the defects implanted with DN hydrogels were almost completely filled with regenerated white opaque tissues without any harmful damage being observed, while the defects without any treatment were insufficiently filled with opaque tissues.

1.4.6.2 Drug delivery

DN hydrogels and other hydrogels have also been used as drug reservoir/delivery systems for different applications[69]. Hydrogels containing high water content provide an aqueous environment for not only loading small organic molecules, but also preserving bioactive conformations of protein drugs and DNA/RNA. Particularly, proteins encapsulated in the hydrogels are more resistant to denaturation than free proteins in solution[70].

Chen et al[71] developed β-cyclodextrin (β-CD) modified graphene–PDMAA DN hydrogels for controlled release of a model anticancer drug camptothecin (CPT). β-CD modified graphene–PDMAA DN hydrogels showed a very slow release of CPT, i.e. 70% of CPT was released within 175 h. Kato et al[72] developed a one-pot method to synthesize silicabased DN hydrogels using silica nanoparticles, sodium silicate, and acrylamide. They found that the encapsulated enzymes (trypsin, pepsin, and urease) in the silica DN hydrogels were able to retain their enzymatic activity. Luo et al[73] recently developed light-responsive DN hydrogel particles with multi-compartmental structures to control-release TRITC dextran. The agarose–alginate DN hydrogels were loaded with polypyrrole (PPy) nanoparticles as photothermal transducers to form a core–shell structure, where the core compartment provides NIR responsiveness while the non-loaded shell provides a barrier to control the release of reagent immobilized in the core. Upon periodic NIR laser switching, the DN hydrogel particles enable one to control the release of TRITC–dextran in a pulsatile manner.

1.4.6.3 Antifouling, sensors and actuators

Hydrogels are also designed and used as antifouling materials to resist protein adsorption, cell adhesion, and microorganism attachment for anti-thrombogenic implants, drug delivery carriers, and membrane separation. Murosaki et al[74] have performed long term antifouling tests for PVA SN and PAMPS–PAAm DN hydrogels in the real marine environment. The surface coverage of barnacle was 92.4%, 7.4%,

and 3.3% on polyethylene (PE as a control), PVA hydrogel, and PAMPS–PAAm DN hydrogel, respectively. They further found that both PVA and PAMPS–PAAm hydrogels also highly resisted other micro/macro organism adhesion. PAMPS–PAAm DN hydrogels showed a better antifouling performance than PVA SN hydrogels, probably because PVA hydrogels are too soft so that barnacles could easily penetrate into the hydrogels via muscle contraction.

DN hydrogels have also been used as highly responsive, selective, and sensitive sensors to detect a wide range of analytes in response to changes in pH, solvent, light, mechanical force, or electric and magnetic field. Liang et al[75] reported ultrathin and tough PAMPS–PAAm DN hydrogels (UTDN hydrogels), which demonstrated very fast and high solvent-triggered force generation. Within several tens of seconds, the UTDN hydrogels can quickly change the stress over a wide range by simply changing the solvent components and ratios (ethanol vs. water). The solvent-induced dramatic changes in the elastic modulus of the UTDN hydrogels were considered the main reason for this response in the contractile stress. Moreover, DN hydrogels can also be used as actuators. Dai et al[76-77] synthesized triple-network (TN) hydrogels composed of PAAc or PAAm and poly(3,4-ethylenedioxythiophene)– poly(styrenesulfonate) (PEDOT–PSS), which possess not only high mechanical toughness, but also outstanding electrochemical activity of the conducting components. The specific capacitance of the PAAc–PEDOT–PSS TN hydrogels is 4.8 F g^{-1}, which is much larger than that of the ordinary commercial capacitors with the order of mF g^{-1}. The combination of mechanical toughness, rheological properties, electrical properties, microstructures and molecular structures of the TN hydrogels allows one to use them as electro-sensors and supercapacitors in some applications.

1.5 References

(1) Williams, D. F. *Biomaterials* **2009**, *30*, 5897.

(2) Huebsch, N.; Mooney, D. J. *Nature* **2009**, *462*, 426.

(3) Hoffman, A. S. *Adv Drug Deliver Rev* **2002**, *54*, 3.

(4) Annabi, N.; Tamayol, A.; Uquillas, J. A.; Akbari, M.; Bertassoni, L. E.; Cha, C.; Camci-Unal, G.; Dokmeci, M. R.; Peppas, N. A.; Khademhosseini, A. *Adv Mater* **2014**, *26*, 85.

(5) Jen, A. C.; Wake, M. C.; Mikos, A. G. *Biotechnol Bioeng* **1996**, *50*, 357.

(6) Peppas, N. A.; Bures, P.; Leobandung, W.; Ichikawa, H. *Eur J Pharm Biopharm* **2000**, *50*, 27.

(7) Peppas, N. A.; Huang, Y.; Torres-Lugo, M.; Ward, J. H.; Zhang, J. *Annual Review of Biomedical Engineering* **2000**, *2*, 9.

(8) Lee, K. Y.; Mooney, D. J. *Chemical Reviews* **2001**, *101*, 1869.

(9) Pérez, R. A.; Won, J.-E.; Knowles, J. C.; Kim, H.-W. *Adv Drug Deliver Rev* **2013**, *65*, 471.

(10) Haraguchi, K.; Takehisa, T. *Adv Mater* **2002**, *14*, 1120.

(11) Karino, T.; Okumura, Y.; Ito, K.; Shibayama, M. *Macromolecules* **2004**, *37*, 6177.

(12) Sakai, T.; Matsunaga, T.; Yamamoto, Y.; Ito, C.; Yoshida, R.; Suzuki, S.; Sasaki, N.; Shibayama, M.; Chung, U. I. *Macromolecules* **2008**, *41*, 5379.

(13) Gong, J. P.; Katsuyama, Y.; Kurokawa, T.; Osada, Y. *Adv Mater* **2003**, *15*, 1155.

(14) Slaughter, B. V.; Khurshid, S. S.; Fisher, O. Z.; Khademhosseini, A.; Peppas, N. A. *Adv Mater* **2009**, *21*, 3307.

(15) Li, Y. L.; Rodrigues, J.; Tomas, H. *Chemical Society Reviews* **2012**, *41*, 2193.

(16) Goding, J.; Vallejo-Giraldo, C.; Syed, O.; Green, R. *Journal of Materials Chemistry B* **2019**, *7*, 1625.

(17) Li, X.; Su, X. *Journal of Materials Chemistry B* **2018**, *6*, 4714.

(18) Stock, S. R. *MicroComputed Tomography: Methodology and Applications*; CRC Press 2009.

(19) Arun, T. A. T.; Soumya, C. K. C.; Saaj, U. S.; Nair, M. B.; Kalliyana, K. V. *Ct 2008: Tomography Confluence* **2008**, *1050*, 68.

(20) Nyangoga, H.; Mercier, P.; Libouban, H.; Baslé, M. F.; Chappard, D. *Plos One* **2011**, *6*, e17336.

(21) Barbetta, A.; Bedini, R.; Pecci, R.; Dentini, M. *Annali dell'Istituto Superiore di Sanità* **2012**, *48*, 10.

(22) Wang, Y.; Chang, H. I.; Wertheim, D. F.; Jones, A. S.; Coombes, A. G. A. *Tissue Eng* **2007**, *13*, 1742.

(23) Dorsey, S. M.; Lin-Gibson, S.; Simon, C. G. *Biomaterials* **2009**, *30*, 2967.

(24) Jennifer Patterson; Ruth Siew; Susan W. Herring; Angela S.P. Lin; Robert Guldberg; Stayton, P. S. *Biomaterials* **2010**, *31*, 6772

(25) Yash M. Kolambkar; Kenneth M. Dupont; Joel D. Boerckel; Nathaniel Huebsch; David J. Mooney; Dietmar W. Hutmacher; Guldberg, R. E. *Biomaterials* **2011**, *32*, 65

(26) Nakajima, T.; Furukawa, H.; Tanaka, Y.; Kurokawa, T.; Osada, Y.; Gong, J. P. *Macromolecules* **2009**, *42*, 2184.

(27) Shestakova, P.; Willem, R.; Vassileva, E. *Chemistry – A European Journal* **2011**, *17*, 14867.

(28) Na, Y.-H.; Kurokawa, T.; Katsuyama, Y.; Tsukeshiba, H.; Gong, J. P.; Osada, Y.; Okabe, S.; Karino, T.; Shibayama, M. *Macromolecules* **2004**, *37*, 5370.

(29) Tirumala, V. R.; Tominaga, T.; Lee, S.; Butler, P. D.; Lin, E. K.; Gong, J. P.; Wu, W. L. *J Phys Chem B* **2008**, *112*, 8024.

(30) Chen, Q.; Chen, H.; Zhu, L.; Zheng, J. *Journal of Materials Chemistry B* **2015**, *3*, 3654.

(31) Nakajima, T.; Sato, H.; Zhao, Y.; Kawahara, S.; Kurokawa, T.; Sugahara, K.; Gong, J. P. *Adv Funct Mater* **2012**, *22*, 4426.

(32) Nakajima, T.; Fukuda, Y.; Kurokawa, T.; Sakai, T.; Chung, U.-i.; Gong, J. P. *Acs Macro Lett* **2013**, *2*, 518.

(33) Chen, Q.; Zhu, L.; Zhao, C.; Wang, Q.; Zheng, J. *Adv Mater* **2013**, *25*, 4171.

(34) Muroi, H.; Hidema, R.; Gong, J.; Furukawa, H. *Journal of Solid Mechanics and Materials Engineering* **2013**, *7*, 163.

(35) Bakarich, S. E.; Panhuis, M. i. h.; Beirne, S.; Wallace, G. G.; Spinks, G. M. *Journal of Materials Chemistry B* **2013**, *1*, 4939.

(36) Nakajima, T.; Takedomi, N.; Kurokawa, T.; Furukawa, H.; Gong, J. P. *Polym Chem-Uk* **2010**, *1*, 693.

(37) Tanaka, Y.; Gong, J. P.; Osada, Y. *Progress in Polymer Science* **2005**, *30*, 1.

(38) Huang, M.; Furukawa, H.; Tanaka, Y.; Nakajima, T.; Osada, Y.; Gong, J. P. *Macromolecules* **2007**, *40*, 6658.

(39) Johnson, J. A.; Turro, N. J.; Koberstein, J. T.; Mark, J. E. *Progress in Polymer Science* **2010**, *35*, 332.

(40) Sun, J.-Y.; Zhao, X.; Illeperuma, W. R. K.; Chaudhuri, O.; Oh, K. H.; Mooney, D. J.; Vlassak, J. J.; Suo, Z. *Nature* **2012**, *489*, 133.

(41) Stevens, L.; Calvert, P.; Wallace, G. G.; Panhuis, M. i. h. *Soft Matter* **2013**, *9*, 3009.

(42) Li, J.; Illeperuma, W. R. K.; Suo, Z.; Vlassak, J. J. *Acs Macro Lett* **2014**, *3*, 520.

(43) Lake, G. J. *Rubber Chem Technol* **1995**, *68*, 435.

(44) Haque, M. A.; Kurokawa, T.; Kamita, G.; Gong, J. P. *Macromolecules* **2011**, *44*, 8916.

(45) Haque, M. A.; Kamita, G.; Kurokawa, T.; Tsujii, K.; Gong, J. P. *Adv Mater* **2010**, *22*, 5110.

(46) Yue, Y. F.; Haque, M. A.; Kurokawa, T.; Nakajima, T.; Gong, J. P. *Adv Mater* **2013**, *25*, 3106.

(47) Haque, M. A.; Kurokawa, T.; Kamita, G.; Yue, Y.; Gong, J. P. *Chemistry of Materials* **2011**, *23*, 5200.

(48) Hu, J.; Hiwatashi, K.; Kurokawa, T.; Liang, S. M.; Wu, Z. L.; Gong, J. P. *Macromolecules* **2011**, *44*, 7775.

(49) Kirchmajer, D. M.; Panhuis, M. i. h. *J Appl Polym Sci* **2014**, *131*, 40557.

(50) Wang, Q.; Hou, R.; Cheng, Y.; Fu, J. *Soft Matter* **2012**, *8*, 6048.

(51) Gao, G.; Du, G.; Cheng, Y.; Fu, J. *Journal of Materials Chemistry B* **2014**, *2*, 1539.

(52) Tsukeshiba, H.; Huang, M.; Na, Y.-H.; Kurokawa, T.; Kuwabara, R.; Tanaka, Y.; Furukawa, H.; Osada, Y.; Gong, J. P. *The Journal of Physical Chemistry B* **2005**, *109*, 16304.

(53) Nakajima, T.; Kurokawa, T.; Ahmed, S.; Wu, W.-l.; Gong, J. P. *Soft Matter* **2013**, 1955

(54) Tominaga, T.; Tirumala, V. R.; Lin, E. K.; Gong, J. P.; Furukawa, H.; Osada, Y.; Wu, W. L. *Polymer* **2007**, *48*, 7449.

(55) Gong, J. P. *Soft Matter* **2010**, *6*, 2583.

(56) Zhang, X.; Guo, X.; Yang, S.; Tan, S.; Li, X.; Dai, H.; Yu, X.; Zhang, X.; Weng, N.; Jian, B.; Xu, J. *J Appl Polym Sci* **2009**, 3063

(57) Azuma, C.; Yasuda, K.; Tanabe, Y.; Taniguro, H.; Kanaya, F.; Nakayama, A.; Chen, Y. M.; Gong, J. P.; Osada, Y. *J Biomed Mater Res A* **2007**, *81*, 373.

(58) Yin, H.; Akasaki, T.; Lin Sun, T.; Nakajima, T.; Kurokawa, T.; Nonoyama, T.; Taira, T.; Saruwatari, Y.; Ping Gong, J. *Journal of Materials Chemistry B* **2013**, *1*, 3685.

(59) Tsukeshiba, H.; Huang, M.; Na, Y. H.; Kurokawa, T.; Kuwabara, R.; Tanaka, Y.; Furukawa, H.; Osada, Y.; Gong, J. P. *J Phys Chem B* **2005**, *109*, 16304.

(60) Ahmed, S.; Nakajima, T.; Kurokawa, T.; Anamul Haque, M.; Gong, J. P. *Polymer* **2014**, *55*, 914.

(61) Chen, Q.; Zhu, L.; Huang, L.; Chen, H.; Xu, K.; Tan, Y.; Wang, P.; Zheng, J. *Macromolecules* **2014**, *47*, 2140.

(62) Langer, R.; Vacanti, J. P. *Science* **1993**, *260*, 920.

(63) Nicodemus, G. D.; Bryant, S. J. *Tissue Engineering Part B: Reviews* **2008**, *14*, 149.

(64) Janmey, P. A.; Winer, J. P.; Murray, M. E.; Wen, Q. *Cell Motility* **2009**, *66*, 597.

(65) Weng, L.; Gouldstone, A.; Wu, Y.; Chen, W. *Biomaterials* **2008**, *29*, 2153.

(66) Zhao, Y.; Nakajima, T.; Yang, J. J.; Kurokawa, T.; Liu, J.; Lu, J.; Mizumoto, S.; Sugahara, K.; Kitamura, N.; Yasuda, K.; Daniels, A. U. D.; Gong, J. P. *Adv Mater* **2014**, *26*, 436.

(67) Yasuda, K.; Kitamura, N.; Gong, J. P.; Arakaki, K.; Kwon, H. J.; Onodera, S.; Chen, Y. M.; Kurokawa, T.; Kanaya, F.; Ohmiya, Y.; Osada, Y. *Macromol Biosci* **2009**, *9*, 307.

(68) Tanabe, Y.; Yasuda, K.; Azuma, C.; Taniguro, H.; Onodera, S.; Suzuki, A.; Chen, Y. M.; Gong, J. P.; Osada, Y. *J Mater Sci Mater Med* **2008**, *19*, 1379.

(69) Bae, K. H.; Wang, L.-S.; Kurisawa, M. *Journal of Materials Chemistry B* **2013**, *1*, 5371.

(70) Gehrke, S. H.; Uhden, L. H.; McBride, J. F. *Journal of Controlled Release* **1998**, *55*, 21.

(71) Chen, P.; Wang, X.; Wang, G. Y.; Duo, Y. R.; Zhang, X. Y.; Hu, X. H.; Zhang, X. J. *Materials Technology* **2014**, *29*, 210.

(72) Kato, M.; Shoda, N.; Yamamoto, T.; Shiratori, R.; Toyo′oka, T. *Analyst* **2009**, *134*, 577.

(73) Luo, R.; Cao, Y.; Shi, P.; Chen, C.-H. *Small* **2014**, *10*, 4886.

(74) Murosaki, T.; Ahmed, N.; Gong, J. P. *Sci Technol Adv Mat* **2011**, *12*.

(75) Liang, S.; Yu, Q. M.; Yin, H.; Wu, Z. L.; Kurokawa, T.; Gong, J. P. *Chemical Communications* **2009**, 7518.

(76) Dai, T.; Qing, X.; Lu, Y.; Xia, Y. *Polymer* **2009**, *50*, 5236.

(77) Dai, T.; Qing, X.; Zhou, H.; Shen, C.; Wang, J.; Lu, Y. *Synthetic Metals* **2010**, *160*, 791.

Scope and Objectives

Chapter – II

In the second chapter, we have discussed the scope and objective of thesis work.

Hydrogels have attracted immense interest in the last few decades due to their ability to mimic the visco-elastic properties of hydrated extracellular matrix (ECM), transport feasibility by diffusion, accommodating soluble active pharmaceutical agents (API) or biological molecules, etc[1]. Affinity of hydrogels towards cells and biological systems can be further enhanced by designing hydrogels from natural macromolecules such as polysaccharides, polypeptides, polymers from protein origin, etc[2]. However, hydrogels derived from polysaccharides and other natural resources lacks the mechanical integrity (modulus $\leq 10^3$ Pa) compared to their synthetic counterpart (modulus $\approx 10^4$ Pa), which restricts their applications in the biomedical field. Recently, a few new concepts such as nano-composite hydrogels[3], slide-ring hydrogels[4], tetra-PEG hydrogels[5], double network (DN) hydrogels[6], etc have been evolved to enhance the mechanical properties of hydrogels.

Polysaccharides, originated from renewable sources, apart from economical advantages over synthetic polymers also possess low toxicity and biocompatibility[7]. A wide variety of polysaccharides are available with specific physico-chemical characteristics. There are some other polysaccharides which are not yet fully explored. One such polysaccharide is xyloglucan (XG), which is non-ionic, neutral, branched polysaccharide, derived from the seeds of the tree *Tamarindus indica*[8-12]. It contains glucose, xylose, and galactose units in the ratio ~ 3:2:1[13-14]. Currently it is used in food and textile industry as a thickening and stabilizing agent. Developing hydrogels from biomimetic resources such as XG, using mild chemical reactions can contribute towards value-addition to such under-utilized resources and such hydrogels can find applications in designing bio-medical devices and implants.

Conventional drug delivery systems often lead to high dosages or repeated administration which reduces its efficacy and patient compliance. In this scenario, controlled drug delivery systems (CDDS) have emerged as a path-breaking solutions, where membranes, liposomes, hydrogels, etc are utilized to design systems which can control the availability of drugs to cells and tissues over time and in space[15]. Hydrogels are also widely used to design CDDS's in all major braches of medicine due to their flexibility to tune cross-link density, permeability, hydrophilicity and inherent excellent biocompatibility. New scientific concepts such as rate pre-programmed delivery, activation modulated delivery and feedback regulated delivery has revolutionalized the CDDS platforms[16]. Such new platforms aim to provide

prolonged and sustainable DDS's to address various challenging issues such as chronic wounds, hormone imbalance, angiopathy, etc[17-19]. XG based DN hydrogel systems; with drug incorporated micro-reservoirs could be employed as a promising solution to design such novel platform for prolonged drug delivery.

Hydrogels based scaffolds have many different functions or roles in the field of tissue engineering and regenerative medicine. They could be applied as space filling agents, three-dimensional structures to organize cells, delivery vehicle for growth factor and drugs, engineering tissue replacements, etc[20-21]. Naturally derived polymers such as polysaccharides are widely utilized in tissue engineering applications due to their macro-molecular properties similar to the natural ECM and their favorable interactions in vivo. However, hydrogels employed as tissue replacements has to overcome the fatigue and stress components experienced at the implant site for a better patient compliance. To enable hydrogels to address such challenges new network designs with improved mechanical properties along with energy dissipating functional moieties need to be evolved. Hence, designing DN hydrogels from a widely available polysaccharide such as carboxymethyl cellulose (CMC), with synthetic moieties such as hydrophobic domains, could provide a promising candidate to address this challenge.

To address the mechanical weakness of hydrogels used in biomedical applications a plethora of new methodologies are adopted. One important strategy among them is autonomous self-healing hydrogels. Self-healing is an inherent property which enables a hydrogel intrinsically and automatically heals damages induced by external deformation, restoring itself back to normalcy[22]. In the case of self-healing hydrogels comprising of two or more polymer networks, presence of reversible non-covalent interactions in all the polymer networks enhance the overall healing efficiency and time of the resultant hydrogel systems. However, healing efficacy and time reduces drastically (< 100%) if only one network possess reversible functional moieties[23]. In bio-simulated medium such as polysaccharide-derived DN hydrogels, self-healing phenomena equips them to promote artificial bio-mineralization, which can enhance the growth or formation of mineralized hard tissues such as bone, cartilage, enamel, etc[24]. This methodology has a far reaching potential to develop value-added solutions for regenerative medicine.

The objectives of the thesis are:

- To design a hydrogel from XG with mild cross-linking strategy and utilize these hydrogels to develop value-added medical devices such as composite microelectrode for applications in neural interface
- To develop a DN hydrogel using XG with robust mechanical properties and to design a micro-reservoir based CDDS for the sustained delivery of a model drug such as curcumin
- To design a DN hydrogel for tissue replacement using CMC, which can impart efficient energy dissipation capabilities to sustain mechanical deformation as well as stress at the implant site
- To design a self-healing DN hydrogel based on alginate and to utilize these DN hydrogels for promoting artificial bio-mineralization process which can enable them for applications in the regeneration of hard-tissues.

References

(1) Patterson, J.; Martino, M. M.; Hubbell, J. A. *Mater Today* **2010**, *13*, 14.

(2) Mano, J. F.; Silva, G. A.; Azevedo, H. S.; Malafaya, P. B.; Sousa, R. A.; Silva, S. S.; Boesel, L. F.; Oliveira, J. M.; Santos, T. C.; Marques, A. P.; Neves, N. M.; Reis, R. L. *J R Soc Interface* **2007**, *4*, 999.

(3) Haraguchi, K.; Takehisa, T. *Adv Mater* **2002**, *14*, 1120.

(4) Karino, T.; Okumura, Y.; Ito, K.; Shibayama, M. *Macromolecules* **2004**, *37*, 6177.

(5) Sakai, T.; Matsunaga, T.; Yamamoto, Y.; Ito, C.; Yoshida, R.; Suzuki, S.; Sasaki, N.; Shibayama, M.; Chung, U. I. *Macromolecules* **2008**, *41*, 5379.

(6) Gong, J. P.; Katsuyama, Y.; Kurokawa, T.; Osada, Y. *Adv Mater* **2003**, *15*, 1155.

(7) Van Vlierberghe, S.; Dubruel, P.; Schacht, E. *Biomacromolecules* **2011**, *12*, 1387.

(8) Lang, P.; Burchard, W. *Makromol Chem* **1993**, *194*, 3157.

(9) Lang, P.; Masci, G.; Dentini, M.; Crescenzi, V.; Cooke, D.; Gidley, M. J.; Fanutti, C.; Reid, J. S. G. *Carbohyd Polym* **1992**, *17*, 185.

(10) Gidley, M. J.; Lillford, P. J.; Rowlands, D. W.; Lang, P.; Dentini, M.; Crescenzi, V.; Edwards, M.; Fanutti, C.; Reid, J. S. G. *Carbohyd Res* **1991**, *214*, 299.

(11) Khan, N. A.; Mukherjee, B. D. *Chem Ind-London* **1959**, 1413.

(12) Savur, G. R.; Sreenivasan, A. *J Biol Chem* **1948**, *172*, 501.

(13) Srivastava, H. C.; Singh, P. P. *Carbohyd Res* **1967**, *4*, 326.

(14) White, E. V.; Rao, P. S. *Journal of the American Chemical Society* **1953**, *75*, 2617.

(15) Li, J.; Mooney, D. J. **2016**, *1*, 16071.

(16) Chien, Y. *Novel Drug Delivery Systems*; 2 ed.; CRC Press: Boca Raton, 1991.

(17) Chien, Y. W. In *Methods in Enzymology*; Academic Press: 1985; Vol. 112, p 461.

(18) Chien, Y. W. In *Recent Advances in Drug Delivery Systems*; Anderson, J. M., Kim, S. W., Eds.; Springer US: Boston, MA, 1984, p 367.

(19) Chien, Y. W.; Cabana, B. E.; Mares, S. E. *Novel drug delivery systems : fundamentals, developmental concepts, biomedical assessments*; Dekker: New York, 1982.

(20) Drury, J. L.; Mooney, D. J. *Biomaterials* **2003**, *24*, 4337.

(21) Lee, K. Y.; Mooney, D. J. *Chemical Reviews* **2001**, *101*, 1869.

(22) Taylor, D. L.; in het Panhuis, M. *Adv Mater* **2016**, *28*, 9060.

(23) Wang, W.; Narain, R.; Zeng, H. *Frontiers in Chemistry* **2018**, *6*.

(24) Asenath-Smith, E.; Li, H.; Keene, E. C.; Seh, Z. W.; Estroff, L. A. *Adv Funct Mater* **2012**, *22*, 2891.

Polysaccharide hydrogel incorporated carbon nanofiber microelectrode for designing neural interfaces

Chapter – III

In the third chapter, we report on the design and synthesis of new microelectrodes, comprising of carbon nano-fiber (CNF) and carboxymethyl xyloglucan (CMX) hydrogel, which enhanced the current density across the interface of artificial prosthesis and human neural system. Microelectrode was prepared by in-situ cross-linking of CMX inside CNF, with optimized CMX: CNF ratio, resulting in continuous ionic channels confined within the hollow core of CNF. The electrochemical studies indicated the enhancement in charge density as well as the active surface area of the microelectrodes upon incorporation of CMX hydrogel network.

Arun Torris and Manohar V. Badiger, *Polysaccharide Hydrogel Incorporated Carbon Nanofiber Microelectrode for Designing Neural Interfaces*,
Journal of Bionic Engineering, 16 (4), 696 - 710 (2019).

3.1 Introduction

Medical bionic devices such as pacemakers and bionic cochlear implants were one of the first successful implants in humans[1]. Development of bionic medical devices is strongly dependent on successfully connecting the device to cellular tissue. In this context, implantable neural microelectrodes have become extremely important, and the electrode materials that facilitate interaction with living cells are crucial for the development of next-generation bionic devices. The emergence of organic polymer conductors is contributing to achieving this success[1]. It is also critical that the materials need to be biodegradable and bio-absorbable with appropriate function and lifetime profiles in developing implants for peripheral nerve or spinal cord repair[1].

Neural interfaces have been evolved over a period of time, mostly in the design of microelectrodes for the efficient transduction of signals. The first generation microelectrodes comprised of an assembly of a substrate coated metal wires namely, micro-wire electrodes, where conducting polymers such as PEDOT:PSS, PPy, PEDOT nanotubes, etc., were coated onto metallic micro-wires made up of silicon[2-3], iridium oxide[4], etc. These intra-cortical implant records neural signals with a higher degree of signal-to-noise ratio and were used for both recording and stimulation. For the prolonged recording of neural signals and to restore the independence of humans with paralysis, microelectrode arrays were developed by the precise micro-fabrication process[5-6]. These devices consists of multiple electrodes of Pt[7], Cr[8], Au, etc, coated with parylene or polyimide[9] and help to attain two-way exchange of signals with nervous system as well as electrical stimulation. However, microelectrode arrays invoke mechanical mismatch and enhanced tissue response at the interface, which leads to major inflammatory response along with higher glial activation around the electrodes. To address this issue, Kozai et al developed new generation soft bio-compatible composite microelectrodes[10-12] which consisted of carbon core coated with conducting polymers and bioactive motifs. These flexible and soft composite systems were engineered to match the modulus of tissues at the site of implantation, regulated the tissue response and enhanced the performance and life-span of neural interfaces[13].

It can be realized that nano-structuring of electrodes based on inert materials improves the performance by reducing impedance and influencing cell compatibility. Nano-

structured carbons provide an inherently electrochemically stable organic interface[1]. Mattson et al. reported carbon nano tube (CNT) as a substrate for neuronal growth[14] and biocompatibility of CNTs as a substrate for neurons was established. CNTs could potentially be used for neural prosthesis. Although CNTs are not biodegradable, they could be used as implants where long term extracellular molecular cues for neurite outgrowth are necessary, such as in regeneration after spinal cord or brain injury. CNTs can also be used to determine the behaviour of neural networks in vitro, an essential step for the design of synthetic biomaterials. Increase in efficiency of neural signal transmission may be related to specific properties of CNT materials, such as the high electrical conductivity[15-16]. CNTs provide safer and efficient solutions for neural prosthesis than metal electrodes. Wang et al. fabricated a new neural interface using vertically aligned multi-walled carbon nano tube (MWCNT) pillars as micro electrodes[15]**.** The surface charge of MWCNTs was used to control the neurite outgrowth as characterized by the presence of more numerous growth cones, longer average neurite length, and elaborate neurite branching[14].

In this study, we report on the design of a microelectrode based on a polysaccharide namely, carboxymethyl xyloglucan (CMX) and carbon nano fiber (CNF), which shows better current density, enhanced biological response. CMX is a biocompatible, biodegradable and ionic biopolymer which is more suitable for making biomedical devices and implants. To the best of our knowledge, this could be the first report on the *in-situ* CMX hydrogel formation inside the CNF to prepare a microelectrode. Gelation process, swelling characteristic and mechanical behaviour of these hydrogels were studied. Microelectrodes were examined for the electrochemical properties to evaluate the current density across the neural interface. Further, cytotoxicity studies were performed to know the feasibility of these systems for applications in the neural interface.

3.2 Materials and methods

3.2.1 Materials

Carboxymethyl tamarind kernel powder was procured from Dabur India Ltd., and purified by washing with acetone, filtered, dissolved in water, centrifuged, dialysed and finally freeze-dried to obtain white coloured cotton-like soft carboxymethyl

xyloglucan (CMX). Divinyl sulphone was obtained from Sigma-Aldrich India Ltd. Sodium hydroxide and acetone were procured from Merck India Ltd. Carbon nano fiber (CNF) was procured from Global Nanotech Pvt. Ltd., India. All reagents were used as received. Distilled water was used for all the experiments unless specified otherwise.

3.2.2 Gel permeation chromatography (GPC) and NMR analysis of CMX

The molecular weight of purified CMX was measured using gel permeation chromatography (Agilent Technologies) with RI detector. 0.2 M $NaNO_3$ was used as the mobile phase with 0.3 ml/min as flow rate, and pullulan was taken as the reference standard. 20 µl of the polymer solution was injected in triplicate. 10mg of pure lyophilized CMX was transferred to NMR vial, dissolved in ~1.5 ml D_2O overnight and ^{1}H NMR spectra were acquired using Bruker 400 MHz spectrometer comprising of 500 scans at $22^{0}C$. The ^{13}C spectrum was recorded at room temperature.

3.2.3 Preparation of CMX hydrogels

A stock solution of CMX was prepared in 50ml closed cylindrical glass vial by adding 0.75 gm of CMX in 30 ml of distilled water, to obtain 2.5 wt-% concentrations. The dissolution was carried out overnight by putting glass vial on a roller mixer rotating at 25 RPM which ensured homogenous solution of CMX.

To a 2ml of CMX stock solution, 2 to 3 drops of 1 M NaOH solution was added to increase the pH up to 12 followed by 1.8 ml (0.18 ml DVS/gm of polymer) of 0.1 N DVS solution and kept at $15^{0}C$ overnight for 24 hours to obtain CMX hydrogels. The hydrogel was washed thrice with distilled water at $15^{0}C$ to remove any residual DVS and stored under refrigeration.

3.2.4 Gelation time and swelling studies

A rheometer (Model 301, Anton Paar, Austria) equipped with cup and bob geometry was used to measure the time required for the gelation of CMX hydrogels cross-linked by DVS. About 4 ml of CMX aqueous solution was charged onto the cup, 8 wt % DVS as added, stirred for 2 minutes. Time sweep measurements were performed at constant strain, frequency and temperature (15^{0} C) within the linear visco-elastic regime. Storage modulus (G') and loss modulus (G") were measured as a function of

time until the gelation of CMX. The swelling behaviour of CMX hydrogels at 25^0C in distilled water was studied by monitoring the water uptake as a function of time and histogram of the swelling ratio (Q) was plotted following the equation:

$$Swelling\ Ratio, (Q) = \frac{W_s - W_d}{W_d} \quad \text{---------- (1)}$$

where, W_s is the mass of hydrogel at time t, and W_d is the mass of xerogel.

3.2.5 Compressive strength and modulus of CMX hydrogels

3.2.5.1 Compressive strength of as-prepared hydrogels

Mechanical behaviour of as-prepared CMX hydrogels was studied using uni-axial compression experiments. CMX hydrogels with 3 different degrees of crosslinking (having DVS concentrations viz. 8, 10 and 12 wt-%) were prepared and punched out into a cylindrical shape with 1:1 aspect ratio (height and diameter). The experiments were done using dynamic mechanical analyser (Model RSA3, TA Instruments USA).

3.2.5.2 Compressive strength of equilibrium swollen hydrogels

Mechanical behaviour of equilibrium swollen CMX hydrogels was studied using uni-axial compression experiments. CMX hydrogels with 3 different degrees of crosslinking (having DVS concentrations viz. 8, 10 and 12 wt-%) were prepared, swollen to equilibirum in DI water and punched out into a cylindrical shape with 1:1 aspect ratio (height and diameter). The experiments were done using dynamic mechanical analyser (Model RSA3, TA Instruments USA).

3.2.6 Preparation of microelectrodes

For preparing micro electrodes, 0.5 mL of CMX solution (4wt-%) was mixed with 60 mg of carbon nano fiber (CNF) under sonication for 10 minutes and kept for stirring overnight (12 hrs) to effect the penetration of CMX into the hollow core of CNFs. Later, DVS solution (0.2 mL of 15-% aq. solution) was added to the mixture to facilitate the cross-linking of CMX at 15^0C for 24 hours. During this process, the pH of the solution was maintained at 12. Finally, the mixture was washed with an excess of distilled water to remove any un-reacted DVS residues, filtered and dried in an oven at 50^0C for 4 hours. The microelectrodes prepared with 0.5 mL of CMX solution was abbreviated as CMX-CNF ME 1 and while those prepared with 1.0 mL & 1.5 mL

CMX solutions were abbreviated as CMX-CNF ME 2 and CMX-CNF ME 3, respectively.

3.2.7 Electron microscopy and electrochemical studies

For SEM analysis, electrodes were placed on carbon tapes before imaging acquisition. Quanta 3D^{TM} scanning electron microscope (FEI, Oregon, USA) was used to analyze the structure and morphology of micro electrodes. For TEM imaging, electrodes were dispersed in isopropyl alcohol with moderate stirring for 4 hours, loaded onto holey carbon grids using micro-pipette and imaged using Tecnai T20^{TM} transmission electron microscope (FEI, Oregon, USA).

Electrochemical studies were performed using potentiostat (Model Autolab PGSTAT30, Metrohm AG, Netherlands) equipped with conventional three-electrode test cell consisting of SCE and platinum foil as a reference electrode and the counter electrode, respectively. A glassy carbon (GC) electrode for the working electrode was polished using 0.3 and 0.05 µm alumina slurries, followed by washing with water and acetone. A slurry was prepared by sonicating 1 mg of CMX-CNF ME 2 with 1 mL isopropyl alcohol and 10 µL aliquote of the slurry was drop coated onto glassy carbon electrode to prepare the working electrode. Later, 2 µL of 0.01 wt% Nafion diluted with ethanol was coated on the surface of CMX-CNF ME 2 layer to obtain a uniform thin film. The electrode was dried in air and used as a working electrode for electrochemical sutides. Similarly, pristine CNF was also coated on to the GC electrode to prepare another working electrode using the protocol described above. Linear voltage sweep was performed using a rotating disk electrode (RDE) to study oxygen reduction reaction (ORR) in oxygen saturated perchloric acid at 1600 RPM and 5 mV/s scan rate.

3.2.8 Cytotoxicity studies

CMX xerogels, micro-electrodes and CNFs were soaked in 70% ethanol/water mixture overnight and dried in vacuum oven followed by 30 minutes UV exposure inside a biosafety cabinet. CMX xerogels, microelectrodes and CNFs were again soaked in sterile PBS before use in a 24 well plate. Healthy L929 fibroblast cell lines (passage number 58) were maintained using complete DMEM. 50,000 cells suspended in 500 µL complete media were plated in each well along with the soaked

xerogels, electrodes and CNFs in triplicates. It was incubated in 5% CO_2 at 37°C for 2 days. 100 µL of 600 µM resazurin solution in DMEM media was added to each well followed by 6 hours incubation in 5% CO_2 at 37°C. The entire plate was read in a plate reader (excitation 530 to 560 nm and emission at 590 nm). For calculating the cell viability, emission due to 100 µM resazurin in DMEM was incorporated, normalized with negative control (only cells) and incorporated with standard error.

3.3 Results and discussion

3.3.1 Chemical structure of carboxymethyl xyloglucan (CMX)

Tamarind kernel powder (TKP) is derived from the seeds (from fruits) of the tree *Tamarindus indica* (**Fig 3.1a-c**). The seed kernel contains around 65 % of Xyloglucan (XG) which is composed of a non-ionic, neutral, branched polysaccharide in which glucose, xylose and galactose units are present in the ratio ~ 3:2:1[17-18]. It is a biodegradable, biocompatible, non-toxic and edible polysaccharide. There are numerous applications of xyloglucan from thickening, gelling and stabilizing agents in food, to sizing and weaving in textiles, to adhesive and binding agents in the industry.

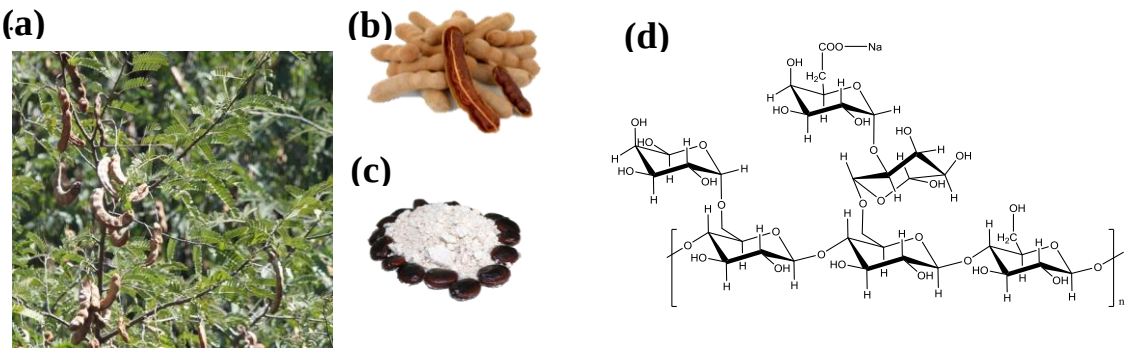

Figure 3.1: (a) Tamarind tree, (b) tamarind fruits, (c) tamarind seeds and TKP, the (d) chemical structure of sodium salt of carboxymethyl xyloglucan (CMX)

Xyloglucan is a neutral polysaccharide with low molecular weight compared to many other polysaccharides and forms a hydrogel at high concentrations. A high water holding capacity with good stability to heat, acids and shear are some unique properties of this particular polysaccharide. The stability of XG to heat and mild acids and bases can be attributed to the high degree of substitution of the backbone, which, to some extent, shields it from hydrolyzing agents. The food industry widely uses XG to improve the rheological and thermal properties of many products. The solubility of

XG in cold water is moderately inhibited by its galactose side chain. Hence, efforts have been made for partial removal of galactose side chains using β-galactosidase[19-20]. Another route towards making enhanced solubility is the carboxymethylation of XG (CMX). Chemical structure of the sodium salt of CMX is given in **fig 3.1d**. The commercial CMX was purified to remove components which are soluble in organic solvents and were dialyzed to remove oligomers. The molecular weight and the polydispersity of CMX were determined by Gel Permeation Chromatography (GPC) and found to be M_n= 1.2 x10^6 g/mol, M_w = 2.3 x10^6 g/mol and PDI = 1.9.

NMR spectroscopy is one of the most important tools to investigate the chemical structure and properties of polysaccharides. In CMX, the presence of a large number of protons in the vicinity of glucose backbone overlaps to a greater extent resulting in a broader NMR spectrum. To resolve the signals from glucose backbone, these protons are partially substituted with deuterium by four repeated lyophilisation cycles of CMX in D_2O. The resulting ^{1}H NMR spectrum is shown in **fig 3.2**. The ^{1}H NMR spectrum shows cumulative signals from the equatorial as well as axial protons from glucose backbone, xylose and galactose residues. The anomeric protons nearer to the glycosidic oxygen linkages appear at 5.10 ppm, and the signal from HOD is observed at 4.71 ppm. The signal from the proton involved in the β 1-4 linkage is seen at 4.49 ppm. The signals from protons coming from H-2 to H-6 appear around 3.6 ppm.

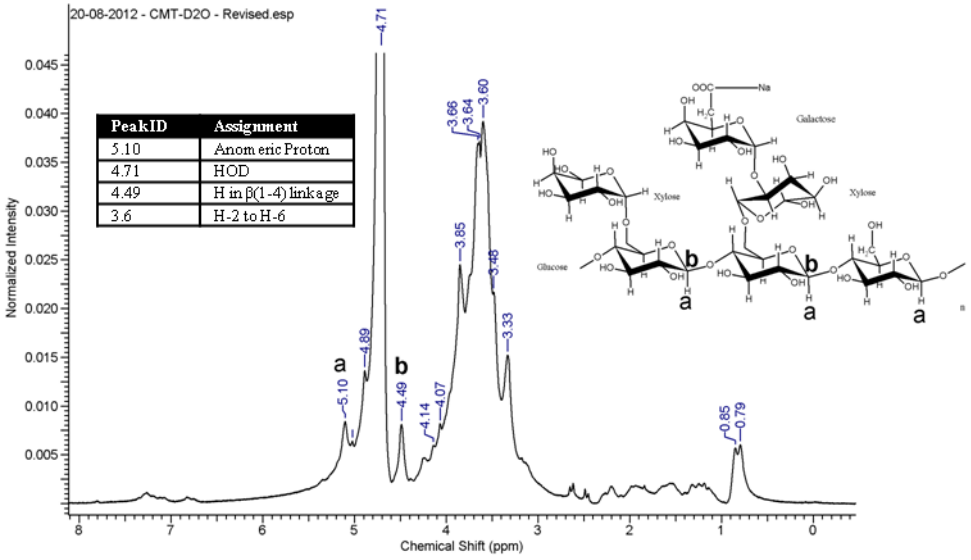

Figure 3.2: ^{1}H NMR spectra of CMX

The ^{13}C spectrum of CMX is also shown in **fig 3.3**. Carboxyl groups show a characteristic peak at 178 ppm whereas, the carbon attached to the primary alcohol group shows a peak at around 61 ppm. Anomeric carbon at the β 1-4 linkage between glucosidic groups is observed at 100 ppm, while the carbon atom at α 1-2 linkage between glucose and xylose was observed at 68 ppm. In the ^{13}C spectrum, the peaks corresponding to the carboxyl carbon and anomeric carbon were well resolved. The analysis from ^{1}H NMR and ^{13}C NMR confirms the chemical structure and purity of CMX.

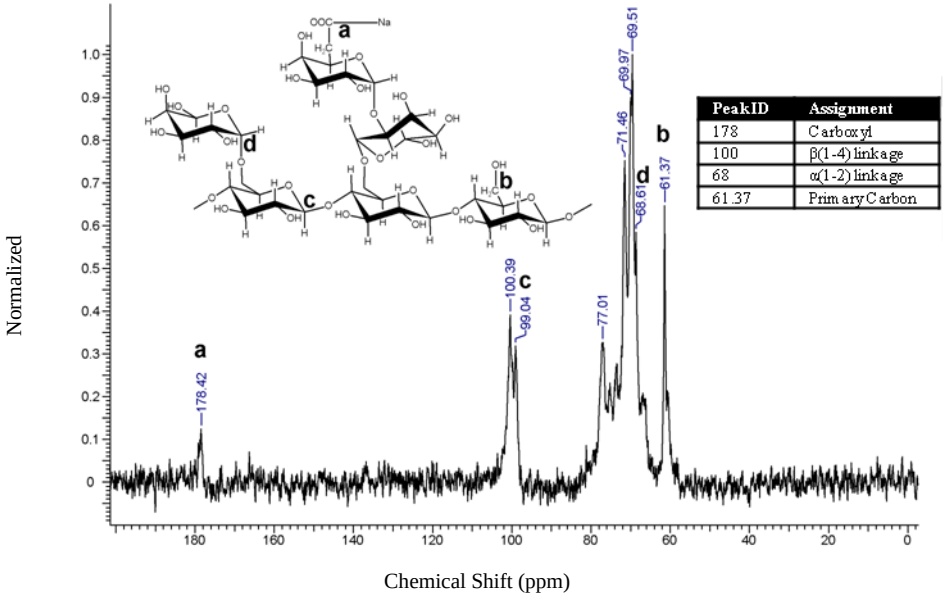

Figure 3.3: ^{13}C NMR spectra of CMX

3.3.2 CMX hydrogels

The CMX hydrogels were prepared by Michael-type addition reaction between purified CMX and divinyl sulphone (DVS) (cross-linker), in the presence of a base (pH 12), resulting in the formation of a cross-linked polymer network, as shown in **fig 3.4a**. At lower DVS concentration (< 8 wt-%), only the viscous solution was formed which may be attributed to insufficient cross-link formation. DVS concentration in the range of 8 to 12 wt-% results in the formation of stable and robust CMX hydrogels after equilibrium swelling. However, concentrations above 12 wt-% lead to very fragile as well as brittle hydrogels at equilibrium.

The rapid gelation was observed at higher DVS concentration (>12 wt-%) with the observed heterogeneity in the cross-linking of the hydrogel. In the gelation mechanism of Michael-type addition, a base-catalyzed reaction between a nucleophile

(Michael donor) and an electrophile (Michael acceptor), resulting in a 'Michael adduct'[21-22], is proposed as shown in **fig 3.4b**. Primary alcohol in CMX acts as nucleophilic Michael donor, and DVS plays the role of electron withdrawing Michael acceptor, catalyzed by the presence of NaOH.

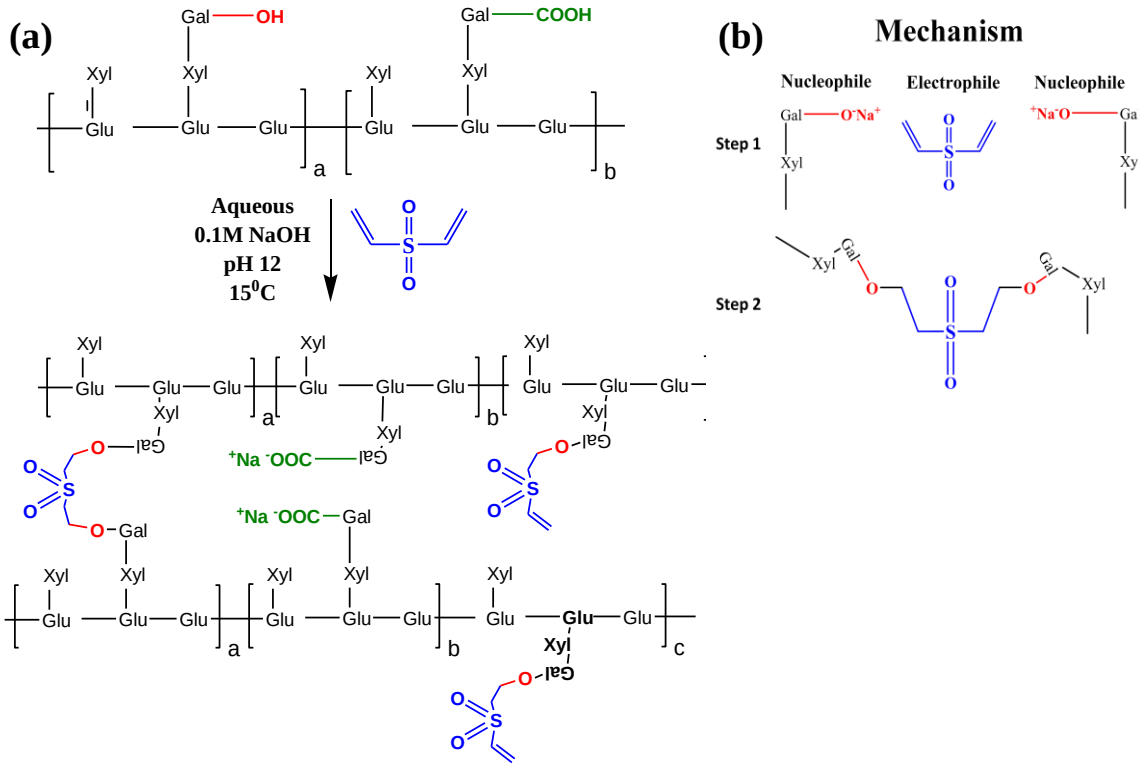

Figure 3.4: (a) Reaction pathway for cross-linking CMX using DVS and (b) mechanism of the cross-linking reaction of CMX with DVS

3.3.3 Gelation and swelling characteristics of CMX hydrogels

Generally, during the cross-linking reaction in polymers, elastic characteristics of polymer solutions gradually increase over and above its viscous counterpart, due to the formation of cross-links between the polymer chains (**fig 3.5**). During the initial stage of the measurement (before 15 mins), G" dominates over G', which indicates the viscous nature of the solution. Gradually, with an increase in time, G' slowly increase, crosses over G" after 15 mins and progressively increases further. This observation shows that gelation takes place in 15 mins after the addition of cross-linker in CMX solution and the modulus of the resultant hydrogels gradually increases further.

Rheological measurements were performed to study the time required for the gelation/formation of CMX hydrogel, cross-linked by DVS. Cross-linker was added to CMX solution and loaded on to Rheometer to study the change in visco-elastic characteristics of the solution. Results are shown in **fig 3.5**, where storage modulus (G') and loss modulus (G") are plotted as a function of time. Storage and loss modulus represents the elastic and viscous response from the solution, respectively.

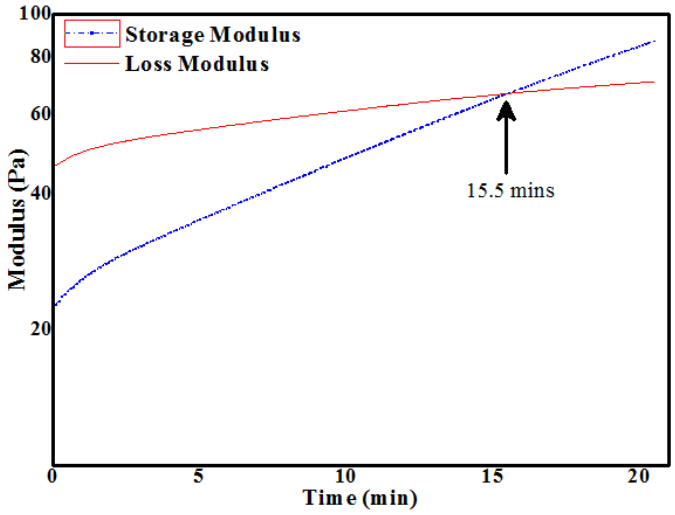

Figure 3.5: Storage modulus (G') versus loss modulus (G") plot of CMX solution containing cross-linker at 15 ^{0}C

The swelling profile of CMX hydrogel with 8 wt-% DVS is given in **fig 3.6a**. Abrupt uptake of water is observed in the initial 20 hours of swelling, after that, a slow gradual increase is observed up to 180 hours. CMX hydrogels with 8, 10 and 12 wt-% DVS has a swelling ratio of 235, 150 and 77 at equilibrium swelling (**fig 3.6b)**. Reduction in the swelling ratio is inversely proportional to the cross-linker concentration.

As shown in **fig 3.6a**, CMX hydrogel with 8 wt-% DVS has attained equilibrium swelling within 24 hours. Thereafter, the increase in swelling is marginal. The equilibrium swollen hydrogel has swelling ratio three times its dry mass. The equilibrium swelling of the hydrogels strongly depend on the degree of crosslinking and the kinetics of the hydrogel swelling depends on the particle size, porosity, hydrophilicity etc. of the hydrogel.

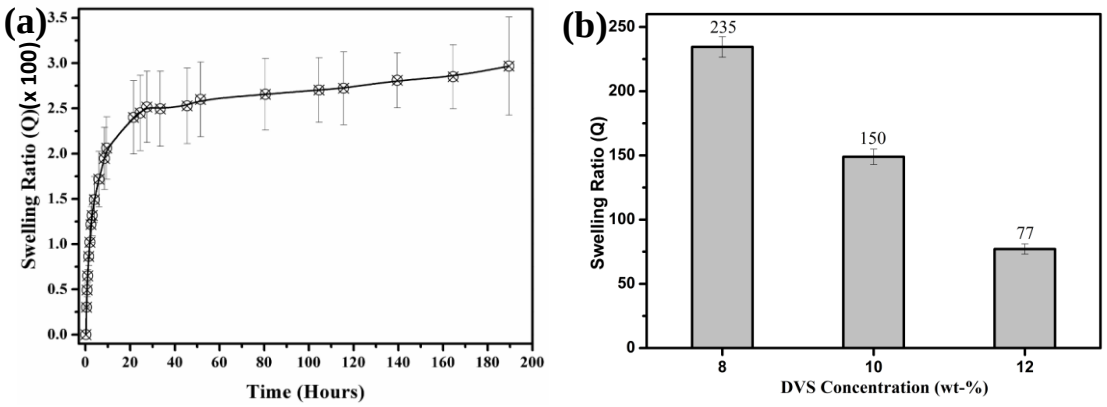

Figure 3.6: (a) Swelling profile of CMX hydrogel cross-linked with 8 wt-% DVS with respect to time and (b) equilibrium swelling ratio of CMX hydrogels with 8, 10 and 12 wt-% DVS

With the increase in cross-linker concentration from 8 to 10 wt-% (**fig 3.6b**), approximately 40% reduction in the swelling ratio is observed. Similarly, approximately 50% reduction is observed in the case of 10 to 12 wt-% concentration. This indicates the formation of higher cross-linking and lower water content with an increase in cross-linker concentration.

3.3.4 Mechanical behaviour of CMX hydrogels

Mechanical properties of hydrogels play a key role in their load-bearing applications. In general, the strength and flexibility of the hydrogel network depend largely on the cross-link density and can be studied by measuring the compressive strength of the hydrogels in the as-prepared state or equilibrium swollen state. The mechanical strength of the hydrogel also strongly depends on the quantity of water present in the hydrogel. Therefore, the studies of mechanical behaviour in equilibrium swollen hydrogels are biased by the volume of water present in it. Hence we have performed the mechanical studies of both as-prepared and equilibrium swollen hydrogels to examine the role of cross-linker concentration and water content on the hydrogel network. Moreover, depending on the water content in the hydrogel, soft and flexible devices are preferred for applications as neural interfaces, since stiff and hard systems evoke undesirable biological responses[23].

3.3.4.1 Compressive strength of as-prepared hydrogels

Mechanical behaviour of as prepared CMX hydrogels was studied using uni-axial compression experiments. CMX hydrogels with 3 different DVS concentrations viz. 8, 10 and 12 wt-% were examined for compressive strength (**fig 3.7a**). During uni-axial compression experiments, cylindrical hydrogel specimens undergo an increase in radial volume, hence true stress is calculated inspite of nominal stress to address the same. **Table 3.1** shows the compressive strength and maximum strain of the as-prepared hydrogels during the compression. CMX hydrogels with 8 wt-% DVS showed 91% strain before failure as compared to 89.9 and 80.2 % strain for 10 and 12 wt-% DVS cross-linked hydrogels. At the same time, the compressive strength of the as-prepared hydrogels showed a gradual increase from 10 to 30 kPa with the increase in cross-linker concentration from 8 to 12 wt-%.

Table 3.1: Mechanical properties of CMX hydrogels with various cross-linker concentration

DVS Conc. (wt-%)	**Compressive Strength (kPa)**		**Strain at Break (%)**		**Elastic Modulus (kPa)**
	as-prepared	at equilibrium	as-prepared	at equilibrium	at equilibrium
8	10	6.2	91.0	39.6	5.3
10	22	7.5	89.9	37.7	7.8
12	30	11.4	80.2	37.9	12.5

3.3.4.2 Compressive strength of equilibrium swollen hydrogels

Stress vs strain graph of the equilibrium swollen CMX hydrogels are shown in **fig 3.7b** and the results are shown in **table 3.1**. CMX hydrogels with 8, 10 and 12 wt-% DVS content show compressive strength of 11.4, 7.5 and 6.2 kPa respectively. Compressive failure occurred within 40 % strain (i.e., $\lambda < 0.6$). True stress vs strain is plotted in **fig 3.7a**, where all the samples show linear deformation during the initial strain values (i.e., from 0 to 70 % strain). After 70% strain (i.e., $\lambda = 0.3$), stress hardening is observed and is consistent with the increase in cross-linker wt-%. The inset of the graph shows the variation in mechanical behaviour during the initial stages of the strain, where the hydrogels with higher cross-linker concentration show

more mechanical resistance compared to others (**Table 3.1**). This behaviour corresponds to mechanical resistance against forcefull deformation, offered by cross-link points in the hydrogel network, against the applied force and the magnitude of resistance depends on the cross-link density of the network[21].

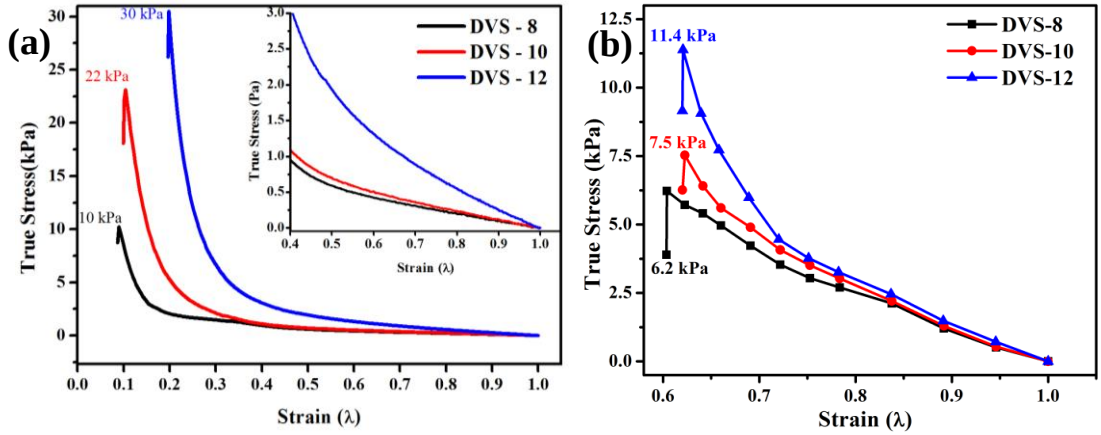

Figure 3.7: Uni-axial compression of (a) as-prepared and (b) equilibrium swollen CMX hydrogels with varying DVS content

As shown in **fig 3.6b**, the amount of water uptake during the swelling of as-prepared hydrogels decreases with increase in cross-linker concentration. During the swelling process, polymer network imbibes water due to its hydrophilic nature and polymer chains between the cross-link points expands to a greater extent. At this stage, polymer chains in the swollen hydrogel network is already in a pre-stretched stage and experience a stress induced by the swelling process. Hence during compression, the equilibrium swollen hydrogel is unable to resist the compressive force to the same degree as exhibited by as-prepared hydrogels (**fig 3.7a**). However, the resistance to compressive force increases with a higher cross-linker concentration in equilibrium swollen hydrogels also.

In short, these studies show that CMX hydrogels exhibit good mechanical strength and modulus compared to some of the hydrogels reported earlier[24]. Hubbell et al. have reported the synthesis of hydrogels using Michael-addition reaction for biomedical applications[25-27], where PEG-co-protein hydrogels were synthesised which possess a modulus of the order of 1 to 3 kPa[25]. Cellulose ethers based hydrogels prepared by Anbergen et al. through Michael-addition route possess a modulus in the range of 0.4

to 1 kPa[28]. Soft and flexible hydrogels can be designed by selecting the optimum cross-linker concentration which is necessary for evoking a better biological response in designing neural interfaces[10].

3.3.5 Preparation of microelectrodes and their microscopic studies

CMX hydrogels possess a higher amount of bound water and ionic conductivity due to the presence of ionic carboxylic groups in the repeating unit. These properties enable them to become a good candidate for the fabrication of ion-conducting channels which are highly desirable for various biomedical applications. One of the major applications of ion-conducting channels is in the development of prosthesis wherein ion-conducting channels called "*neural interfaces"* are required to establish dynamic contact between the electronic prosthesis and the amputated organ.

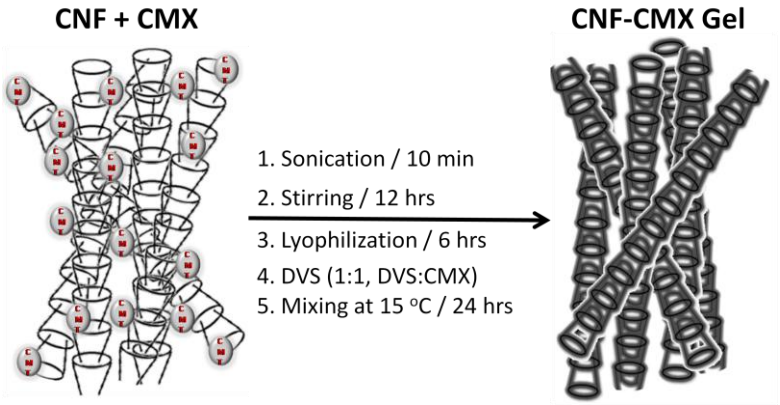

Figure 3.8: Schematic diagram showing the preparation of microelectrodes using CNF and CMX

Neural interfaces are "*communication bridges"* between the artificial electronic prosthesis and the central nervous system of the physically challenged personnel[10]. To act as a neural interface, CMX hydrogels need to be fabricated in the form of microelectrodes, which possess ionic conductivity, relative moisture and a conducting channel. Therefore, ion conducting channels in carbon nanofiber (CNF) were prepared using CMX hydrogels inside the hollow CNF as shown in **fig 3.8.**

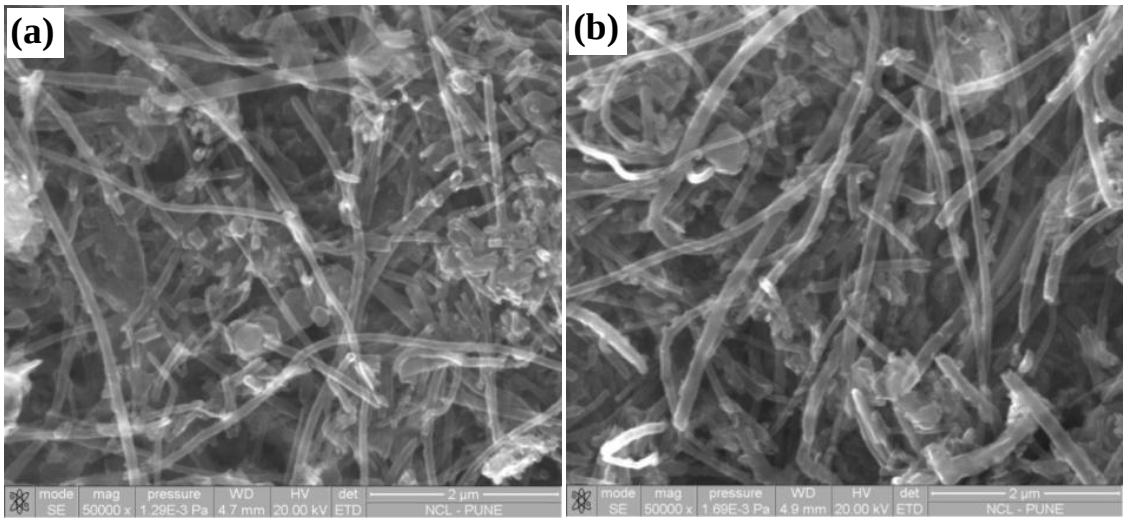

Figure 3.9: SEM images of (a) CMX-CNF ME 1 and (b) CMX-CNF ME 2 microelectrodes where CNFs are impregnated with CMX hydrogel in its hollow core. Scale bar is 2 microns

In the preparation of microelectrodes, the CMX in-situ gelation was effected in the hollow core of the CNF as depicted in **fig 3.8**. SEM images of CMX-CNF ME 1 and 2 are shown in **fig 3.9 a and b**, where microelectrodes are seen, oriented in various directions without any major distortions in their shape. SEM images also clearly show individual CNFs without any significant aggregates among them, which indicates the absence of CMX on their surface.

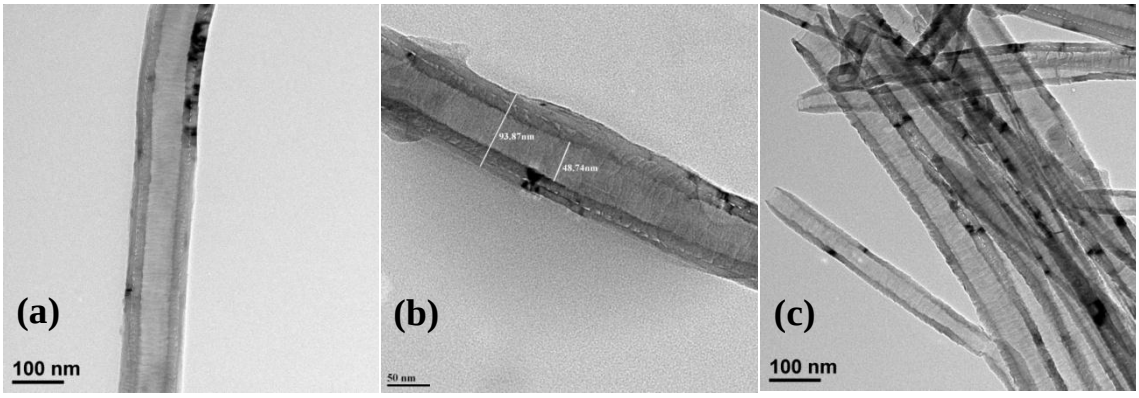

Figure 3.10: TEM images of (a) single pristine CNF with hollow core (scale bar is 100 nm), (b) single CNF with outer diameter (94 nm) and core diameter (49 nm) marked on it (scale bar is 50 nm) and (c) collection of CNFs with length higher than 1 micron (scale bar is 100 nm)

TEM image of a single pristine CNF is shown in **fig 3.10a**, where the nanofiber has a hollow core which is surrounded by a crystalline carbonaceous cylinder[29]. This '*stacked cup'* like morphology provides more exposed edge planes and facilitates intercalation of foreign moieties. CNF possess a typical external diameter of ~100 nm and internal hollow core of ~50 nm (**fig 3.10 b**), with length ranging from 50 to 100 microns (**fig 3.10 c**).

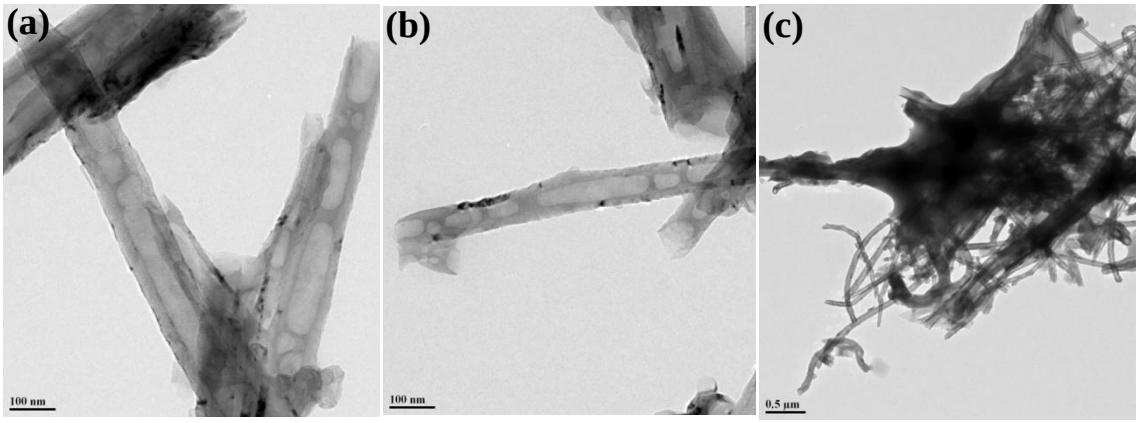

Fig. 3.11 TEM images of (a) and (b) CMX-CNF ME 1 shows partially filed CMX hydrogel inside hollow cores of CNFs (Scale bar is 100 nm). TEM image of (c) CMX-CNF ME 3 shows aggregated microelectrodes (Scale bar is 0.5 microns)

During the preparation of CMX-CNF ME 1, the hollow core of CNF seems to be partially filled with CMX hydrogel network, as seen in the TEM images shown in **fig 3.11**. The morphology of CMX-CNF ME 3 is quite different from its counterparts, where CMX wrapped around the outer surface of CNFs due to higher concentration, resulting in bulky aggregates of microelectrodes (**fig 3.12 a**). A higher magnified image of CMX-CNF ME 3 shows that CMX wraps individual CNFs from top to bottom of their entire length (**fig 3.12 b**).

Preparation of microelectrodes with three different CMX: CNF ratios resulted in the formation of microelectrodes with three distinct morphologies. Lower CMX: CNF ratio (0.5 mL CMX to 60 mg CNF) resulted in the formation of CMX-CNF microelectrodes (CMX CNF ME 1) with partially filed CMX hydrogel network inside the hollow cores of CNF, as evidenced from TEM images shown in **fig 3.11 a and b**. Adequate incorporation of CMX onto CNF hollow cores were realized after

increasing the volume of CMX from 0.5 to 1.0 mL (CMX CNF ME 2) during the preparation process.

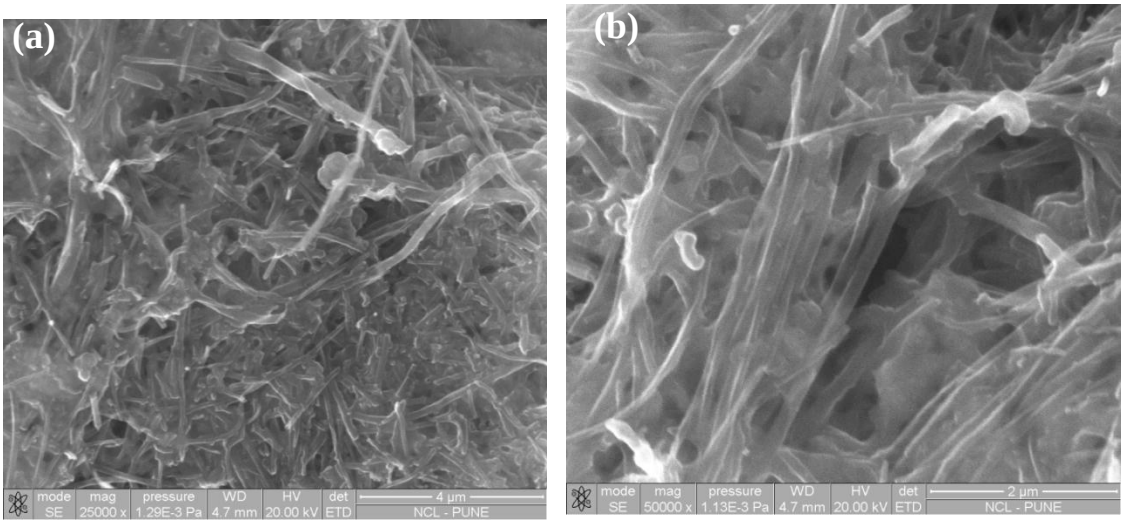

Figure 3.12: SEM images of (a) CMX-CNF ME 3 shows bulky aggregates of microelectrodes wrapped by CMX around the outer surface of CNFs (scale bar is 4 microns). (b) Higher magnification shows individual CNFs among the aggregate (scale bar is 2 microns).

TEM images of CMX CNF ME 2 at various magnifications shown in **fig 3.13** supports this observation. In these images, CNF seems to be filled significantly with CMX hydrogel network in its entire inner diameter (**fig 3.13 a and b**) and across the length of the hollow core (**fig 3.13 c**), without any major deposition of CMX on the surface of CNFs. It can be realized that the volume of CMX added during the preparation of CMX-CNF ME 2 is crucial to obtain microelectrodes filled with the hydrogel matrix. The ability of CNFs to intercalate foreign bodies resulted in the formation of microelectrodes where highly crystalline as well as carbonaceous outer cylinder facilitates conductivity of electrical signals whereas continuous hydrogel network of polyelectrolyte inside its hollow core enhances ionic mobility across the length of the CNF. However, increasing the concentration of CMX further from 1.0 to 1.5 mL resulted in the formation of bulky aggregates of microelectrodes (CMX-CNF ME 3), as evident from the electron microscopic images shown in **fig 3.11 c and 3.12**. This aggregation may be driven by the wrapping of CMX over the surface of CNFs followed by subsequent cross-linking of CMX on the surface. Such aggregation of CMX on the surface may adversely affect the conductivity of microelectrodes.

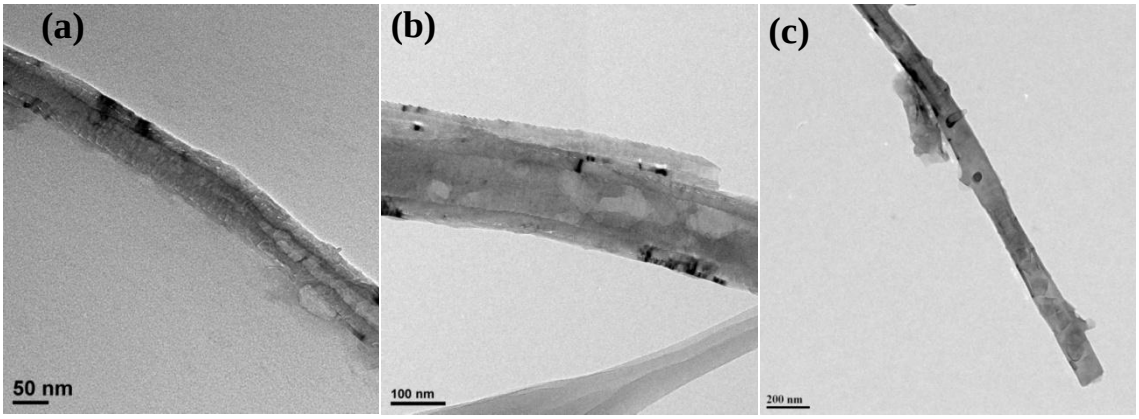

Figure 3.13: TEM images of individual CMX-CNF ME 2 microelectrodes containing CMX hydrogel in its hollow core with scale bars (a) 50, (b) 100 and (c) 200 nm, respectively.

3.3.6 Electrochemical studies

One of the crucial roles of implanted electrodes is an efficient translation of signals between the electronic form in leads and ionic signals in tissue. This transition involves electrochemical processes which has to be carefully controlled and not to be detrimental either to the electrode itself or to the surrounding tissue. Furthermore, in the absence of a rigid anatomical structure where the electrodes can be implanted, soft nervous tissue, has to be in intimate contact with the electrode surface for the signal transition[1-3].

The signal transduction in the nervous system is both electrical and chemical and interacting with either pathway, opens up the possibility for artificial interfacing with the neuron. For electrical interfacing, the electrodes record the electrical activity of the neurons and evoke action potentials by electrical stimuli. Since the electrical current is transported as ions in biological tissue, and as electrons in the electrode material, the interface works as a transducer between ionic and electronic currents. The efficiency of this conversion is limited by the electrical impedance, with higher impedance leading to the greater energy loss of signal to be exchanged[5-7].

To compensate for high impedance, the applied potential can be increased in order to generate a satisfactory current density for stimulation. However, for high potentials applied to the electrode, there are electrochemical considerations that have to be taken into account.

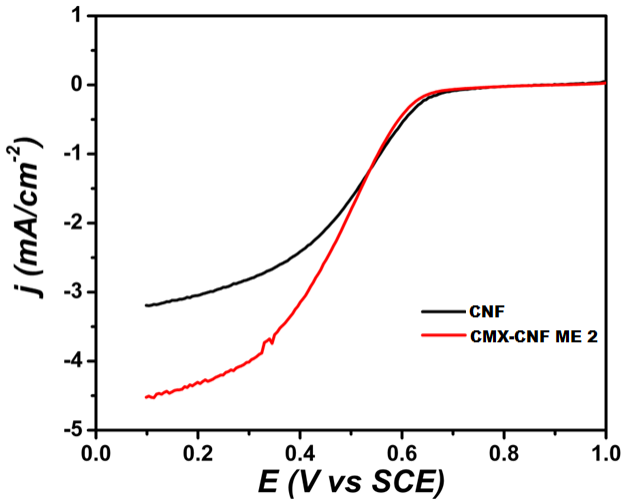

Fig. 3.14 Linear sweep voltammetry of CMX-CNF ME 2 and pristine CNF at 1600 RPM in 5mV/s scan rate in oxygen saturated perchloric acid

The incorporation of CMX hydrogel into CNF can enhance the current density without compromising the increase in impedance. Accordingly, we show in **fig 3.14** a linear sweep voltammograms of CMX-CNF ME 2 and pristine CNF in oxygen saturated perchloric acid at a scan rate of 5mV/s. Voltammograms were recorded using a rotating disk electrode (RDE) at 1600 RPM for oxygen reduction reaction (ORR) on the microelectrode modified GC disk electrode at room temperature.

The ORR limiting current density is higher for CMX-CNF ME 2 than CNF as observed in the voltammograms. This significant increase in current density may be attributed to the presence of the hydrogel network inside the hollow channels of the CNF which alleviate limitations of diffusion in perchloric acid. These observations are in line with the previous reports, wherein CNFs decorated with platinum[30] and polyethylenedioxythiophene (PEDOT)[31] in its hollow core, possess more electro-catalytic activity and charge storage capacity, respectively.

Further, the electrochemical active area (EAA) calculated from the electrochemical studies also shows a significant difference between both CNF and CMX-CNF ME 2 microelectrodes. The electrochemically active area represents the area of the electrode which is accessible to the electrolyte for charge transfer. The EAA of 50.3 m^2/g obtained for CMX-CNF ME 2 microelectrode is 20 % higher as compared with 41.8 m^2/g obtained for pristine CNF. Hence the presence of the hydrogel network in

the hollow core of CNF has enhanced the available active surface of the microelectrode for charge transfer. This study shows that the presence of electrochemical signal transduction and the stable organic interface is supported by nano-structured carbon in the CMX-CNF microelectrodes. The higher electrical conductivity of the resulting microelectrodes can contribute towards the enhanced efficacy of neural signal transmission at the cell-electrode interface.

3.3.7 Cytotoxicity studies

In-vitro cell viability tests were performed using resazurin assay on CMX hydrogel, CNF and CMX-CNF ME 2 with L929 fibroblast cell lines for 72 hours, to evaluate their toxicity and cell viability. Results of the study are shown in **fig 3.15**, where negative control (only cells) is plotted along with CMX hydrogel, CNF and CMX-CNF ME 2. Histogram reveals the difference in metabolism of cells grown on these three systems and cell proliferation is significantly reduced in CNFs as compared to CMX hydrogel and microelectrode.

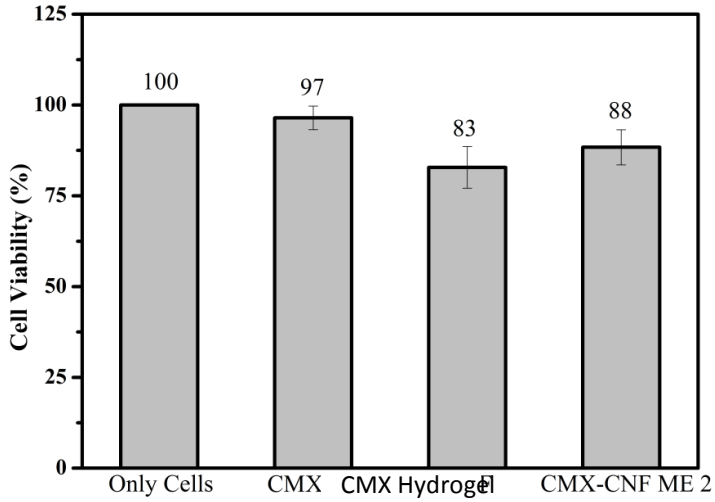

Figure 3.15: Cell viability of CMX hydrogel, CNF and CMX-CNF ME 2 along with a negative control

As shown in **fig 3.15**, there is a significant difference in cell proliferation among CMX hydrogels, CNFs and microelectrode. While considering the error bar limits, CMX hydrogels show similar cell viability as that of negative control, whereas CNF shows a 14 % reduction in cell viability. Polysaccharide hydrogels derived from natural sources are highly biocompatible due to their sugar-rich backbone and other bio-mimetic characteristics; however synthetic systems such as CNF without any

bioactive moieties and cell recognition sites on their surface were unable to enhance cell attachment and growth. Microelectrode which contains both CMX hydrogel and CNF shows a significant increase in its biocompatibility as compared with pristine CNFs. However, more detailed *in-vivo* biological investigations of these microelectrodes are necessary, before taking them forward to the next phase of device development. The biocompatibility exhibited by CMX-CNF ME after 2 days of incubation reveals their stability as well as response to cells in the hydrated environment. This observation underlines the absence of adverse events during the interaction of microelectrodes with the physiological environment, wherein any major electrochemical or charge transfer reactions at the electrode-cell interface may lead to significant variations in the cell viability with respect to control. It also emphasizes the suitability of the synthetic pathway adopted for the preparation of these microelectrodes.

3.4 Conclusions

To make further advancement in the microelectrode technology, we have integrated CNF with CMX hydrogel network to design a flexible microelectrode with enhanced cell-electrode interface which can provide significant electrochemical signal transduction at the neural interface and enhance the intrinsic biological processes.

CMX hydrogels with 12 wt-% DVS crosslinking showed compressive strength of 11.4 kPa at equilibrium which can be further tuned to attain the desired mechanical integrity required for implantation. Microelectrodes were designed by the integration of CMX inside the hollow core of CNF, by *in situ* gelation of CMX. The concentration of CMX was optimized for adequate and continuous formation of a hydrogel network inside the CNF. Voltammograms of microelectrodes showed higher current density and electrochemical active surface area than that of pristine CNFs. This observation signifies the presence of stable electrochemical signal transduction at the CMX-CNF interface, necessary for artificial interfacing with the neuron. Therefore these microelectrodes can work as a transducer between ionic and electronic currents with necessary current density for stimulation. Cytotoxicity studies showed 88% cell viability for microelectrodes which indicates the biocompatible characteristics of these microelectrodes.

Based on their morphology and function, these microelectrodes can be suitable to the generation of flexible composite microelectrodes, wherein the soft cell-electrode interface may encourage the higher proliferation of neuronal growth towards the electrodes. The results indicate the potential of these microelectrodes for their applications in designing new generation neural interfaces. Detailed *in-vitro* and *in-vivo* experiments are nevertheless necessary to establish the long-term efficacy of signal transductions and tissue integration of these microelectrodes.

3.5 References

(1) Wallace, G. G.; Moulton, S. E.; Clark, G. M. *Science* **2009**, *324*, 185.

(2) Cui, X.; Martin, D. C. *Sensors and Actuators B: Chemical* **2003**, *89*, 92.

(3) Abidian, M. R.; Martin, D. C. *Biomaterials* **2008**, *29*, 1273.

(4) Lu, Y.; Wang, D.; Li, T.; Zhao, X.; Cao, Y.; Yang, H.; Duan, Y. Y. *Biomaterials* **2009**, *30*, 4143.

(5) Fattahi, P.; Yang, G.; Kim, G.; Abidian, M. R. *Adv Mater* **2014**, *26*, 1846.

(6) Cheung, K. C. *Biomed Microdevices* **2007**, *9*, 923.

(7) Rodger, D. C.; Fong, A. J.; Li, W.; Ameri, H.; Ahuja, A. K.; Gutierrez, C.; Lavrov, I.; Zhong, H.; Menon, P. R.; Meng, E.; Burdick, J. W.; Roy, R. R.; Edgerton, V. R.; Weiland, J. D.; Humayun, M. S.; Tai, Y.-C. *Sensors and Actuators B: Chemical* **2008**, *132*, 449.

(8) Kim, D.-H.; Viventi, J.; Amsden, J. J.; Xiao, J.; Vigeland, L.; Kim, Y.-S.; Blanco, J. A.; Panilaitis, B.; Frechette, E. S.; Contreras, D.; Kaplan, D. L.; Omenetto, F. G.; Huang, Y.; Hwang, K.-C.; Zakin, M. R.; Litt, B.; Rogers, J. A. *Nature Materials* **2010**, *9*, 511.

(9) Birthe, R.; Conrado, B.; Robert, O.; Pascal, F.; Thomas, S. *J Neural Eng* **2009**, *6*, 036003.

(10) Kozai, T. D. Y.; Langhals, N. B.; Patel, P. R.; Deng, X. P.; Zhang, H. N.; Smith, K. L.; Lahann, J.; Kotov, N. A.; Kipke, D. R. *Nature Materials* **2012**, *11*, 1065.

(11) Righi, M.; Puleo, G. L.; Tonazzini, I.; Giudetti, G.; Cecchini, M.; Micera, S. *Sci Rep-Uk* **2018**, *8*, 502.

(12) Shi, J.; Fang, Y. *Adv Mater* **2018**, *0*, 1804895.

(13) Grill, W. M.; Norman, S. E.; Bellamkonda, R. V. *Annual Review of Biomedical Engineering* **2009**, *11*, 1.

(14) Hu, H.; Ni, Y.; Montana, V.; Haddon, R. C.; Parpura, V. *Nano Letters* **2004**, *4*, 507.

(15) Saito, N.; Usui, Y.; Aoki, K.; Narita, N.; Shimizu, M.; Hara, K.; Ogiwara, N.; Nakamura, K.; Ishigaki, N.; Kato, H.; Taruta, S.; Endo, M. *Chemical Society Reviews* **2009**, *38*, 1897.

(16) Lovat, V.; Pantarotto, D.; Lagostena, L.; Cacciari, B.; Grandolfo, M.; Righi, M.; Spalluto, G.; Prato, M.; Ballerini, L. *Nano Letters* **2005**, *5*, 1107.

(17) White, E. V.; Rao, P. S. *Journal of the American Chemical Society* **1953**, *75*, 2617.

(18) Srivastava, H. C.; Singh, P. P. *Carbohyd Res* **1967**, *4*, 326.

(19) Gidley, M. J.; Lillford, P. J.; Rowlands, D. W.; Lang, P.; Dentini, M.; Crescenzi, V.; Edwards, M.; Fanutti, C.; Reid, J. S. G. *Carbohyd Res* **1991**, *214*, 299.

(20) Shirakawa, M.; Yamatoya, K.; Nishinari, K. *Food Hydrocolloid* **1998**, *12*, 25.

(21) Little, R. D.; Masjedizadeh, M. R.; Wallquist, O.; McLoughlin, J. I. *Organic Reactions* **2004**, *47*, 315.

(22) Mather, B. D.; Viswanathan, K.; Miller, K. M.; Long, T. E. *Progress in Polymer Science* **2006**, *31*, 487.

(23) Hochberg, L. R.; Serruya, M. D.; Friehs, G. M.; Mukand, J. A.; Saleh, M.; Caplan, A. H.; Branner, A.; Chen, D.; Penn, R. D.; Donoghue, J. P. *Nature* **2006**, *442*, 164.

(24) Anseth, K. S.; Bowman, C. N.; Brannon-Peppas, L. *Biomaterials* **1996**, *17*, 1647.

(25) Rizzi, S. C.; Hubbell, J. A. *Biomacromolecules* **2005**, *6*, 1226.

(26) Metters, A.; Hubbell, J. *Biomacromolecules* **2005**, *6*, 290.

(27) Vernon, B.; Tirelli, N.; Bächi, T.; Haldimann, D.; Hubbell, J. A. *Journal of Biomedical Materials Research Part A* **2003**, *64A*, 447.

(28) Anbergen, U.; Oppermann, W. *Polymer* **1990**, *31*, 1854.

(29) Endo, M.; Kim, Y. A.; Hayashi, T.; Fukai, Y.; Oshida, K.; Terrones, M.; Yanagisawa, T.; Higaki, S.; Dresselhaus, M. S. *Applied Physics Letters* **2002**, *80*, 1267.

(30) Balan, B. K.; Unni, S. M.; Kurungot, S. *The Journal of Physical Chemistry C* **2009**, *113*, 17572.

(31) Anothumakkool, B.; Bhange, S. N.; Unni, S. M.; Kurungot, S. *Rsc Adv* **2013**, *3*, 11877.

Development of micro-gel incorporated double network hydrogels from carboxymethyl xyloglucan for rate pre-programmed drug delivery

Chapter – IV

In the fourth chapter, double network (DN) hydrogels comprising of CMX as the first network and poly(hydroxyethyl acrylate) (PHEA) as the second network were proposed using a sequential process. These DN hydrogels exhibited a compressive strength of 3.5 MPa, whereas the first and second network showed compressive strength of 0.02 and 2.3 MPa, respectively. Microgels (MGs) were prepared by the photo-polymerization of stearyl methacrylate (SM) and hydroxyethyl acrylate (HEA) using oil-in-water (O/W) method. Release of curcumin in PBS from these MGs embedded in the DN hydrogels showed release pattern dependent on the concentration of HEA.

4.1 Introduction

Hydrogels are one of the ideal candidates among biomaterials for applications in controlled or sustained drug delivery systems (DDS)[1-2]. However, inherent mechanical weakness and burst release profiles had limited their applications to a large extent. In the recent years, a few new concepts have been evolved to enhance the mechanical property of hydrogels, such as nano-composite hydrogels[3], slide-ring hydrogels[4], double network[5] (DN) hydrogels, etc. Among these methods DN hydrogels has attracted much attention due to their ability to enhance the mechanical property by the combination two different polymer networks; brittle, hard networks with ductile, soft networks.

New scientific concepts such as rate pre-programmed delivery, activation modulated delivery and feedback regulated delivery have revolutionized the arena of controlled / sustainable drug delivery platforms[6]. These concepts provide various solutions to design smart DDS which can address various challenges involved in chronic wounds, hormone imbalance, angiopathy, neuropathy, etc[7]. Among these concepts, rate pre-programmed drug delivery systems (RPPDDS) are ideal for applications in polymeric systems to develop smart DDS for sustained / controlled release for a prolonged time periods with multiple depots.

Major objective of this study is to develop mechanically robust DN hydrogel using biocompatible polymer such as carboxymethyl xyloglucan (CMX) and to design a RPPDDS for sustained release of a model drug such as curcumin, at three different rates, for potential applications in burn wounds or diabetic ulcers. Four different technical principles of RPPDDS are membrane permeation systems, matrix diffusion systems, hybrid membrane/matrix systems and micro-reservoir partition systems. Among these, micro-reservoir partition systems are selected for application in the proposed CMX-based DN hydrogels due to their potential to embed microgel-based micro-reservoirs for sustained / controlled release.

Gong *et al*[8] has reported microgel reinforced hydrogel films to enhance the mechanical strength of polyacrylamide-based hydrogels where embedded microgels effectively reduce the crack during deformation and enhances the fracture propagation

resistance of the films. Khademhosseini *et al*[9] has designed gellan gum microgel reinforced cell-laden gelatin hydrogels with cell-compatible conditions and higher strength. Preosteblasts encapsulated in these hydrogels possess better metabolic activity and higher mineralization. However, a very few reports are available on microgel laden DN hydrogels for designing sustained / controlled DDS. In this study oil-in-water emulsion methodology is employed for the preparation of drug incorporated microgels with varying hydrophobic – hydrophilic balance, which acts as micro-reservoir partition-controlled DDS.

4.2 Materials and methods

4.2.1 Materials

Carboxymethyl tamarind kernel powder was procured from Dabur India Ltd., and purified by washing with acetone, filtered, dissolved in water, centrifuged, dialysed and finally freeze-dried to obtain white coloured cotton-like soft carboxymethyl xyloglucan (CMX). Divinyl sulphone (DVS), hydroxyethyl acrylate (HEA), stearyl methacrylate (SM) and hydroxylmethylpropiophenone (HMPP) were purchased from Sigma Aldrich, India. Tween-80 was purchased from Merck India Pvt. Ltd. All reagents were used as received. Distilled water was used for all the experiments unless specified otherwise.

4.2.2 Preparation of CMX DN hydrogels

Preparation of DN hydrogels consisted of two-step sequential process, where first hydrogel network (from CMX) was prepared initially, followed by the in-situ preparation of the second hydrogel network (from PHEA). First and second hydrogel networks were also prepared separately and named single network (SN) hydrogels.

4.2.2.1 Preparation of SN hydrogels

Solution of CMX was prepared by dissolving 0.35 gms of CMX in 10 ml of 0.1 M NaOH solution. 0.042 ml of DVS (12 Wt% of CMX) was added onto CMX solution, stirred for 5 minutes, poured onto cylindrical teflon moulds (8 mm x 8 mm), stored at 15 ^{0}C for 12 hours and later the resultant hydrogels (as-prepared SN hydrogels) were swollen to equilibrium in distilled water with regular replenishment. These CMX hydrogels were abbreviated as CMX single network (CMX-SN) hydrogels.

A homogeneous aqueous solution containing 30 wt % HEA, 0.045 wt % SDS and 1 µL of photo initiator (HMPP) were poured onto cylindrical teflon moulds (8 mm x 8 mm) and exposed to UV irradiation in a closed chamber for 21 minutes. Hydrogels formed after irradiations were named as PHEA-SN hydrogels which were then swollen to equilibrium in distilled water.

4.2.2.2 Preparation of DN hydrogels

For the preparation of DN hydrogels, as prepared CMX-SN hydrogels were immersed in 20 ml aqueous solution containing 50 wt % HEA, 0.045 wt % SDS and 1 µL of photo initiator (HMPP) and kept in roller mixer for 72 hours. The equilibrium swollen hydrogels in HEA, HMPP and SDS solution were irradiated with UV in a closed chamber for 21 minutes. Irradiated hydrogels were again swollen to equilibrium in distilled water with regular replenishment of distilled water at specific time intervals. Resultant DN hydrogels were composed of poly(hydroxyl ethyl acrylate) as the second network and were abbreviated as CMX-PHEA double network (CMX-PHEA-DN) hydrogels.

4.2.3 Swelling studies

As-prepared hydrogels (both SN and DN) were kept immersed in distilled water until equilibrium, with replenishment of distilled water at regular time intervals. The weight of the equilibrium swollen hydrogels was noted (*Ws*) and dried in an oven at 50 ^{o}C until the weight remained constant. The weight of these vacuum dried xerogels was noted (*Wd*). Swelling ratio (Q) was calculated, as shown in eqn (1).

4.2.4 NMR spectroscopy and gelation time

^{1}H NMR spectra of xerogels were recorded using a Bruker Avance AQS spectrometer (Bruker, Germany). The spectrometer was operated at a carbon frequency of 75MHz, and the samples were spun at 8 kHz in a 4mm triple resonance probe. About 4000 scans were accumulated with an inter-scan delay of 2.5s.

Rheometer (Model 301, Anton Paar, Austria) equipped with a cup and bob geometry was used to measure the time required for the gelation of CMX single network hydrogels cross-linked by DVS. About 4 ml of CMX solution was charged onto the cup, 12 wt % DVS as added, stirred for 2 minutes. Time sweep measurements were performed at constant strain, frequency and temperature (15 ^{0}C) within the linear

visco-elastic regime. Storage modulus (G') and loss modulus (G") were measured as a function of time until the gelation occurred.

4.2.5 Compressive strength of SN and DN hydrogels

Universal testing machine (UTM) (Model 5943, Instron, MA, USA) was used to measure the compressive strength of the equilibrium swollen hydrogels. The hydrogel was placed in the lower compression plate, and the upper compression plate was set at a speed of 3 mm/min to measure the compressive strength of hydrogel during fracture. Stress and strain were recorded and plotted by Bluehill software (Instron, MA, USA). Measurements were repeated thrice, and average values were reported.

4.2.6 Elastic modulus of CMX hydrogels

The elastic modulus of CMX hydrogels was measured using dynamic mechanical analyser (Model RSA3, TA Instruments USA). CMX hydrogels with 3 different degrees of crosslinking (having DVS concentrations viz. 8, 10 and 12 wt-%) were prepared and punched out into a cylindrical shape with 1:1 aspect ratio (height and diameter) and swollen to equilibrium. These equilibrium swollen hydrogels were subjected to dynamic compression experiment within their linear visco-elastic region. During the experiments, specimens were moistened with dodecane to prevent de-hyradation and to reduce the friction between compressive platens.

4.2.7 Preparation of drug-incorporated PHEA-co-SM microgels

Microgels based on PHEA-co-SM were prepared by co-polymerization of SM and HEA using oil-in-water (O/W) emulsion method[9]. 3 wt% solution of SM in paraffin oil was mixed with 5 mol % HEA, along with 30 wt% curcumin and 1 wt% photo-initiator (HMPP). From this solution, 0.4 ml of the mixture was homogenized with 5 ml DI water containing 0.02 ml tween-80 for 3 min by homogenizer (Heidolph, Germany). Emulsion formed was exposed to UV irradiation for 20 mins and dried overnight at 40^0C to evaporate water. Microgels were separated by centrifugation, washed with isopropanol, hexane, acetone and finally dried under vacuum. Experiments were repeated with 10 and 15 mol% HEA to prepared microgels with three different contents of PHEA in the copolymer.

4.2.8 Preparation of microgels incorporated DN hydrogels

Microgels (50 mg) were allowed to swell in 10 ml of 0.1 M NaOH solution and 0.35 gms of CMX was added and dissolved. 0.042 ml of DVS (12 Wt% of CMX) was

added onto CMX solution, stirred for 5 minutes, poured onto cylindrical teflon moulds (8 mm x 8 mm), stored at 15 ^{0}C for 12 hours and later the resultant hydrogels (as-prepared SN hydrogels) were swollen in a homogeneous aqueous solution containing 30 wt % HEA, 0.045 wt % SDS and 1 µL of photo initiator (HMPP). Mixture was poured onto cylindrical teflon moulds (8 mm x 8 mm) and exposed to UV irradiation in a closed chamber for 21 minutes. Hydrogels formed after irradiations were swollen to equilibrium in distilled water and named as CMX-PHEA-MG-DN hydrogels.

4.2.9 3D imaging and size distribution of microgels in CMX-PHEA-MG-DN xerogels

Equilibrium swollen CMX-PHEA-MG-DN hydrogels were dried overnight in vacuum oven at 50^{0}C. CMX-PHEA-MG-DN xerogels with an approximate size of 4 x 4 mm were loaded onto micro-computed tomography (micro-CT) (Model Xradia Versa 510, Carl Zeiss X-ray Microscopy, Pleasanton, CA) where 3201 X-ray projections were acquired with 360^0 rotation at 50 kV X-ray source, with a pixel size of 3.98 microns. Acquired projections were subjected to back projection algorithm to reconstruct a series of virtual cross-sectional 2D images of microgel laden xerogels. 2D images were cropped to a size of 1300 x 900 x 1000 microns, filtered with non-local means filter and segmented using PoroDict® (Math2Market GmbH, Kaiserslautern, Germany) image processing software to construct a three-dimensional image of microgels to visualize its spatial distribution within the DN xerogels matrix. Image segmentation process also differentiates microgels in the xerogels with the aid of Otsu global threshold selection method and quantifies its diameter and size distribution.

4.2.10 Drug release studies from microgels incorporated DN hydrogels

CMX-PHEA-MG-DN hydrogels in triplicate with 5, 10 and 15 mol% HEA loading were trimmed into equal weight and placed in three different beaker sets containing PBS with 10 wt% tween-80. Beakers were placed in a shaking water bath set at 37^{0}C. Media was replaced at specific time intervals to maintain perfect sink conditions. Standard curve was erected with different concentrations of curcumin dissolved in PBS with 10% tween-90, using UV-Vis spectrophotometer. Representative aliquot from replaced media was analyzed against the standard curve and curcumin release into the media was calculated. Cumulative release is plotted as a function of time for a

period of 60 hours from the three data sets pertaining to DN hydrogels containing 5, 10 and 15 mol% HEA loadings.

4.3. Results and discussion

4.3.1 Preparation of CMX DN hydrogels

CMXs are an important class of polysaccharides with branched structure and constitute a significant percentage of the cell walls of plant tissues[10]. It possess a backbone of β-1,4 linked D-glucose, xylose residues are attached to 60 – 75% of the glucoses by α-1,6 linkages and galactose residues are attached to 25 – 30 % of xyloses by β-1,2 linkages (**Fig 4.1**). Its structure contains glucose, xylose and galactose units in a molecular ratio of 3:2:1[11-14]. NMR spectroscopic studies to investigate the chemical structure and purity of CMX are given in **Chapter III section 3.3.1**.

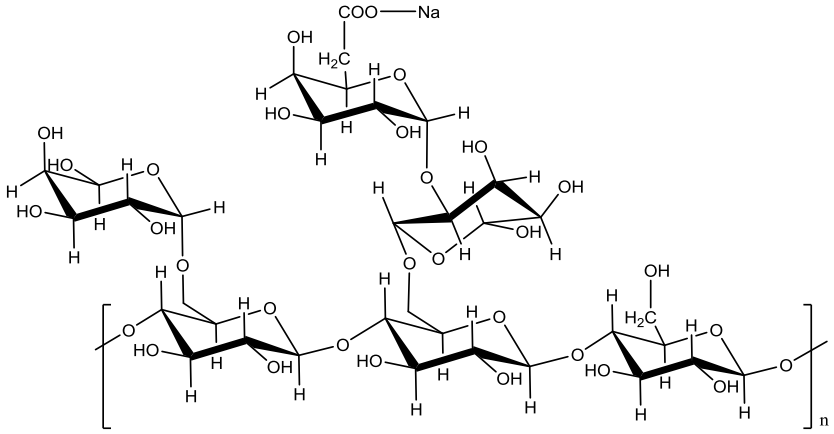

Figure 4.1: Chemical structure of CMX

Preparation of CMX hydrogels via Michael-type addition reaction between CMX and DVS are also detailed in **Chapter III section 3.3.2**. As-prepared CMX hydrogels were washed, dried to constant weight, swollen in the monomer solution of HEA containing photo-initiator and polymerized using UV irradiation. Thus a two-step sequential preparation protocol was employed for the preparation of CMX DN hydrogels.

4.3.2 Gelation and swelling of CMX hydrogels

Results of gelation and swelling studies on CMX hydrogels are described in **Chapter III section 3.3.3**.

4.3.3 Elastic modulus of CMX hydrogels

There are several methods used to study visco-elasticity of polymers and hydrogels. These methods basically determine the relationships between stress, the relative deformation and time required for deformation. Among these methods, oscillatory techniques are used in this study, where the relative deformation varies with time according to a sinusoidal relationship. To establish zone of linear visco-elasticity of the hydrogels, an oscillatory amplitude sweep test was performed for each hydrogel at ambient temperature and constant frequency. Linear zone is defined based on the independence of moduli to the oscillatory shear stress and accordingly the value of strain is selected in the linear visco-elastic regime.

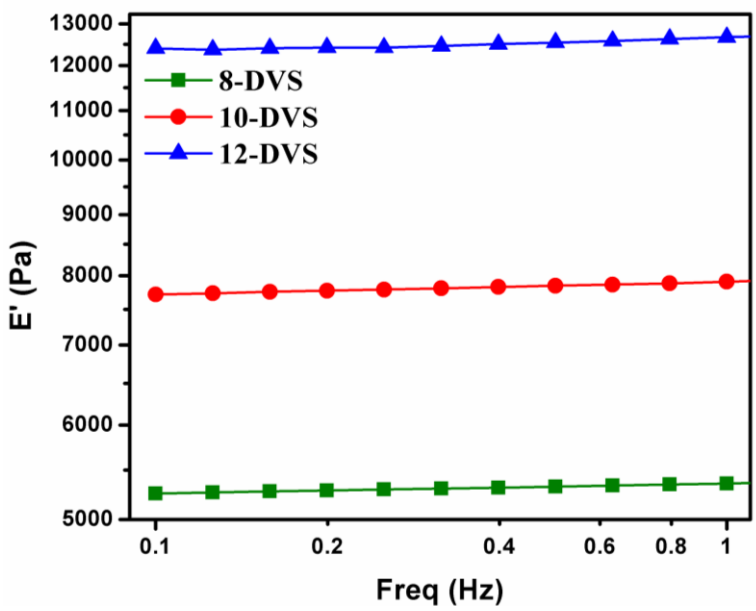

Figure 4.2: Frequency sweep of equilibrium swollen CMX hydrogels with varying DVS content

Fig 4.2 shows the dynamic mechanical response of CMX hydrogels within their linear visco-elastic region. Elastic modulus of CMX hydrogels were obtained by a frequency sweep between 0.1 and 1.0 Hz. CMX hydrogels with 8, 10 and 12 wt-% DVS show a gradual increase in their elastic modulus with an increase in the cross-linker concentration. **Fig 4.2** presents the effect of cross-linker concentration on the dynamic modulus of hydrogels where the elastic character of the hydrogels prevails and is more independent of the frequency, which indicates the existence of three-dimensional network.

4.3.4 Compressive strength of CMX-PHEA-co-SM DN hydrogels and SN hydrogels

Compressive strength of equilibrium swollen SN and DN hydrogels was studied by UTM. **Fig 4.3** shows the stress versus strain plot of SN and DN hydrogels, where CMX-PHEA DN hydrogels possess a compressive strength of 3.5 MPa which is 34 % higher than that of PHEA SN hydrogels and 99 % that of CMX SN hydrogels. Fracture strain of both CMX-PHEA DN hydrogels and its counterpart PHEA SN hydrogels are 82 and 88 respectively, whereas CMX SN hydrogels possess only 40% compressibility.

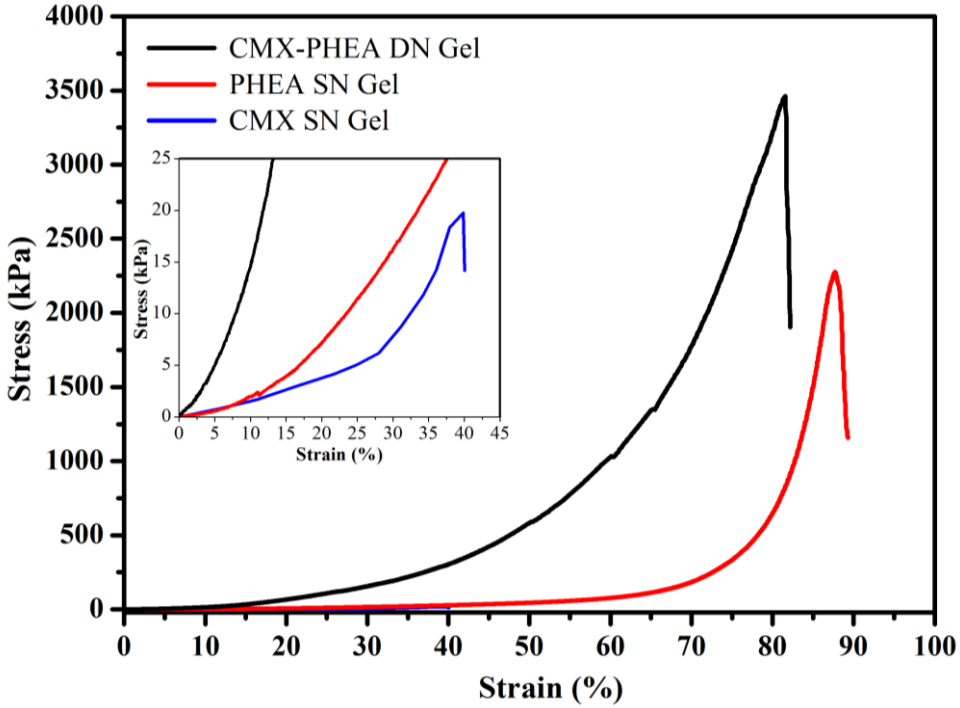

Figure 4.3: Stress versus strain plot CMX SN hydrogel, PHEA SN hydrogel and CMX-PHEA DN hydrogel

The results points out a drastic increase in the mechanical properties of DN hydrogels as compared to their SN counterparts, which signifies the combination of brittle and ductile characteristics of individual SN networks, as reported by Gong et al[5]. DN hydrogel shows 175 times increase in compressive strength and 2 times increase in compressive stress, as compared to CMX SN hydrogel. Hence, this DN strategy has been successful in the preparation of mechanically robust CMX hydrogels and is the first report on CMX based DN hydrogels so far.

4.3.5 Preparation of drug-incorporated PHEA-co-SM microgels

O/W emulsion methodology was employed for the preparation of PHEA-co-SM microgels containing curcumin as model drug; with varying concentrations of HEA (5, 10 and 15 mol% of SM) (**fig 4.4**). Curcumin being a hydrophobic drug molecule, the objective was to design a polymer drug carrier, such as microgels, with varying hydrophilic – hydrophobic volume fractions, to control the permeability of the drug molecules to the external medium. Such rate-controlling strategy has far reaching possibilities in designing pre-programmable drug delivery systems.

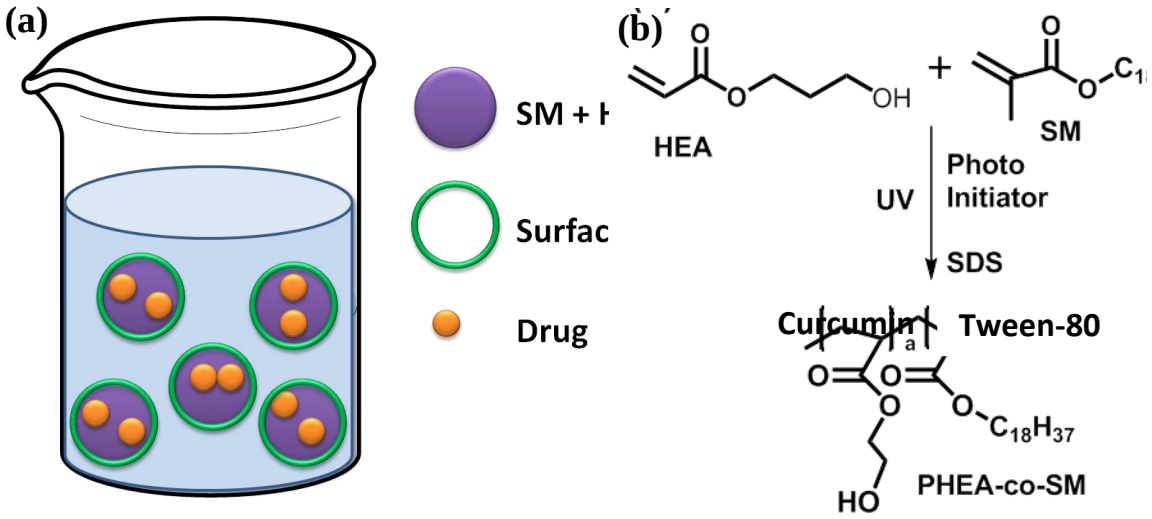

Figure 4.4: (a) Schematic representation of O/W emulsion process of the preparation of microgels and (b) copolymerization reaction of HEA and SM in the presence of drug and surfactant

4.3.6 3D imaging and size distribution of microgels

Vacuum dried microgels were imaged using micro-CT to study their morphology and size distribution. During micro-CT imaging, X-ray radiographic projections were recorded and reconstructed using back-projection algorithm to generate virtual cross-sectional images. These images were later segmented using image analysis package to visualize microgels and to quantify their size-distribution (**Fig 4.5**). Colour-coded 3D images of microgels are shown in **fig 4.5a** with respect to its colour legend. Based on the colour legend, spherical microgels with red colour are those with diameter 500 microns and higher. Similarly, specific colours are given to microgels with diameter below 500 microns. Corresponding histogram on the size distribution of these

microgels is given in **fig 4.5b**. As per the histogram diameter of these microgels ranges from 4 to 580 microns and their average diameter is 295 microns.

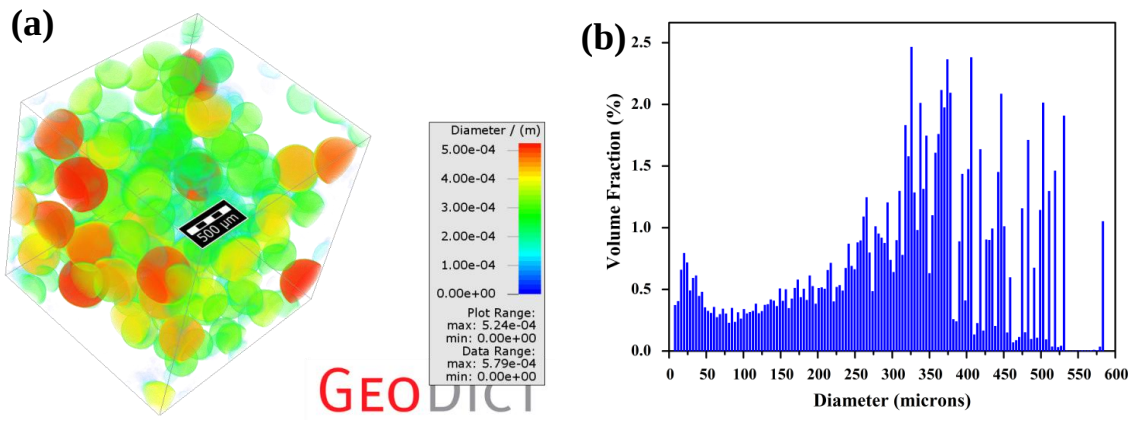

Figure 4.5: (a) 3D visualization of microgels with colour-code based on colour legend (Scale bar is 500 microns) and (b) size distribution of the microgels as a function of its volume fraction

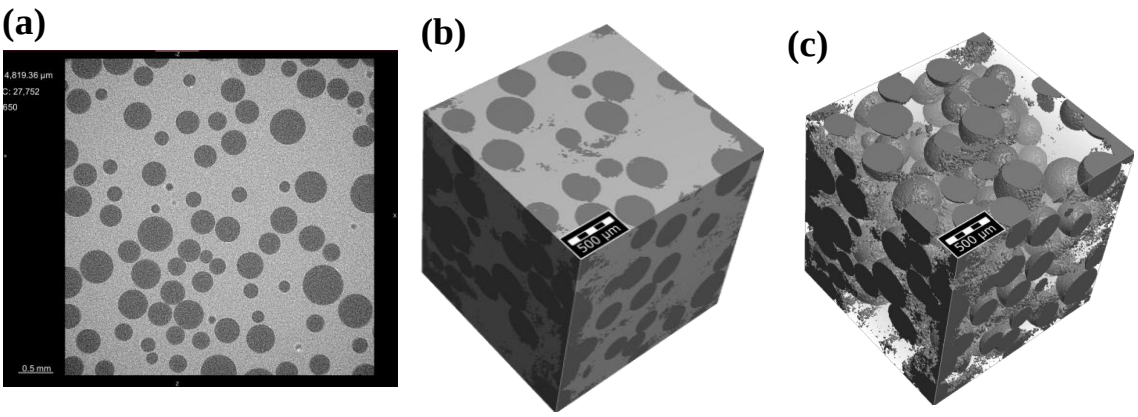

Figure 4.6: (a) 2D virtual cross-sectional image of microgels inside DN hydrogel, (b) 3D reconstructed image of microgels inside DN hydrogel and (c) 3D visualization of the spatial distribution of microgels inside DN hydrogel (Scale bar is 500 microns)

4.3.7 Microgels incorporated DN hydrogels

To prepare microgel incorporated DN hydrogels, as prepared microgels were mixed with CMX solution and two step sequential DN hydrogel preparation process was repeated as described before. The resultant microgel incorporated DN hydrogels were designated as CMX-PHEA-MG DN hydrogels.

4.3.8 Pre-programmed drug release from DN hydrogels

UV-Vis spectroscopy was employed to obtain standard curve of curcumin to estimate the concentration of curcumin released into the external medium. Release media collected at different time intervals were subjected to UV-Vis spectroscopic analysis at λ_{max} of 425 nm and the resultant absorption intensity was correlated with the standard curve to calculate the concentration of curcumin released into the medium (**Fig 4.7a**).

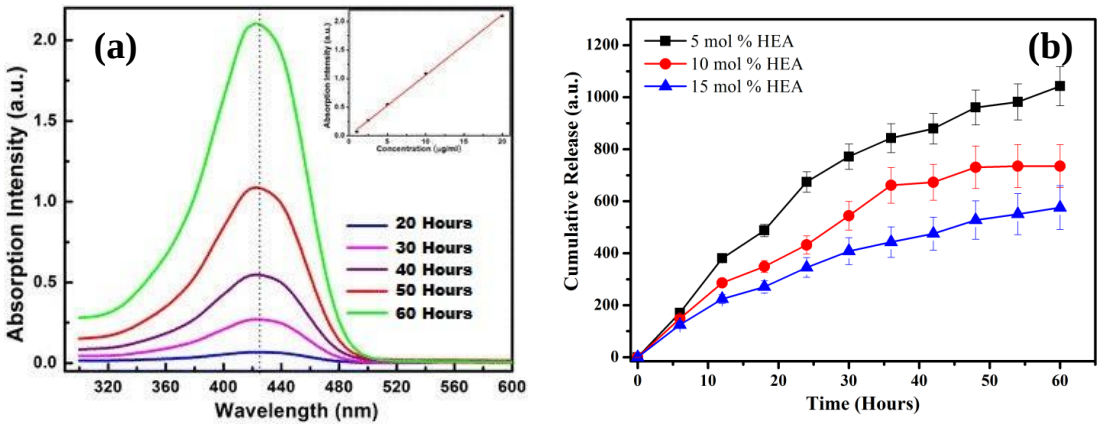

Figure 4.7: (a) Representative UV-Vis spectrum of curcumin released from 20 to 60 hours and its corresponding relation to the standard curve given in inset, (b) cumulative release profile of curcumin from microgels with varying amount of PHEA, as a function of time

Cumulative release profile of curcumin at specific time intervals were calculated from collated UV-Vis spectrum and plotted as a function of time, for three microgel datasets with varying HEA content (**Fig 4.7b**). With increase in HEA content in the microgels, amount of curcumin released into the external medium is decreased which signifies the restricted permeability of curcumin through hydrophilic PHEA fraction. Such modulated release profile helps to design rate pre-programmed drug delivery systems (**RPPDDS**) which are essential to address the challenging dynamic clinical conditions such a chronic wounds, neuropathy, etc[15].

Conventional drug delivery systems often fail to address the challenges during the healing process of chronic wounds such as burn wounds or diabetic ulcers[15-17]. In chronic wounds such as burn wounds, a series of cascading events takes place simultaneously in a synchronized mode during the entire time period involved in the

healing process[18]. Healing process starts with hemostasis followed by inflammation, proliferation and remodeling, which spans across weeks to months, depending on the patho-physiology of the wound[7]. Time scale of these individual stages and bioactive agents required for each stages varies from each other. Therefore, a delivery system with pre-programmed rate is highly recommended to address such patho-physiological conditions.

Generally in RPPDDS, the release of drug molecules are pre-programmed with a specific rate profile and are attained by optimizing the system design of DDS to control the molecular diffusion of drug molecules in and/or across the barrier medium within or surrounding the DDS. Here, Fick's laws of diffusion does not apply and such systems are classified further into; i) polymer membrane permeation-controlled DDS; ii) polymer matrix diffusion-controlled DDS; iii) polymer (membrane/matrix) hybrid-type DDS; and iv) micro-reservoir partition-controlled DDS[6]. RPPDDS discussed in this **chapter** pertains to a modified version of micro-reservoir partition-controlled DDS (**Fig 8**), where drug reservoir is a microgel containing solid drug particles suspended in an hydrogel matrix, which in turn is prepared using hydrophilic polymers, without any external membrane. Release of drug from the micro-reservoir type RPPDDS follows either dissolution- or a matrix diffusion-controlled process[19]. Typical commercial RPPDDS include transdermal delivery of nitroglycerin (Nitrodisc® System)[20-21], subdermal implant for the delivery of norgestomet (Syncro-Mate-C Implant)[19], transdermal delivery of levenorgestrol[20], etc, which are capable of sustained release for a period of 20 to 160 days.

As shown in **fig 7b**, release of curcumin from microgels with three different HEA contents exhibit three rates independent of time. Such modulated release rate can be employed for the efficient delivery of three different active agents such as anti-inflammatory agents, re-epithelialization promoter and growth factors to the wound bed. Effective healing of chronic wounds such as burn wounds and diabetic ulcers requires such time-bound delivery of multiple active agents at different time scale to foster the cascading healing process.

4.4. Conclusions

In this study, we report on the preparation of new DN hydrogel based on CMX and PHEA with robust mechanical properties compared to their SN hydrogels. Microgels prepared by the UV-assisted free-radical co-polymerization of HEA and SM using O/W emulsion technique, containing curcumin as the model drug, was embedded in the DN hydrogel matrix to design RPPDDS for sustained / controlled release of drugs. Three different drug delivery profiles were obtained by varying the hydrophilic – hydrophobic balance of the PHEA-co-SM copolymer, thereby modulating the permeability profile of hydrophobic drug molecule. Such DN hydrogel based DDS can be utilized for the efficient and optimized treatment of challenging patho-physiological scenarios.

4.5 References

(1) Peppas, N. A.; Huang, Y.; Torres-Lugo, M.; Ward, J. H.; Zhang, J. *Annual Review of Biomedical Engineering* **2000**, *2*, 9.

(2) Peppas, N. A.; Bures, P.; Leobandung, W.; Ichikawa, H. *Eur J Pharm Biopharm* **2000**, *50*, 27.

(3) Haraguchi, K.; Takehisa, T. *Adv Mater* **2002**, *14*, 1120.

(4) Karino, T.; Okumura, Y.; Ito, K.; Shibayama, M. *Macromolecules* **2004**, *37*, 6177.

(5) Gong, J. P.; Katsuyama, Y.; Kurokawa, T.; Osada, Y. *Adv Mater* **2003**, *15*, 1155.

(6) Chien, Y. W.; Lin, S. *Clinical Pharmacokinetics* **2002**, *41*, 1267.

(7) Frykberg, R. G.; Banks, J. *Advances in Wound Care* **2015**, *4*, 560.

(8) Hu, J.; Hiwatashi, K.; Kurokawa, T.; Liang, S. M.; Wu, Z. L.; Gong, J. P. *Macromolecules* **2011**, *44*, 7775.

(9) Shin, H.; Olsen, B. D.; Khademhosseini, A. *Journal of Materials Chemistry B* **2014**, *2*, 2508.

(10) York, W. S.; van Halbeek, H.; Darvill, A. G.; Albersheim, P. *Carbohyd Res* **1990**, *200*, 9.

(11) Savur, G. R.; Sreenivasan, A. *J Biol Chem* **1948**, *172*, 501.

(12) White, E. V.; Rao, P. S. *Journal of the American Chemical Society* **1953**, *75*, 2617.

(13) Khan, N. A.; Mukherjee, B. D. *Chem Ind-London* **1959**, 1413.

(14) Srivastava, H. C.; Singh, P. P. *Carbohyd Res* **1967**, *4*, 326.

(15) Davoodi, P.; Lee, L. Y.; Xu, Q.; Sunil, V.; Sun, Y.; Soh, S.; Wang, C.-H. *Adv Drug Deliver Rev* **2018**, *132*, 104.

(16) Pop, M. A.; Almquist, B. D. *Exp Dermatol* **2017**, *26*, 760.

(17) Mir, M.; Ali, M. N.; Barakullah, A.; Gulzar, A.; Arshad, M.; Fatima, S.; Asad, M. *Progress in Biomaterials* **2018**, *7*, 1.

(18) Saghazadeh, S.; Rinoldi, C.; Schot, M.; Kashaf, S. S.; Sharifi, F.; Jalilian, E.; Nuutila, K.; Giatsidis, G.; Mostafalu, P.; Derakhshandeh, H.; Yue, K.; Swieszkowski, W.; Memic, A.; Tamayol, A.; Khademhosseini, A. *Adv Drug Deliver Rev* **2018**, *127*, 138.

(19) Chien, Y. W. In *Methods in Enzymology*; Academic Press: 1985; Vol. 112, p 461.

(20) Karim, A. *Drug Dev Ind Pharm* **1983**, *9*, 671.

(21) Schneeweiss, A.; Marmor, A. *The American Journal of Cardiology* **1988**, *61*, 36.

Design and development of double network hydrogels from carboxymethyl cellulose for tissue-substitutes

Chapter – V

In the fifth chapter, DN hydrogels consisting of tightly cross linked carboxymethylcellulose (CMC) as the first network and loosely cross linked poly(hydroxyethylacrylate) (PHEA) as a second network were synthesized. The second network also contained a small amount of stearyl methacrylate (SM) as a co-monomer along with hydroxyl ethyl acrylate (HEA). Compressive strength of the CMC-PEHA-DN hydrogel was 280 times more than that of CMC-SN hydrogel and with increase in SM concentration DN hydrogels showed better recovery after mechanical deformation. Cell viability studies showed that the biocompatibility of DN hydrogels was enhanced as compared to SN hydrogels.

5.1 Introduction

Hydrogels are three-dimensional network of hydrophilic polymers which can imbibe copious amount of water and mimic the body tissues like extra cellular matrix (ECM). Hydrogels continue to find wide range of applications in drug delivery, tissue engineering, bio-implants, scaffolds, etc due to their unique physico-chemical properties such as softness, biocompatibility, water permeability, stimuli responsiveness, self-healing etc[1-5]. However, one of the major drawbacks of hydrogels is the lack of mechanical strength when they are subjected to load-bearing tissue applications. Therefore, efforts are being made to design and develop novel hydrogels with enhanced mechanical properties. For example, nanocomposite (NC) hydrogels[6], slide-ring (SR) hydrogels[7-8], tetra-PEG hydrogels[9] and double network (DN) hydrogels[10] which exhibit very good mechanical properties despite high water content have been reported in the recent past.

Amongst these new strategies to make robust hydrogels, DN hydrogels are becoming important[10]. Double network (DN) hydrogels comprises of two hydrogel networks in which the first and second networks are prepared sequentially. Two most crucial parameters involved in making the DN hydrogels are i) molar compositions of both networks and ii) the crosslinking ratio of first and second hydrogel networks. The molar ratio of second to first network is in the range of 10-30, contrary to inter-penetrating networks, which are in the range of 1-4. The first network is a highly crosslinked, rigid and serves as a sacrificial bond and the second network, a sparsely crosslinked, is ductile and flexible. Despite containing 60-90 % water, DN hydrogels exhibit very high fracture strength which is of the order of tens of Megapascals and show high wear resistance because of their very low coefficient of friction.

The DN hydrogels reported earlier were mainly prepared from synthetic polymers[10] and very little focus is given on synthesizing DN hydrogels based on natural polymers (**Table 5.1**) which are most desired for their bio-medical applications. For example, DN hydrogels prepared from natural polymers were reported on bacterial cellulose/gelatin[11-12], chitosan/PEG[13], etc.

Table 5.1: Double-network hydrogels reported in the literature which comprises of polysaccharide as either one or both networks, prepared with sequential two step process

Sl. No.	First Network	Second Network	Tensile Strength (MPa)	Compressive Strength (MPa)	Fracture Strength (MPa)
1.	Bacterial cellulose	Gelatin	2.7	3	-
2.	Bacterial Cellulose	PAAm	-	-	40 ± 10
3.	Methacrylated Chondroitin sulphate-co-PEGDA	PAAm	3.3	-	-
4.	Agar	PAAm	-	-	38
5.	Konjac glucoman - PVA	PAAm	0.1	30	-
6.	Hydroxy propyl guar gum	PAAm	-	-	0.843

In this work, we adopt a strategy to synthesize DN hydrogel from a polysaccharide viz. carboxymethylcellulose (CMC) and a synthetic poly(hydroxyethyl acrylate) (PHEA). The resulting DN hydrogel consisted of a tightly crosslinked CMC as the first network and loosely crosslinked PHEA as the second network. We also prepared DN hydrogels incorporating the hydrophobic stearyl methacrylate (SM) in the PHEA network. The presence of SM in the PHEA network enhances the viscous modulus keeping the overall elastic modulus constant and helps in energy dissipation mechanism through hydrophobic associations. The hydrophobic groups in SM associate and contribute to the enhanced stability of the network which is the most desired property of the medical applications. Hysteresis energy measurements demonstrated the role of SM in the energy dissipation mechanism. The morphology of the DN hydrogels was investigated by the state-of-the-art X-ray micro-computed tomography imaging technique.

5.2. Materials and Methods

5.2.1 Materials

Carboxymethyl cellulose sodium salt (CMC) was procured from Merck, India. Divinyl sulphone (DVS), hydroxyethyl acrylate (HEA), stearyl methacrylate (SM) and hydroxylmethylpropiophenone (HMPP) were purchased from Sigma Aldrich, India. Sodium dodecyl sulphate (SDS) was procured from Loba Chem, India. Dulbecco's modified Eagle medium (DMEM) was purchased from Invitrogen, USA. All the chemicals were of analytical grade and used as received. Distilled water was used for all the reactions unless specified otherwise.

5.2.2 Preparation of hydrogels and xerogels

Preparation of DN hydrogels consisted of two-step sequential process, where the first hydrogel network (from CMC) was prepared initially, followed by the in-situ preparation of the second hydrogel network (from PHEA or PHEA-co-SM). First and second hydrogel networks were also prepared separately and called single network (SN) hydrogels. Porous xerogels were prepared by lyophilization and non-porous xerogels were prepared by the vacuum drying process.

5.2.2.1 Preparation of SN hydrogels and xerogels

Solution of carboxymethyl cellulose was prepared by dissolving 0.4 gms of CMC in 10 ml of 0.1 M NaOH solution. 0.12 gms of 30 wt % DVS was added onto CMC solution, stirred for about 5 minutes, poured onto cylindrical teflon moulds (8 mm x 8 mm), stored at 15 ^{0}C for 12 hours and later the resultant hydrogels (as-prepared SN hydrogels) were swollen to equilibrium in distilled water with regular replenishment with distilled water. These CMC hydrogels were abbreviated as CMC single network (CMC-SN) hydrogels. Xerogels of CMC-SN were prepared by vacuum drying of equilibrium swollen CMC-SN at 50 ^{0}C.

A homogeneous aqueous solution containing 30 wt % HEA, 0.045 wt % SDS and 1 µL of photo initiator (HMPP) were poured onto cylindrical teflon moulds (8 mm x 8 mm) and exposed to UV irradiation in a closed chamber for 21 minutes. Hydrogels formed after irradiations were named as PHEA-SN hydrogels which were then swollen to equilibrium in distilled water. A hydrophobic co-monomer, namely, stearyl methacrylate (SM) was incorporated in the HEA monomer. The concentration of SM was varied from 2, 4 and 6 mol % of HEA content and the resultant SN hydrogels

were abbreviated as PHEA-co-SMx-SN hydrogels, wherein x denotes the mol % of SM. Xerogels of PHEA-SN and PHEA-co-SMx-SN's were prepared by vacuum drying of equilibrium swollen PHEA-SN and PHEA-co-SMx-SN's hydrogels at 50 ^{0}C.

5.2.2.2 Preparation of DN hydrogels

For the preparation of DN hydrogels, CMC-SN xerogels were immersed in 20 ml aqueous solution containing 30 wt % HEA, 0.045 wt % SDS and 1 µL of photo initiator (HMPP) and kept in roller mixer for 72 hours. The equilibrium swollen hydrogels with HEA, HMPP were irradiated with UV in a closed chamber for 21 minutes. Irradiated hydrogels (as-prepared DN hydrogels) were again swollen to equilibrium in distilled water with regular replenishment of distilled water at specific time intervals. Resultant DN hydrogels were composed of poly(hydroxyl ethyl acrylate) as the second network and were abbreviated as CMC-PHEA double network (CMC-PHEA-DN) hydrogels.

DN hydrogels with the second network comprising of poly (hydroxyl ethyl acrylate – co – stearyl methacrylate) copolymer were prepared by UV irradiation of equilibrium swollen CMC-SN hydrogels in 30 wt % aqueous solution of HEA with 2 mol % SM, 0.045 wt % SDS and one µL HMPP. The concentration of SM was varied from 2, 4 and 6 mol % of HEA. The as-prepared DN hydrogels after UV irradiation were swollen again in distilled water and were abbreviated as CMC-PHEA-co-SMx-DN, wherein x denotes the mol % of SM. Porous xerogels were prepared from DN hydrogels (CMC-PHEA-co-SM0-DN) by lyophilization technique, and non-porous xerogels were prepared by vacuum drying of equilibrium swollen CMC-PHEA-co-SMx-DN hydrogels.

5.2.3 Swelling studies

As-prepared hydrogels (both SN and DN) were kept immersed in distilled water until equilibrium, with replenishment of distilled water at regular time intervals. The weight of the equilibrium swollen hydrogels was noted (*Ws*) and dried in an oven at 50 ^{o}C until the weight remained constant. The weight of these vacuum dried xerogels was noted (*Wd*). Swelling percentage was calculated from eqn. (1).

5.2.4 FTIR spectroscopy

Xerogels of both SN and DN were powdered, mixed with KBr to form pellets. FTIR measurements were performed using Perkin Elmer Spectrum One IR spectroscope.

5.2.5 NMR spectroscopy

Liquid-state ^{1}H NMR spectra of xerogels were recorded using a Bruker Avance AQS spectrometer (Bruker, Germany). The spectrometer was operated at a carbon frequency of 75MHz, and the samples were spun at 8 kHz in a 4mm triple resonance probe. About 4000 scans were accumulated with an inter-scan delay of 2.5 s.

5.2.6 Gelation time

Rheometer (Model 301, Anton Paar, Austria) equipped with a cup and bob geometry was used to measure the time required for the gelation of CMC single network hydrogels cross-linked by DVS. About 4 ml of CMC solution was charged onto the cup, 30 wt % DVS as added, stirred for 2 minutes. Time sweep measurements were performed at constant strain, frequency and temperature (15 ^{0}C) within the linear visco-elastic regime. Storage modulus (G') and loss modulus (G") were measured as a function of time until the gelation occurred.

5.2.7 Uni-axial compression studies

5.2.7.1 Uni-axial compressive strength

Universal testing machine (UTM) (Model 5943, Instron, MA, USA) was used to measure the compressive strength of the equilibrium swollen hydrogels. The hydrogel was placed on the lower compression plate, and the upper compression plate was set at a speed of 3 mm/min to measure the compressive strength of hydrogel during fracture. Stress and strain were recorded and plotted by Bluehill software (Instron, MA, USA). Measurements were repeated thrice, and average values were reported.

5.2.7.2 Cyclic-strain and step-strain measurements

Two types of repeated compressive strain measurements were performed by applying viz., cyclic-strain and step-stain using UTM. These measurements were carried out using an experimental setup shown in **fig 5.1**, where compression experiments were performed on hydrogel, immersed in a temperature-controlled water bath (BioPuls Bath, Instron, MA, USA) kept at $37^{0}C$, which creates an *in-vitro* environment closer to the physiological conditions. These simulated conditions could overcome the errors

caused by de-hydration of hydrogels, especially during compression experiments which require a prolonged time period.

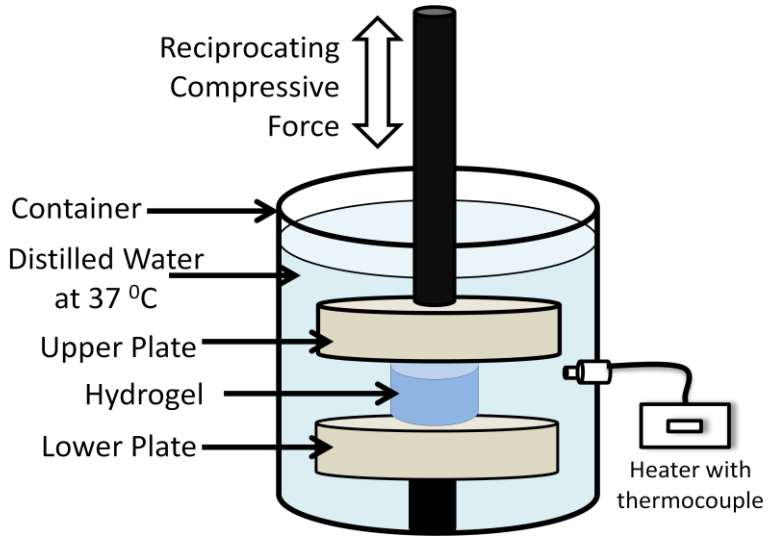

Figure 5.1: Schematic representation of the setup for simulated mechanical experiments

In the cyclic-strain experiment, a constant compressive strain (50%) was applied for 50 consecutive loading and unloading cycles without any time interval between the cycles. Upper compression plate was set at a speed of 10 mm/min and the hydrogel was compressed upto 50 % strain and the platen was returned to the initial position to complete one cycle. Similarly, 50 cycles were repeated on a single hydrogel and the measurements were replicated. During the measurements, hydrogel was placed in a water bath which was kept at 37 ± 0.5 ^{0}C (**fig 5.1**).

In a step-strain experiment, 10 % compressive strain was applied in the first compressive cycle followed by a linear increase of 10 % strain per cycle up to a maximum of 60 % strain, without any interval between the loading and unloading cycles. Upper compression plate was set at a speed of 10 mm / min and the measurements were repeated thrice. During the measurements, hydrogel was placed in a water bath which was kept at 37 ± 0.5 ^{0}C (**fig 5.1**).

5.2.7.3 Stress relaxation

Stress relaxation measurements were performed using UTM equipped with the experimental setup shown in **fig 5.1**. The hydrogel was placed in a water bath which is kept at 37 ^{0}C. Upper compression plate was used to apply a constant compressive

strain (50%) continuously for 60 mins and released afterwards. Compressive stress was measured and recorded as a function of time.

5.2.8 3D micro-CT imaging and simulation of flow velocity

As prepared CMC-PHEA-SM0-DN hydrogels were swollen to equilibrium in distilled water and lyophilized for 48 hours to prepare porous xerogels. Porous xerogels with an approximate size of 4 x 4 mm were loaded onto micro-computed tomography (micro-CT) (Model Xradia Versa 510, Carl Zeiss X-ray Microscopy, Pleasanton, CA) where 3201 X-ray projections were acquired with 360^0 rotation at 50 kV X-ray source, with a pixel size of 3.98 microns. Acquired projections were subjected to back projection algorithm to reconstruct a series of virtual cross-sectional 2D images of porous xerogels. 2D images were cropped to a size of 1300 x 900 x 1000 microns, filtered with non-local means filter and segmented using PoroDict® (Math2Market GmbH, Kaiserslautern, Germany) image processing software to constructa three-dimensional image of porous xerogels to visualise its microstructure. Image segmentation process also differentiates pores in the xerogels with the aid of Otsu global threshold selection method and quantifies porosity and pore-size distribution in xerogels.

Three-dimensional micro-structural geometry data of porous xerogels was loaded onto FlowDict® software (Math2Market GmbH, Kaiserslautern, Germany) and flow velocity of water through the porous microstructure at a given pressure drop were computed (Darcy's Law) along three different axes (X, Y and Z) at 25^0 C. Periodic boundary condition and 20 Pa limiting pressure drop were two major experimental process parameters adopted during the flow simulation experiment. Average flow velocity was computed in three axes with <1 % error. 2D virtual cross-sections and 3D images depicting the visualization of flow velocity in porous xerogels were also computed.

Fluid flow properties of porous xerogels were computed from their respective 3D image data sets using *FlowDict*® software package (Math2Market GmbH, Kaiserslautern, Germany). Mean flow velocity in all three axes of the 3D model is predicted for a given pressure drop using this image solver. In FlowDict®'s post-processing step, the relationship between the predicted pressure drop, fluid viscosity

and media thickness expressed in Darcy's law is used to compute and output the material's permeability.

5.2.9 *In-vitro* cytotoxicity studies

Hydrogels were soaked in 70% ethanol/water mixture overnight and dried in vacuum oven followed by 30 minutes UV exposure inside a biosafety cabinet. Vacuum dried xerogels were again soaked in sterile PBS before use in a 24 well plate. Healthy L929 fibroblast cell lines (passage number 58) were maintained using complete DMEM. 50,000 cells suspended in 500 μL complete media were plated in each well along with the soaked hydrogels in triplicates. It was incubated in 5% CO_2 at 37°C for two days. 100 μL of 600 μM resazurin solution in DMEM media was added to each well followed by 6 hours incubation in 5% CO_2 at 37°C. The entire plate was read in a plate reader (excitation 530 to 560 nm and emission at 590 nm). For calculating the cell viability, emission due to 100 μM resazurin in DMEM was incorporated, normalized with negative control (only cells) and incorporated with standard error.

5.3. Results and discussion

5.3.1 Preparation of double network hydrogels and xerogels

The concept of double network hydrogels proposed by J P Gong *et al*[10], essentially consisted of two synthetic networks, *viz.*; brittle and hard first network followed by the ductile second network. Many of the earlier works report on the use of fully synthetic polymers for the preparation of DN hydrogels. Our objective in this work was to prepare a semi-synthetic DN hydrogel using a biopolymer namely, carboxy methyl cellulose (CMC) as a first network (**Scheme 5.1**) and PHEA as the second network (**Scheme 5.2**).

CMC is a biocompatible, biodegradable and inexpensive, simple polysaccharide. It is an FDA approved polymer for several biomedical applications. PHEA is also a biocompatible polymer and provides good visco-elastic properties to the hydrogel. In order to provide more elasticity to the first network, a long chain (C_{18}) monomer, SM was copolymerized with PHEA. SM induces an efficient energy dissipation mechanism due to the formation of hydrophobic associations.

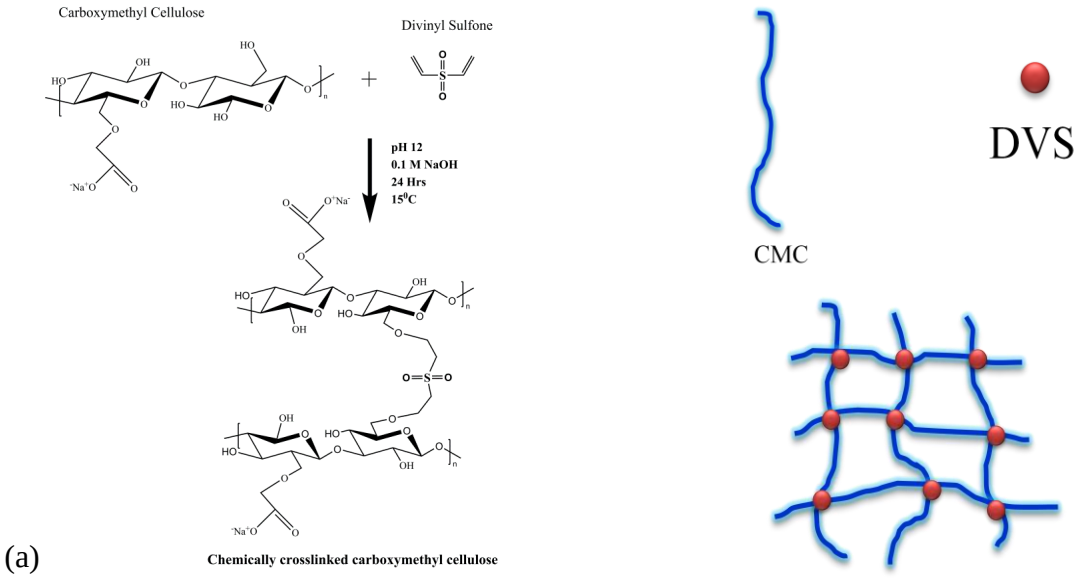

Scheme 5.1: (a) Cross-linking reaction of CMC with DVS and (b) schematic representation of CMC hydrogel network

The post-crosslinking of CMC network was performed using Michael-type addition reaction between the primary alcohols groups of CMC and the vinyl groups of di vinyl sulphone, catalyzed by a base in an aqueous medium. The cross-linking reaction pathway is shown in **Scheme 5.1**.

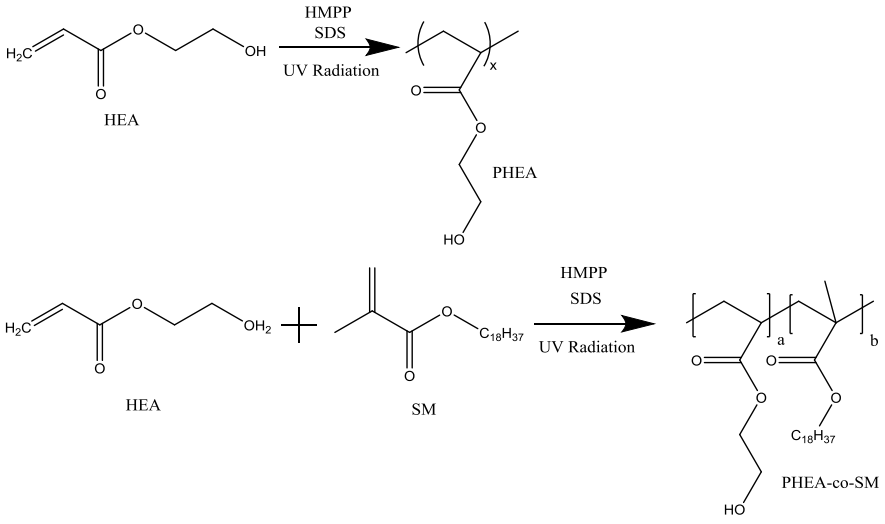

Scheme 5.2: Reaction pathway for PHEA and PHEA-co-SM

Subsequently, the xerogel of the CMC first network was swollen in the monomer solution containing HEA and HEA-SM along with the surfactant and in-situ

polymerized using a UV initiator (**Scheme 5.3**). The reaction pathway is shown in **Scheme 5.2**. Hence, DN strategy, which generally follows a dual-step sequential preparation protocol, provides a pathway to combine the physico-chemical characteristics of both CMC and PHEA. This is distinctly different from the IPN preparation where single-pot preparation protocols are invariably followed. Schematic representation of the sequential preparation of CMC-PHEA-co-SM DN hydrogels are given in **scheme 5.3**.

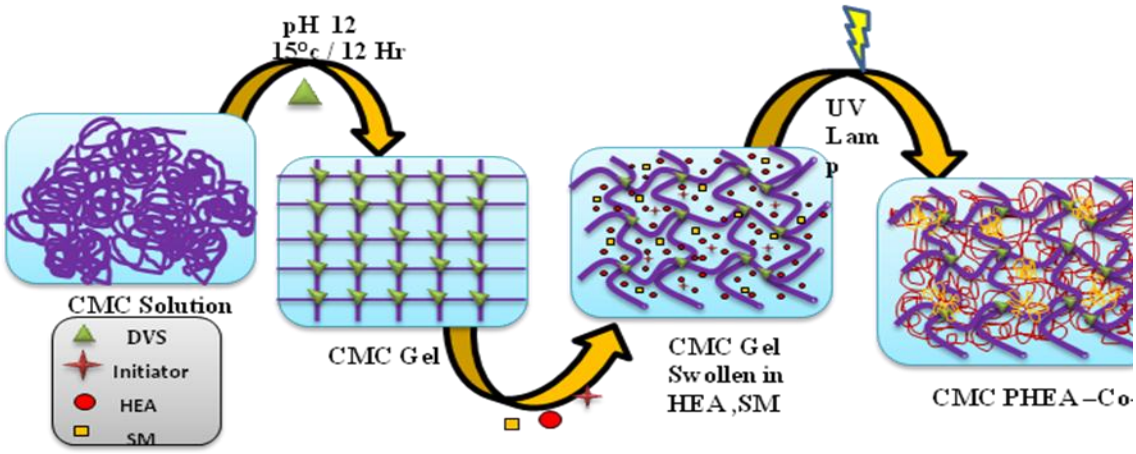

Scheme 5.3: Two-stage preparation process for CMC-PHEA-co-SM-DN hydrogel

5.3.2 Spectroscopic studies

NMR spectroscopic studies were performed to elucidate the chemical structure of CMC, PHEA, PHEA-co-SM and CMC-PHEA-co-SM6 DN xerogels. ^{1}H NMR spectra of CMC (**Fig 5.2**) shows cumulative signals from both equatorial and axial protons pertaining to glucose backbone. Signals from anomeric protons appear around 5.0 to 5.6 ppm and those from the protons involved in β 1-4 linkage appears at 4.46 ppm. **Fig 5.3** shows ^{1}H spectra of PHEA with their characteristic peaks assigned to the chemical structure. **Fig 5.4** shows ^{1}H NMR spectra of PHEA-co-SM with their characteristic peaks assigned to the chemical structure. **Fig 5.5** shows the ^{1}H NMR spectra of CMC-PHEA-co-SM6 DN.

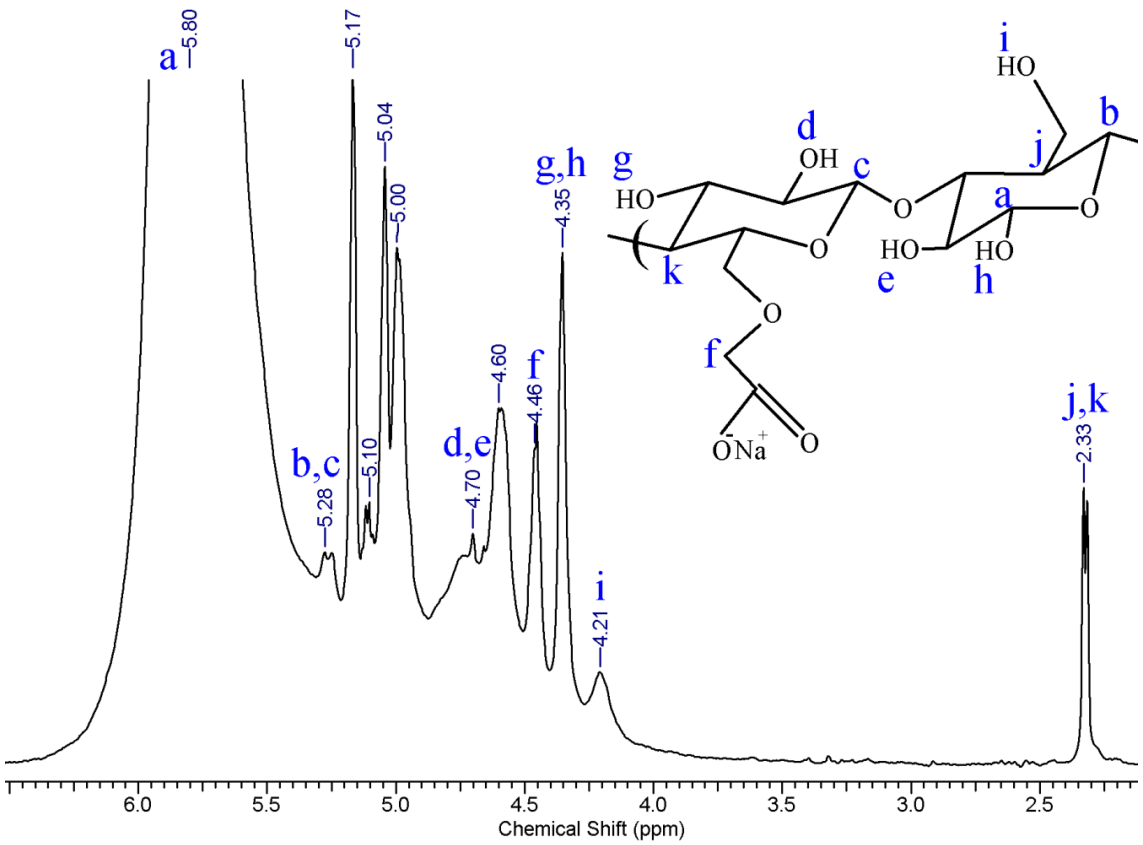

Figure 5.2: ^{1}H NMR spectrum of **CMC**

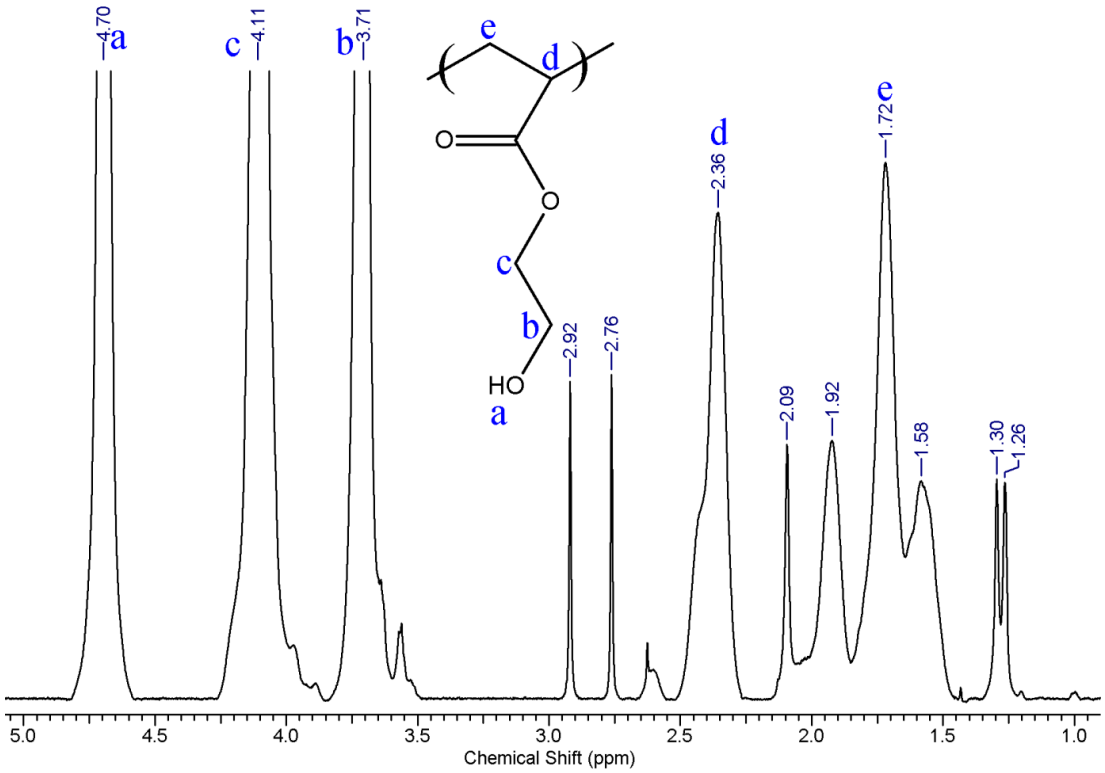

Figure 5.3: ^{1}H NMR spectrum of **PHEA**

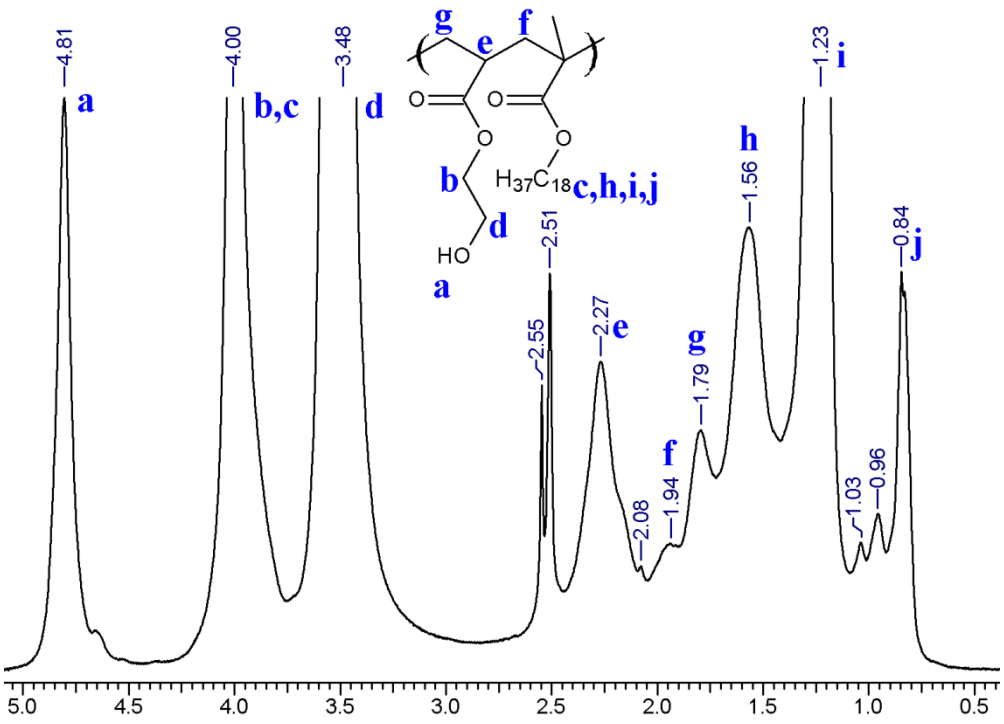

Figure 5.4: ^{1}H NMR spectrum of **PHEA-co-SM6**

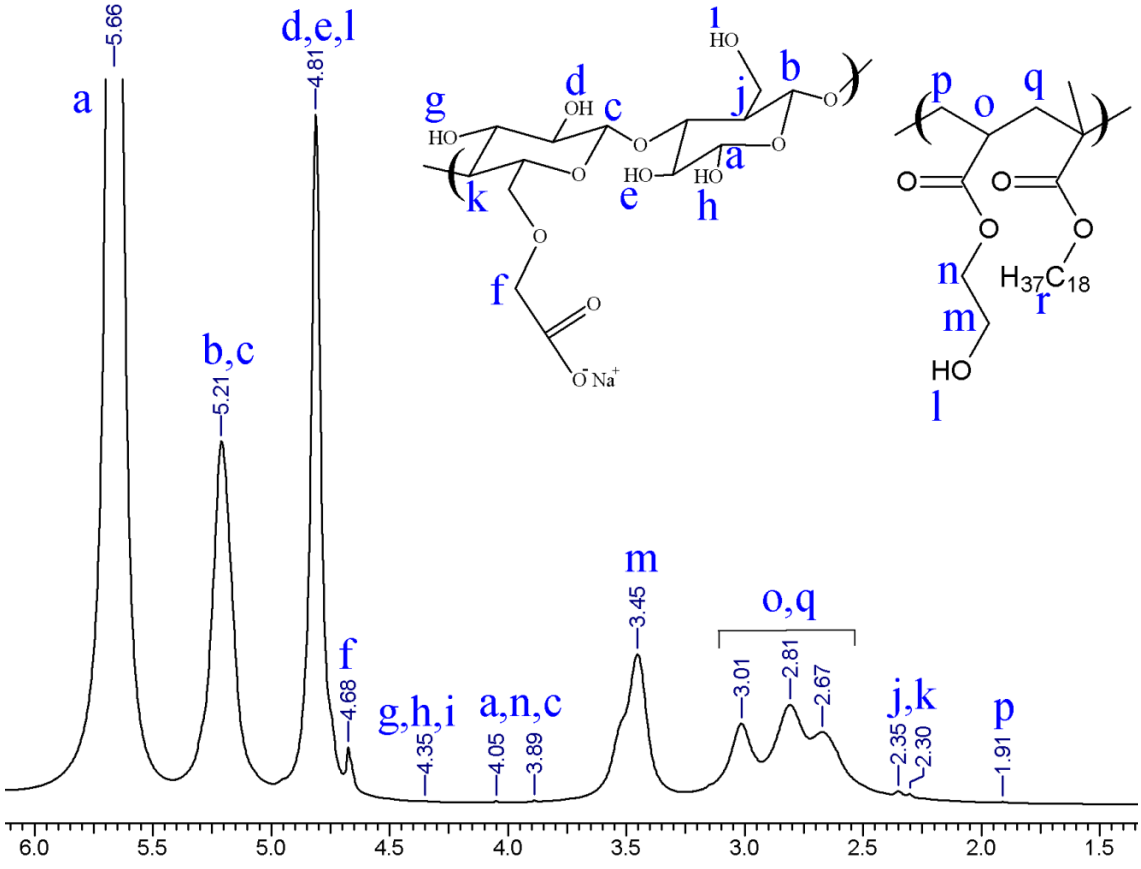

Figure 5.5: ^{1}H NMR spectrum of **CMC-PHEA-co-SM6 DN**

FTIR spectra of CMC-SN, PHEA-SN, PHEA-co-SM-SN, CMC-PHEA-DN and CMC-PHEA-co-SM-DN xerogels are shown in **fig 5.6**. Characteristics peaks are assigned in **Table 5.2,** where CMC SN shows C=O stretching of its carboxyl group at 1700 cm^{-1} and C-O-H in-plane bending at 1430 cm^{-1}. These two characteristic peaks were also seen in the DN xerogels. Aliphatic C=O stretching peak of PHEA-SN at 1750 cm^{-1} and its second overtone of C-H stretching at 1165 cm^{-1} are seen in PHEA-co-SM-SN and DN xerogels. Asymmetric C-H stretching of methyl group in SM are shown at 2890 cm^{-1} which is also evident in CMC-PHEA-co-SM DN xerogels. This confirms the chemical structure of the DN xerogels.

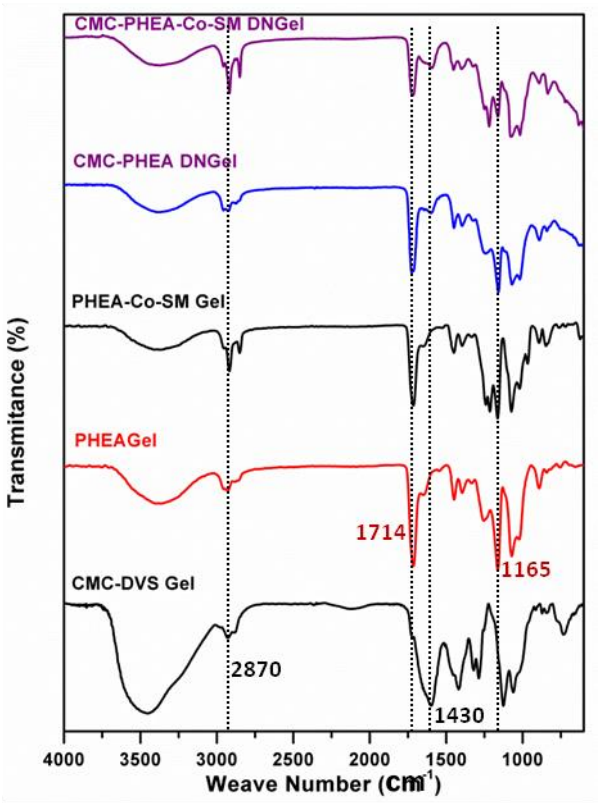

Figure 5.6: FTIR spectra of CMC-SN, PHEA-SN, PHEA-co-SM6-SN, CMC-PHEA-DN and CMC-PHEA-co-SM6-DN xerogels

5.3.3 Swelling behaviour of hydrogels

The swelling ratios of SN and DN hydrogels were given in **fig 5.7a**. CMC-SN hydrogels show lower swelling ratio compared to PHEA-SN and all other DN hydrogels. This could be attributed to the fact that, although polyelectrolyte-based hydrogels generally exhibit high swelling ratios, the presence of high crosslink

density in CMC-SN hydrogels predominates over the charge repulsion and results into lower swelling ratios.

Table 5.2: Assignment of peaks in FTIR spectra

FTIR Spectral Assignment					
CMC-PHEA-co-SM6-DN Xerogel					
Peak Position (cm^{-1})	1165	1430	1700	1750	2870
Assignment	Second overtone of C-H stretching	C-O-H in-plane bending	C=O stretching of carboxyl group	Aliphatic C=O stretching	Methyl Assymetric C-H stretching
CMC-PHEA-DN Xerogel					
Peak Position (cm^{-1})	1165	1430	1700	1750	-
Assignment	Second overtone of C-H stretching	C-O-H in-plane bending	C=O stretching of carboxyl group	Aliphatic C=O stretching	-
PHEA-co-SM6 Xerogel					
Peak Position (cm^{-1})	1165	-	1714	1750	2870
Assignment	Second overtone of C-H stretching	-	First overtone of C-H stretching	Aliphatic C=O stretching	Methyl asymmetric C-H stretching
PHEA-SN Xerogel					
Peak Position (cm^{-1})	1165	-	1714	1750	-
Assignment	Second overtone of C-H stretching	-	First overtone of C-H stretching	Aliphatic C=O stretching	-
CMC-SN Xerogel					
Peak Position (cm^{-1})	-	1430	1700	-	-
Assignment	-	C-O-H in-plane bending	C=O stretching of carboxyl group	-	-

The selling ratio of PHEA-SN hydrogel is approximately five times more than the CMC-SN hydrogel which is due to the low crosslink density of the PHEA-SN hydrogel. On the other hand, DN hydrogels with 0, 4 and 6 mol % SM show swelling ratios similar to that of PHEA-SN hydrogels with a small gradual increase from 2 to 6 mol % SM. The error bars of all hydrogels except CMC-SN shows a high degree of overlap with each other, which indicates an insignificant effect of hydrophobic SM on the swelling ratios.

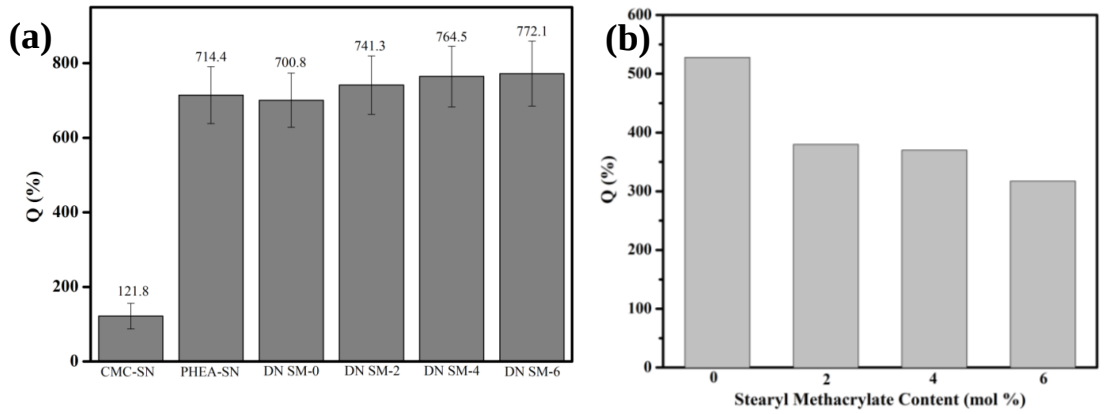

Figure 5.7: Swelling percentage of (a) single network and double network hydrogels and (b) PHEA-SN hydrogels with 0, 2, 4 and 6 mol % SM, in the absence of SDS

Generally, the presence of hydrophobic moiety in the hydrophilic polymer network is expected to reduce the swelling of the overall network in water. However, in the presence of surfactants, which is residual and tightly bound to the hydrophobic moiety, micelle formation helps to enhance swelling, which is evident from **fig 5.7a and b**. Similar swelling profile in the presence of surfactants is reported earlier in micellar co-polymerized hydrogels[14]. In the absence of SDS, the swelling decreases with an increase in SM content. **Fig 5.7b** shows the swelling percentage of PHEA-SN hydrogels with 0, 2, 4 and 6 mol % SM in the absence of SDS.

5.3.4 Gelation time

Rheological measurements were performed to study the time required for the formation of CMC-SN hydrogel, cross-linked by DVS. Cross-linker is added to the CMC solution and loaded on to Rheometer to study the change in visco-elastic characteristics of the solution. Generally, during the cross-linking reaction in

polymers, elastic characteristics of polymer solutions gradually increase over and above its viscous counterpart, due to the formation of cross-links between the polymer chains. Results were shown in **fig 5.8**, where storage modulus (G') and loss modulus (G") were plotted as a function of time. Storage and loss modulus represents the elastic and viscous response from the solution, respectively. During the initial stage of the measurement (before 10 mins), G" dominates over G', which indicates viscous nature of the solution. Gradually, over a period of time, G' slowly increases, crosses over G" after 15 mins and progressively increases further. This observation shows that gelation takes place 15 mins after the addition of cross-linker in CMC solution and the modulus of the resultant hydrogels gradually increase further.

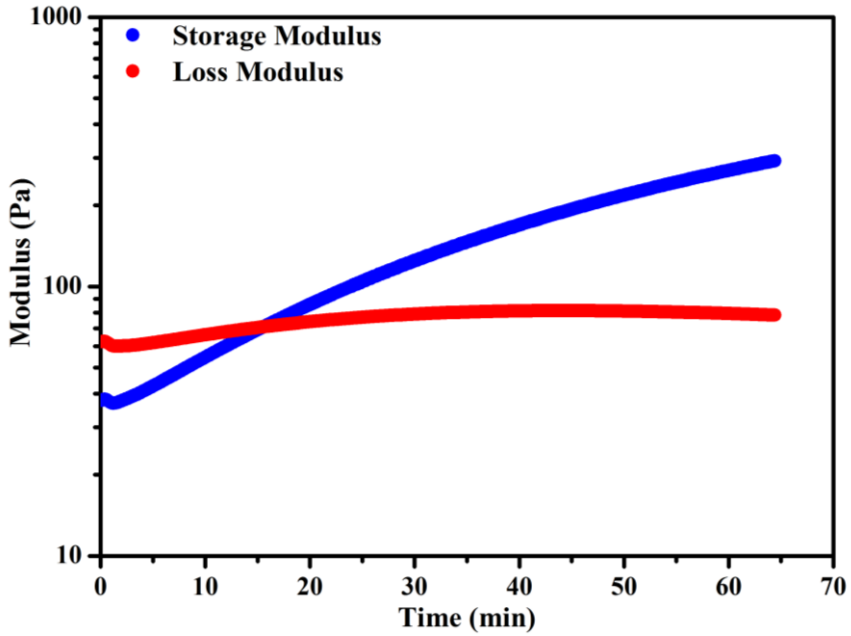

Figure 5.8: Plot of storage modulus (G') and loss modulus (G") as a function of time of CMC-SN hydrogel with 30 wt % DVS

5.3.5 Uni-axial compression

The mechanical strength of equilibrium swollen SN and DN hydrogels were evaluated by measuring their compressive strength using UTM. Initially, the mechanical strength of as-prepared CMC-SN hydrogels were measured with an increase in cross-linker concentration (**Fig 5.9a**). Cross-linker concentration was increased from 20, 25 and 30 wt % DVS and measurements were performed on the as-prepared hydrogels to study the effect of cross-linker concentration on the compressive strength of as prepared CMC SN hydrogels. As seen in **fig 5.9a**, as- prepared CMC-SN hydrogels with 30 wt. % DVS showed a threefold increase in compressive strength as compared

to the one with 25 wt. % DVS. The equilibrium swollen CMC-SN and PHEA-SN hydrogels showed compressive strengths of 5 and 615 kPa respectively, whereas DN hydrogel showed the compressive strength of 1.4 MPa (**Fig 5.10a**).

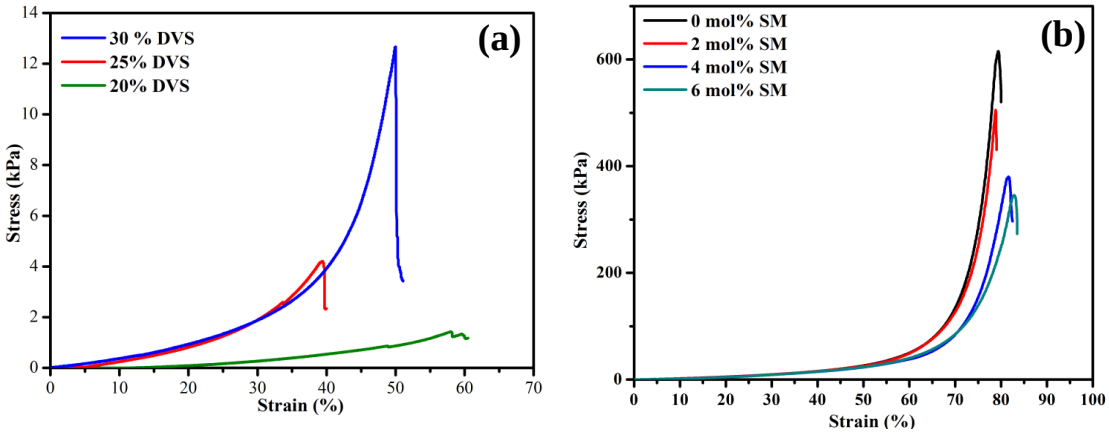

Figure 5.9: Stress vs strain plot of (a) as prepared CMC-SN hydrogels with 20, 25, 30 wt. % DVS and (b) equilibrium swollen PHEA-SN hydrogels with 0, 2, 4 and 6 mol % SM

As seen in **fig 5.10a**, equilibrium swollen CMC-SN hydrogel is very brittle, weak and fractures at very lower stress (~5 kPa). PHEA-SN hydrogel, on the other hand, can withstand major compressive force and strain compared with CMC-SN hydrogels. PHEA-SN network is also highly compressible as evident from the strain at break (~ 80 %). DN hydrogel shows a remarkable increase in its compressive strength, which is more than two-folds of that of PHEA-SN.

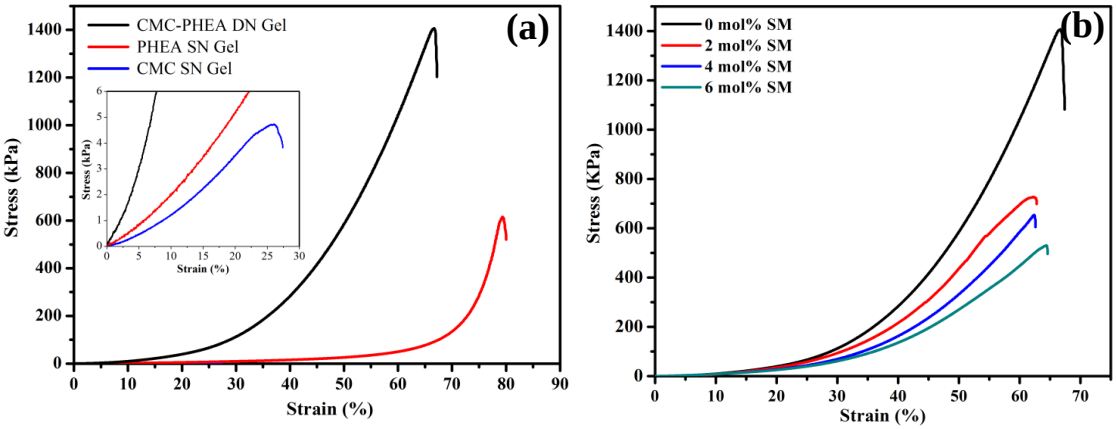

Figure 5.10: Stress vs strain plot of (a) CMC-SN, PHEA-SN, CMC-PHEA-DN and (b) CMC-PHEA-co-SM-DN hydrogels with 0, 2, 4 and 6 mol % SM

The compressive strength of as prepared CMC-PHEA-DN hydrogels is 5 MPa, which is 3.5 times higher than that of equilibrium swollen hydrogels (**Fig 5.11**) and attains very high compressibility before fracture (~ 90%). This observation is primarily due to the lower fraction of water content in the as prepared hydrogels compared to equilibrium swollen hydrogels. In the as prepared hydrogels, upon compression, entangled polymer chains of the network have potential for volumetric expansion, which leads to higher compressibility and simultaneously, can impart higher resistance against the compressive force. On the contrary, in the equilibrium swollen hydrogels, the polymer networks are already pre-stretched to a higher extent, within the limitations of their mesh size (ξ), hence attains lower compressibility. Also, these networks cannot withstand higher compressive force before fracture, compared to as prepared hydrogels. In the previous reports on DN hydrogels, the outstanding mechanical properties[10,15] were investigated mostly in as prepared hydrogels. However, considering the swelling characteristics of hydrogels and their applications in the biomedical areas, mechanical properties in the equilibrium swollen hydrogels are important. Hence, in this work, mechanical properties of equilibrium swollen hydrogels are studied in detail.

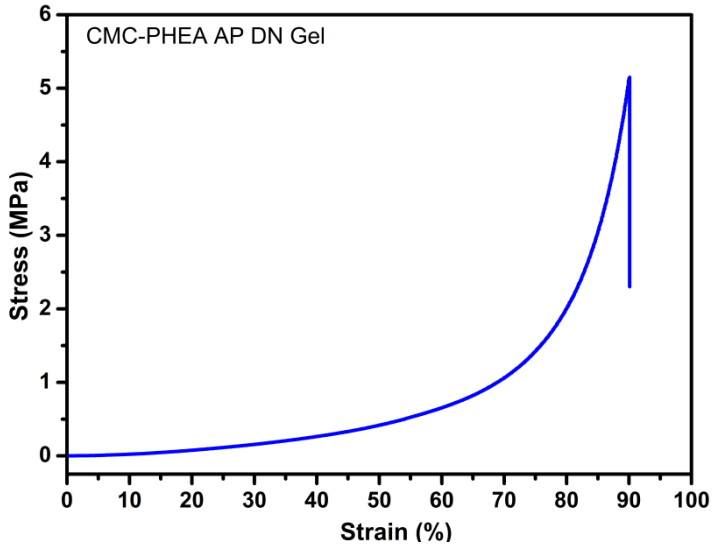

Figure 5.11: Stress vs strain plot of as prepared CMC-PHEA-DN hydrogels.

The enhancement of the compressive strength in DN hydrogel is attributed to the effective stress distribution which arises from the synergistic combination of brittle CMC network and ductile PHEA network. This observation is in line with the Double network hydrogels, first reported by Jian Ping Gong et al [10,16-18]. Further, the role of SM in modulating the mechanical behaviour of PHEA-SN and CMC-PHEA-DN

hydrogels was investigated by measuring the compressive strength of PHEA-SN (**fig 5.9b**) and CMC-PHEA-DN hydrogels with 0, 2, 4, and 6 mol % SM (**fig 5.10b**). With an increase in SM concentration, compressive strength shows a gradual decrease in PHEA-SN hydrogels. However, the strain at break increases with an increase in SM concentration. This is attributable to the formation of more ductile and soft hydrogel network with an increase in SM concentration. The role of SM in the energy dissipation of DN hydrogels was further studied by cyclic-strain, step-strain and stress relaxation measurements.

Entanglement of the second network is another parameter which contributes to toughening of DN hydrogels[18], that arises from its higher molecular weight. Therefore, DN hydrogels derived from poly(acrylamide) possess robust mechanical characteristics due to their inherent high molecular weight. In this work, photo-polymerization of HEA inside partially swollen first network leads to the formation of PHEA network with infinite molecular weight which in turn results in a mechanically robust DN hydrogels. IPNs are a well-known conventional method to prepare hydrogels with higher mechanical strength by combining two or more polymer networks. However, in this case, phase separation inhibits the process to prepare IPN hydrogels from CMC and PHEA. Therefore, to the best of our knowledge, the sequential preparation process reported in this work is the first one to prepare hydrogels from CMC and PHEA.

5.3.6 Hysteresis energy

Cyclic-strain compression measurements were performed on DN hydrogels with varying SM concentration to study the role of SM in modulating energy dissipation mechanism in the network. During the cyclic-strain compression studies, DN hydrogels were compressed up to 50 % strain and relaxed consecutively to its initial state to complete one compression cycle. Such repeated loading and un-loading cycles were carried out upto a total of 50 cycles, without any interval between the cycles. **Fig 5.12a** shows the stress vs. strain plots of 50 loading and unloading cycles of DN hydrogels with 0, 2, 4 and 6 mol % SM, wherein a major difference in hysteresis is observed between first cycle and the rest. Resultant hysteresis energy is calculated using eqn. (4) and plotted in **fig 5.12b**.

$$U_{50} = \frac{\int_0^{0.5\ loading} Fds - \int_0^{0.5\ unloading} Fds}{\pi R^2} \quad \ldots\ldots\ldots\ldots\ldots\ldots\ldots\ldots (2)$$

Where, U_{50} represents dissipated energy, F is the loading, s is the displacement and R is the radius. U_{50}It is calculated by measuring the area of the cycle and the surface area of the hydrogel. It implies that higher dissipation energy in the first cycle may be due to the breakage of bonds primarily in the first network during the compression.

Hysteresis energy is a direct indication of the energy dissipation in hydrogels, which is a ratio of energy absorbed during its mechanical compression and released during the reversal of compressive force. Lower the loss of energy during the reversal of compressive force, higher the efficacy in the dissipation of energy by the hydrogels[19].

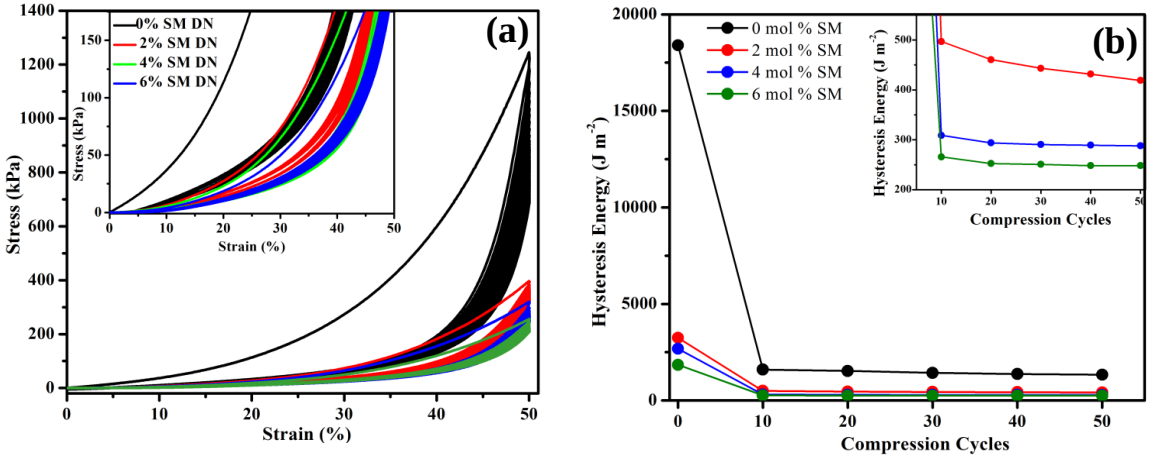

Figure 5.12: (a) Stress – strain plot of cyclic-strain measurements of DN hydrogels and (b) corresponding hysteresis energy is plotted as a function of compression cycles

It is evident from **fig 5.12a**, that in DN hydrogels, with increase in SM concentration, the hysteresis loop size and respective compressive stress decreases. There exists a major difference in loop size between DN hydrogel without SM and the one with 2 mol % SM. This major difference is reflected in the hysteresis energy of DN hydrogel with and without SM. This clearly indicates the role of SM in increasing the energy dissipation capability of DN hydrogels at lower SM concentration. DN hydrogel with 2 mol % SM shows 4.5 times lower energy compared to the DN hydrogel without SM. However, beyond 10 cycles of compression, any significant reduction in energy is not observed.

There exists a considerable difference between the hysteresis area observed in the first and second cycle. It may be attributed to the irreversible fracture of network during the loading of first cycle [19]. However, from second cycle onwards, a more or less elastic loading is observed with limited hysteresis and strain hardening.

5.3.7 Step-strain cycles

Step-strain compression cycles were performed on DN hydrogels to analyze the variation in energy dissipation with increase in compressive strain. During the measurement, 10 %strain was applied in the first loading and unloading cycle followed by 20, 30, 40, 50 and 60 % strain in the subsequent cycles. DN hydrogels with 0, 2, 4 and 6 mol % SM were studied.

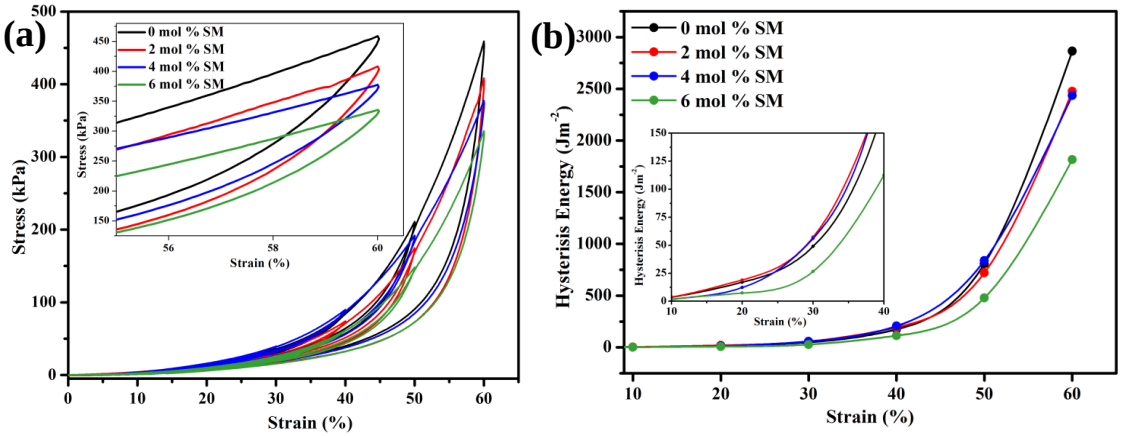

Figure 5.13: (a) Stress – strain plot of step-strain experiments and (b) hysteresis energy of DN hydrogels with 0, 2, 4 and 6 mol % SM

Fig 5.13a shows the loading and unloading curves of step-strain compression experiments for all DN hydrogels and the corresponding hysteresis energy per cycle is plotted as a function of strain in **fig 5.13b**. In **fig 5.13a**, it is observed that hysteresis between the loading and un-loading cycles are prominent after 30 % strain. Below 30 % strain, loading and unloading curves show major overlapping between each other which is an indication of significantly lower energy loss between the cycles. Hysteresis energy difference is evident in the higher strain cycles (as shown in inset of **fig 5.13a** and **fig 5.13b**), where with increase in SM (**fig 5.14**), energy loss is reduced significantly.

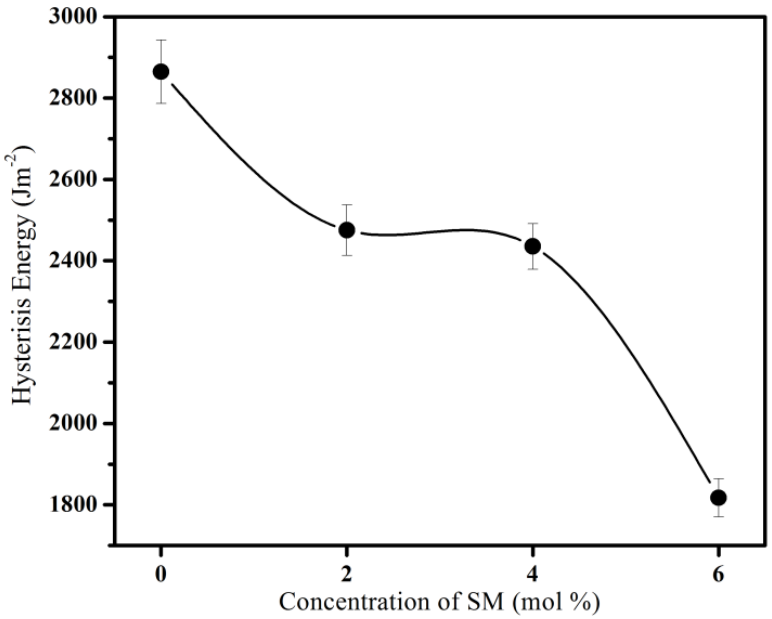

Figure 5.14: Hysteresis energy calculated from 60 % compression cycle of step-strain measurements were plotted as a function of SM concentration

5.3.8 Stress relaxation

The ability of a hydrogel network to recover from prolonged force of deformation is studied by stress relaxation experiment using UTM. In this experiment, the hydrogel was placed in the bath at 37 ^{0}C and immediately subjected to 50 % compression, and kept on hold for 60 minutes. The resisting force of the hydrogel was recorded, normalised and plotted as stress vs. time (log scale) in **fig 5.15a**. It can be readily seen from **fig 5.15a** that, stress decays gradually over a period in the case of DN hydrogel with 0 and 2 mol % SM. However, DN hydrogels with 4 and 6 mol % SM show better resistivity towards the applied deformation force and their stress decay is significantly lower.

In **fig 5.15b**, the slopes of the curves are plotted as a function of SM concentration, wherein the dotted line is a guide to the eye, with a slope value of 1. It denotes a linear relationship among the SM concentration and the recovery behaviour of DN hydrogels. Stress relaxation plot of CMC-SN and PHEA-SN hydrogels are given in **fig 5.16**, where it is evident that gradual stress decay is shown by CMC-SN, whereas PHEA-SN shows two different stages of decay. Both SN hydrogels were not able to withstand force of deformation and the network structure deteriorates over a period of time.

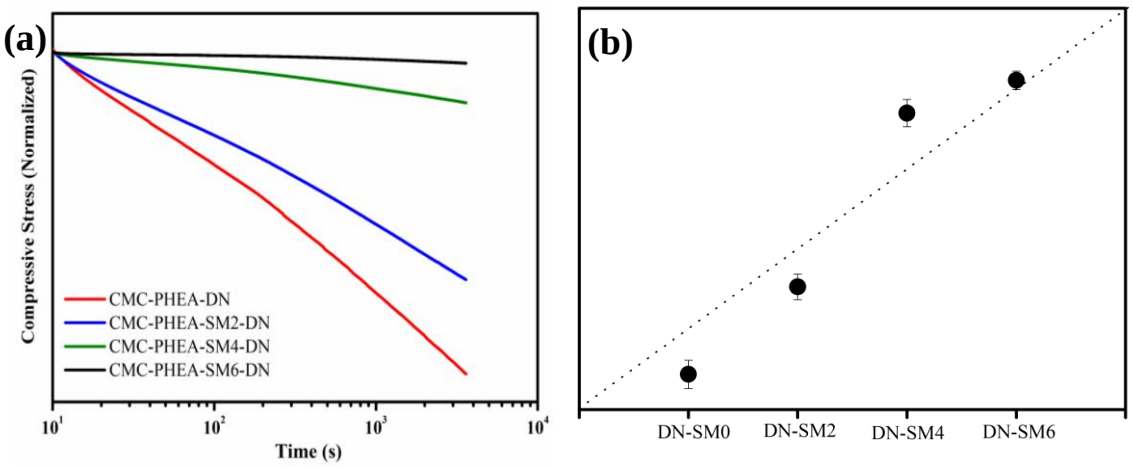

Figure 5.15: Stress relaxation: (a) Normalized stress vs. time plot of DN hydrogels with 2, 4 and 6 mol % SM and (b) their corresponding slope were plotted with an increase in SM concentration

SM volume fraction is responsible for dissipation of energy within in the DN network as evident from relaxation experiments (**fig 5.15a**). This hydrophobic co-monomer, solvated by surfactant (SDS) molecules, in the hydrophilic environment, positions themselves in a rather coiled or entangled state. During compression, they un-coil and/or stretch out themselves, for which more energy is consumed during the process. However, during the un-loading cycle, they coil back to their native state, enabling the network to recover the initial volume.

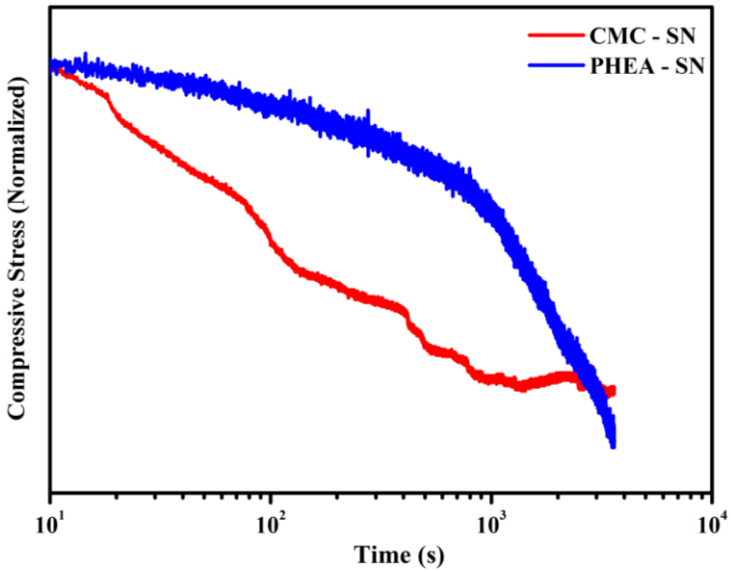

Figure 5.16: Stress relaxation plot of CMC-SN (25 % Strain) and PHEA-SN hydrogels (50% Strain).

Conventional hydrogels used for biomedical applications are found to be vulnerable to stress-induced formation of cracks and voids, which affects the integrity of hydrogel network, resulting in the loss of functionality and service life of devices or implants. Tough hydrogel networks with inherent energy dissipation mechanism are ideal for such environments, which mimic the self-regeneration mechanism of natural tissues. These two major properties can be merged through the design of DN hydrogels, where one network contributes towards the toughness of the hydrogel and other imparts ductility.

CMC-PHEA-SM6-DN hydrogels reported in this work pertains to the class of *truly independent*-DN hydrogels[20], where first and second network does not possess any covalent bonds between each other. Higher mechanical strength of such DN hydrogels may be attributed to the entanglements arising from the second network. Such DN hydrogel networks can be further toughened by imparting cross-links in the second network. However, in this study, we incorporated hydrophobic co-monomer in the second network which can further enhance the energy dissipation mechanism of the DN hydrogels. Interconnected spherical domains of micelles containing the surfactant and hydrophobic blocks plays a key role in this process, supported by hydrophobic association of the alkyl chains[21].

5.3.9 3D micro-CT imaging of porous xerogels

Porous polymeric structures have found potential applications in tissue engineering and regenerative medicine[22-26]. Micro-CT, a non-destructive three-dimensional X-ray imaging technique was used to study the microstructure of DN hydrogels. During the imaging process, radiographic projections (**Fig 5.17**) of the specimen are recorded at different angles by rotating the specimen. 2D cross-sectional images or slices shown in f**ig 5.17 b & c** were generated from these radiographic projections using back-projection reconstruction algorithm. Image segmentation process helps to generate 3D image of the xerogels (**Fig 5.18a**) after differentiating voxels pertaining to xerogels and those of pores.

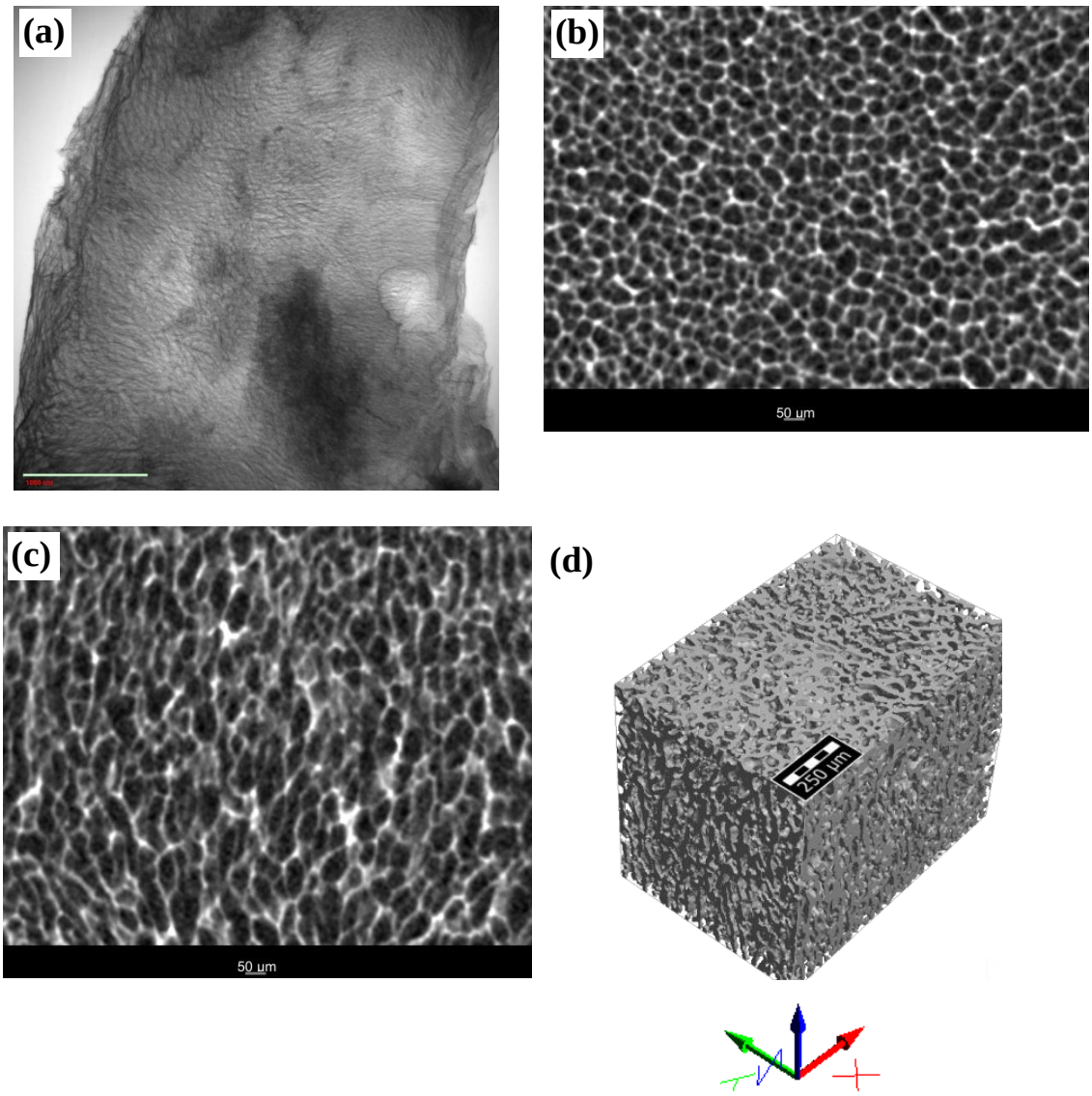

Figure 5.17: Images generated by micro-CT during the image acquisition process of CMC-PHEA-DN porous xerogel: (a) X-ray projection image (scale bar in 1mm), (b) 2D slice in horizontal axis (scale bar in 50 microns), (c) 2D slice in vertical axis (scale bar in 50 microns) and (d) 3D image of porous xerogel (scale bar in 250 microns)

Fig 5.18a shows the 3D image of porous xerogels (1300 x 900 x 1000 microns size) which has 70 % porosity. Porosity and pore-size distribution of these xerogels were calculated with the aid of image analysis package (PoroDict®, Math2Market GmbH, Kaiserslautern, Germany) and the resultant 3D visualization of pore-size distribution is given in **fig 5.18b** along with color-coded scale. Xerogels contains pores in the

range of 4 to 70 microns as depicted in the color-scale, with an average size of 36 microns **(Fig 5.19 & 5.20)**.

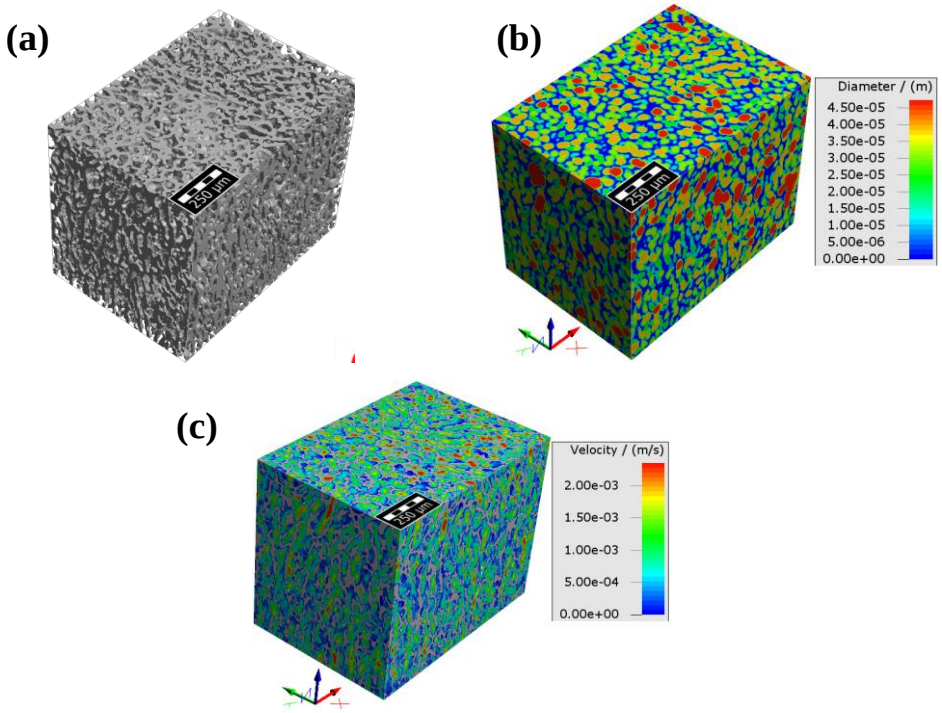

Figure 5.18: (a) 3D image of porous xerogel (CMC-PHEA-SM0-DN) (scale bar is 250 microns), (b) its pore-size distribution and (c) flow velocity visualization with color-code scale

3D visualizations of pores differentiated based on their size with appropriate color-code are shown in **fig 5.19 (a, b & c)**. Visualization of pores in the entire size range (4 to 70 microns) are shown in **fig 5.19a**, whereas pores in the size range of 35 to 70 microns are shown in **fig 5.19b** and **fig 5.19c** shows pores in the range of 45 to 70 microns. These observations provide insight into the spatial distribution of pores in the overall 3D volume of xerogels relative to their size.

Results of the colour-coded visualization of flow simulation studies were shown in **fig 5.21** and **fig 5.22** with appropriate colour-scale. Three axes (X, Y and Z) along with the vertical as well as horizontal cross-sectional faces of the 3D micro-structure geometry of the xerogels were shown in **fig 5.21b**.

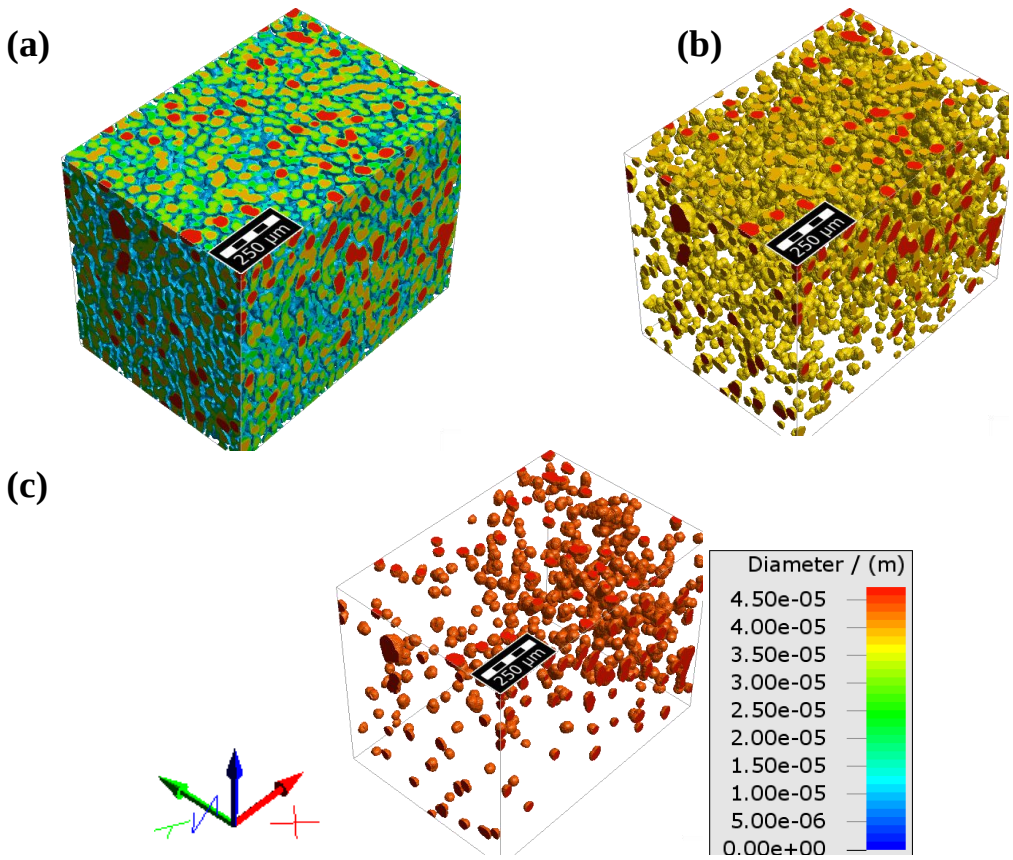

Fig 5.19: 3D visualizations of pores in the (a) 4 to 70 microns range, (b) 35 to 70 microns range and (c) 45 to 70 microns range in CMC-PHEA-DN porous xerogel with color-code

(scale bar in 250 microns)

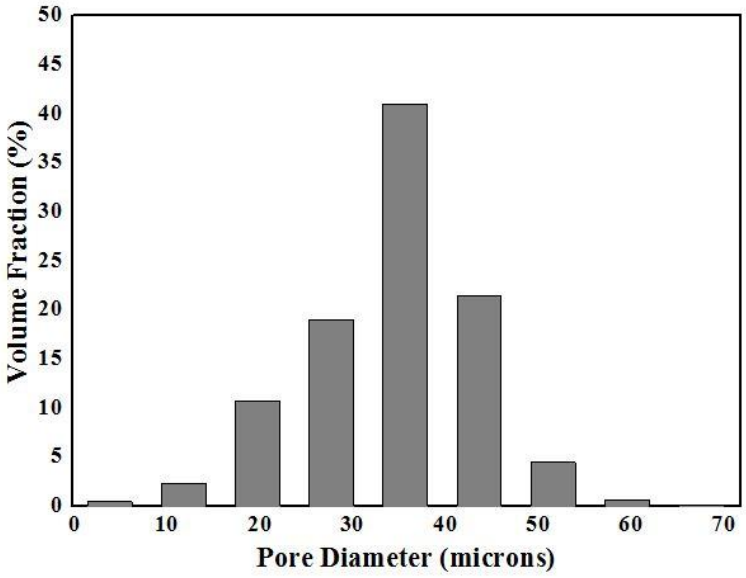

Figure 5.20: Histogram of pore-size distribution is given as a function of pore-volume fraction

Mapping of the flow velocity in horizontal and vertical cross-sections are shown in **fig 5.21 a** and **b**. As shown in colour legend, region of red represents higher flow velocity and decrease down the order and low velocity profiles are represented by blue. Maximum flow velocity in Z-axis was 5.47 x 10^{-4} m/s whereas that in the X and Y axes were 2.84 x 10^{-4} m/s and 2.0 x 10^{-4} m/s, respectively. This clearly indicates a higher flow velocity in the Z-axis which denotes orientation of pores in the Z-axis. This observation is supported by the flow mapping observed in Z-axis (**fig 5.21a**), where flow channels shows more or less a cylindrical shape, aligned in Z-axis.

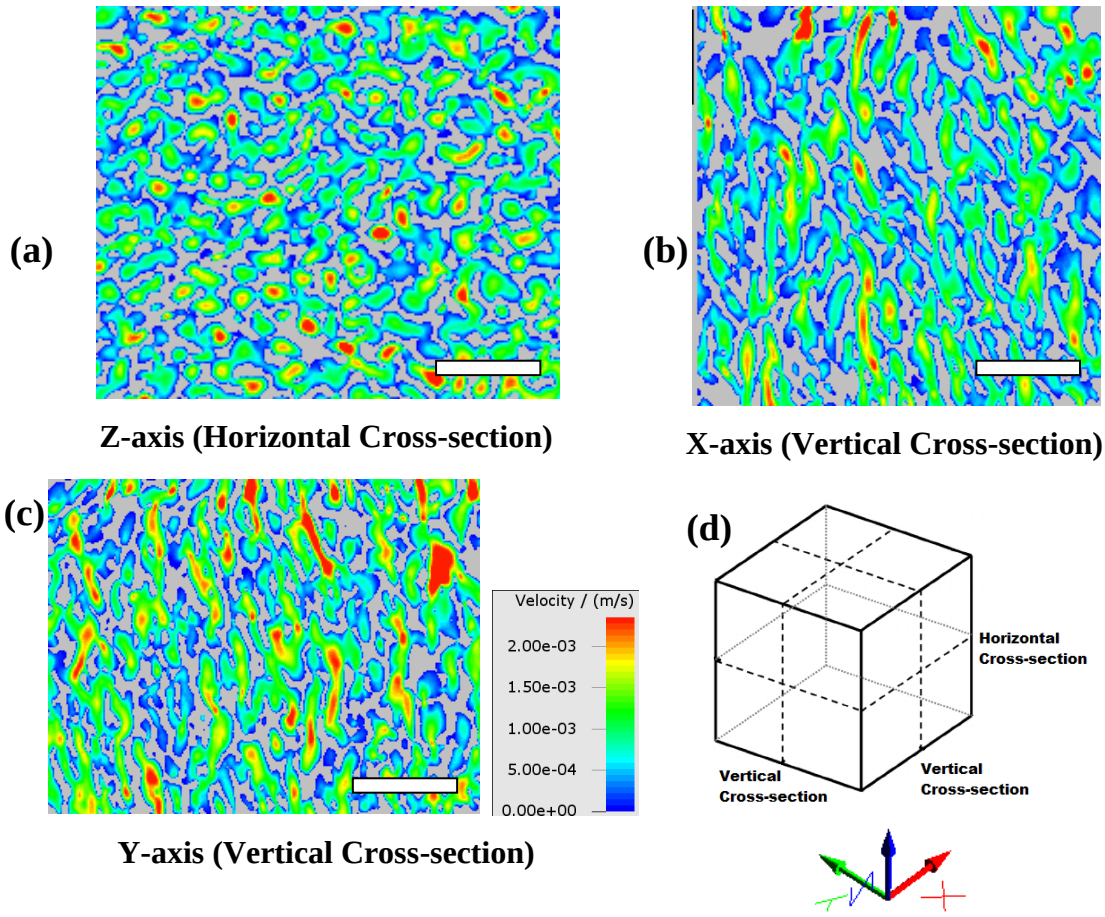

Figure 5.21: 2D cross-sections of flow visualizations in (a) horizontal and (b), (c) two lateral vertical cross-sections with color-coded velocity (scale bar is 150 microns) in porous xerogels,
(d) cube-model as a guidance to identify vertical and horizontal cross-sections

We have used the 3D micro-structural geometry of the porous xerogels obtained through micro-CT imaging to study the flow velocity of water through these pores in all the three coordinates[27-29]. Flow of water is simulated along all the three axis of segmented 3D image models with pressure drop of 20 Pa under ambient conditions.

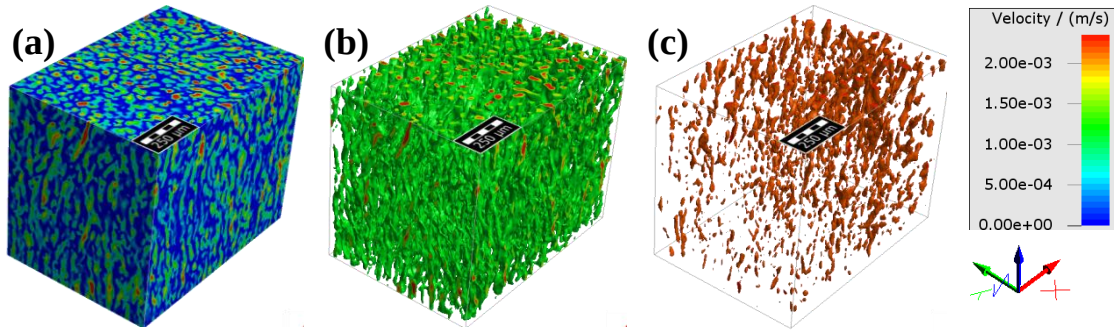

Figure 5.22: 3D visualizations of (a) overall flow velocity (from 0 to 2.5 (x 10^{-3} m/s), (b) velocity in the range 0.5 to 1.5 (x 10^{-3} m/s) and (c) velocity in the range 2 to 2.5 (x 10^{-3} m/s) with color-code (scale bar in 250 microns).

The flow velocity of water through pores with numerical simulations was performed using *FlowDict*® software. Flow channels were categorized based on their flow velocity and shown in **fig 5.22**, where flow channels with higher flow velocity are depicted with red colour (**fig 5.22 c**). Orientation of these high velocity channels are also in the Z-axis which could be due to different ways of formation of pores in these systems. Lyophilization technique utilizes forced sublimation in the uni-axial direction which results in the formation of pores oriented in that direction. Xerogels with such oriented pores are ideal for applications in polymer scaffolds for the regeneration of vascular tissue, which possess oriented multi-layer tissue constructs.

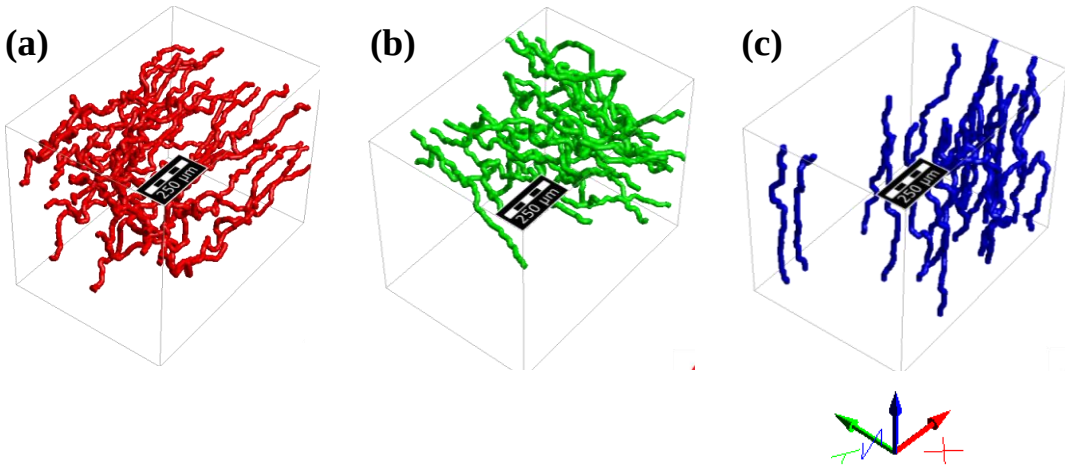

Figure 5.23: 3D visualizations of end-to-end percolation paths inside porous xerogels in (a) X, (b) Y and (c) Z axis (scale bar in 250 microns)

Cell proliferation and migration of cell clusters inside porous scaffolds are essential for the development of viable tissue constructs for their regeneration, which requires inter-connected pores in scaffold[24-25]. We performed simulation of percolation pathways inside the 3D micro-structural geometry to verify the presence of end-to-end connected pores. Percolations of 20 spheres with 35 micron diameter were simulated from one side of the xerogel to the other and their pathways in all three axes were shown in **fig 5.23**. Since the average pore size were 35 microns, these pathways represent the probable inter-connected pores available across the entire axis for the proliferation and migration of cell clusters throughout the 3D micro-structure.

5.3.10 *In-vitro* cytotoxicity

In-vitro cell viability tests were performed on SN and DN hydrogels using L929 fibroblast cell lines, to evaluate their toxicity and cell viability. Results of the study are shown in **fig 5.24**, where a negative control (only cells) is also plotted along with SN and DN hydrogels. While considering the error bar limits, CMC-SN hydrogels showed similar cell viability as that of negative control, whereas PHEA- SN showed 16 % reduction in cell viability. Polysaccharide hydrogels are generally highly biocompatible due to their sugar-rich backbone and other bio-mimetic characteristics, whereas, synthetic polymers without any bioactive moieties were unable to enhance cell proliferation[30].

Significant increase in cell viability was observed in the case of DN hydrogels with 0, 2 and 4 mol % SM. This is due to the fact that, DN hydrogels could be more flexible with enhanced diffusion characteristics. Further, the incorporation of SM might induce more elastic property and relaxation to the hydrogel which helps in the transport of cells. However, at high content of SM, the hydrophobic effect may curtail the cell viability. These observations are in line with the earlier report where, the cell proliferation and differentiation are enhanced in hydrogels with higher relaxation[31]. Hence, this remarkable increase in cell viability of DN hydrogels may be attributed to the engineered network structure which possesses higher energy dissipation mechanism compared to its SN counterparts.

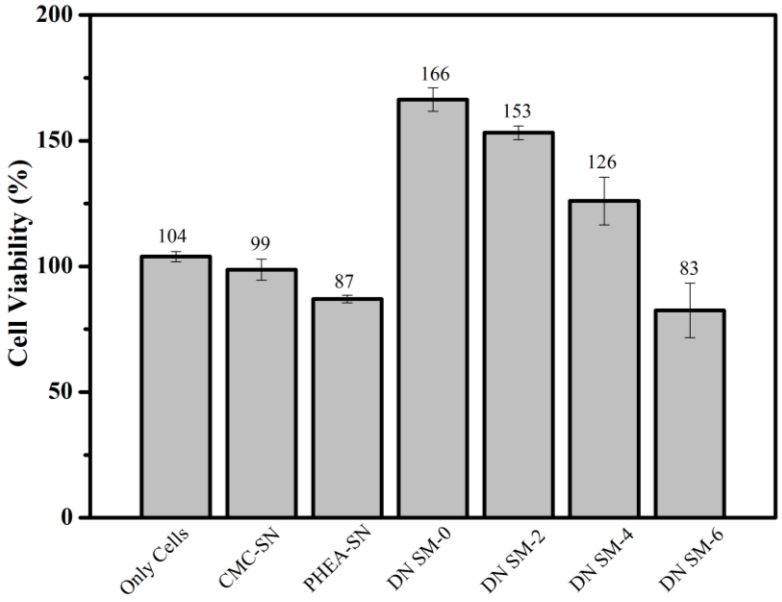

Figure 5.24: Cell viability of SN and DN hydrogels along with control

Biocompatibility of hydrophilic polymer hydrogels such as poly(HEMA) and poly(HEA) are well studied and reported [32], however hydrogels derived from poly(acrylamide) are known to induce significant inflammatory responses[32-34]. Therefore, biomedical applications of DN hydrogels prepared from poly(acrylamide) are limited even though they possess higher mechanical strength[10]. In this scenario, DN hydrogels prepared from PHEA are more superior over poly(acrylamide) counterparts due to their applicability in the biomedical scenario.

DN hydrogels prepared from bacterial cellulose[11] are reported to have significantly higher mechanical strength (3.7 MPa). However, their mechanical performance depends upon the directionality of the applied force and is due to the stratified structure of fiber network in bacterial cellulose. On the other hand, DN hydrogels prepared using plant-derived cellulose, one of the most abundant renewable polymer resource, is direction independent and provides more sustainable solution.

5.4. Conclusions

In this study, we have reported on the preparation of a new DN hydrogel based on CMC and PHEA which possess higher compressive strength compared to its SN hydrogels. We also demonstrated that, the incorporation of a hydrophobic co-monomer, SM in the second network imparts efficient energy dissipation mechanism which is evidenced from the hysteresis energy measurements. Compressive strength

of the CMC-PEHA-DN hydrogel was found to be 280 times more than that of CMC-SN hydrogel. With increase in SM concentration, DN hydrogels showed better recovery after deformation. Stress relaxation measurements showed the ability of DN hydrogels to recover from force of deformation after a prolonged time period. This was possible due to the coiled nature of hydrophobic polymer fractions within the DN structure. Results of micro-CT 3D imaging and simulation studies shows the presence of oriented and inter-connected pores in the xerogels with an average pore-size of 35 microns.

DN hydrogels showed very good cell viability and the biocompatibility of DN hydrogels was enhanced due to better response of cells towards hydrogel network structure with faster relaxation rates and also due to the presence of bioactive polysaccharide units in it. These hydrogels have great potential in tissue engineering, implant coating, surface modification, etc.

5.5 References

(1) Annabi, N.; Tamayol, A.; Uquillas, J. A.; Akbari, M.; Bertassoni, L. E.; Cha, C.; Camci-Unal, G.; Dokmeci, M. R.; Peppas, N. A.; Khademhosseini, A. *Adv Mater* **2014**, *26*, 85.

(2) Tanaka, Y.; Gong, J. P.; Osada, Y. *Progress in Polymer Science* **2005**, *30*, 1.

(3) Li, J.; Mooney, D. J. **2016**, *1*, 16071.

(4) Lim, H. L.; Hwang, Y.; Kar, M.; Varghese, S. *Biomaterials Science* **2014**, *2*, 603.

(5) Hunt, J. A.; Chen, R.; van Veen, T.; Bryan, N. *Journal of Materials Chemistry B* **2014**, *2*, 5319.

(6) Haraguchi, K.; Takehisa, T. *Adv Mater* **2002**, *14*, 1120.

(7) Karino, T.; Okumura, Y.; Ito, K.; Shibayama, M. *Macromolecules* **2004**, *37*, 6177.

(8) Karino, T.; Shibayama, M.; Ito, K. *Physica B-Condensed Matter* **2006**, *385*, 692.

(9) Sakai, T.; Matsunaga, T.; Yamamoto, Y.; Ito, C.; Yoshida, R.; Suzuki, S.; Sasaki, N.; Shibayama, M.; Chung, U. I. *Macromolecules* **2008**, *41*, 5379.

(10) Gong, J. P.; Katsuyama, Y.; Kurokawa, T.; Osada, Y. *Adv Mater* **2003**, *15*, 1155.

(11) Nakayama, A.; Kakugo, A.; Gong, J. P.; Osada, Y.; Takai, M.; Erata, T.; Kawano, S. *Adv Funct Mater* **2004**, *14*, 1124.

(12) Yasuda, K.; Gong, J. P.; Katsuyama, Y.; Nakayama, A.; Tanabe, Y.; Kondo, E.; Ueno, M.; Osada, Y. *Biomaterials* **2005**, *26*, 4468.

(13) Xu, Y.; Xie, J.; Gao, H.; Cao, Y.; Chen, M.; Liu, Y.; Zeng, B.; Chang, F.-C.; Dai, L. *Macromol Res* **2015**, *23*, 2.

(14) Algi, M. P.; Okay, O. *Eur Polym J* **2014**, *59*, 113.

(15) Sun, J. Y.; Zhao, X. H.; Illeperuma, W. R. K.; Chaudhuri, O.; Oh, K. H.; Mooney, D. J.; Vlassak, J. J.; Suo, Z. G. *Nature* **2012**, *489*, 133.

(16) Gong, J. P. *Soft Matter* **2010**, *6*, 2583.

(17) Na, Y. H.; Kurokawa, T.; Katsuyama, Y.; Tsukeshiba, H.; Gong, J. P.; Osada, Y.; Okabe, S.; Karino, T.; Shibayama, M. *Macromolecules* **2004**, *37*, 5370.

(18) Tsukeshiba, H.; Huang, M.; Na, Y. H.; Kurokawa, T.; Kuwabara, R.; Tanaka, Y.; Furukawa, H.; Osada, Y.; Gong, J. P. *J Phys Chem B* **2005**, *109*, 16304.

(19) Webber, R. E.; Creton, C.; Brown, H. R.; Gong, J. P. *Macromolecules* **2007**, *40*, 2919.

(20) Nakajima, T.; Furukawa, H.; Tanaka, Y.; Kurokawa, T.; Osada, Y.; Gong, J. P. *Macromolecules* **2009**, *42*, 2184.

(21) Can, V.; Kochovski, Z.; Reiter, V.; Severin, N.; Siebenbürger, M.; Kent, B.; Just, J.; Rabe, J. P.; Ballauff, M.; Okay, O. *Macromolecules* **2016**, *49*, 2281.

(22) Langer, R.; Vacanti, J. P. *Science* **1993**, *260*, 920.

(23) Yang, S.; Leong, K.-F.; Du, Z.; Chua, C.-K. *Tissue Eng* **2001**, *7*, 679.

(24) Hutmacher, D. W. *Biomaterials* **2000**, *21*, 2529.

(25) Mooney, D. J. *Cranio Grow* **1998**, *34*, 225.

(26) Kretlow, J. D.; Mikos, A. G. *Aiche J* **2008**, *54*, 3048.

(27) Van Cleynenbreugel, T.; Schrooten, J.; Van Oosterwyck, H.; Vander Sloten, J. *Medical and Biological Engineering and Computing* **2006**, *44*, 517.

(28) Ohser, J.; Schladitz, K. *3D Images of Materials Structures: Processing and Analysis*; John Wiley & Sons, 2010.

(29) Ohser, J.; Mücklich, F. *Statistical Analysis of Microstructures in Materials Science*; John Wiley & Sons: Chichester, 2000.

(30) Shoichet, M. S. *Macromolecules* **2010**, *43*, 581.

(31) Chaudhuri, O.; Gu, L.; Klumpers, D.; Darnell, M.; Bencherif, S. A.; Weaver, J. C.; Huebsch, N.; Lee, H.-p.; Lippens, E.; Duda, G. N.; Mooney, D. J. *Nature Materials* **2016**, *15*, 326.

(32) Langer, R.; Brem, H.; Tapper, D. *J Biomed Mater Res* **1981**, *15*, 267.

(33) Aras, D.; Cakar, Z.; Ozkavukcu, S.; Can, A.; Cinar, O. *Plos One* **2017**, *12*, e0172026.

(34) Manjanatha, M. G.; Aidoo, A.; Shelton, S. D.; Bishop, M. E.; McDaniel, L. P.; Lyn-Cook, L. E.; Doerge, D. R. *Environmental and Molecular Mutagenesis* **2006**, *47*, 6.

Design and development of self-healing double network hydrogels from alginate for enhanced bio-mineralization

Chapter – VI

In the sixth chapter, we designed and synthesized self-healing DN hydrogels, comprising of alginate as the first network and PHEA-co-SM as the second network. Salt-assisted co-polymerization route helped to incorporate 10 Wt. % of SM onto the second network which in turn exhibited self-healing property. Elastic modulus and thermo-reversible characteristics of the first network were studied by rheology. Step strain oscillatory rheological measurements and uni-axial tensile measurements were used to study the self-healing characteristics of the second network hydrogels and the DN hydrogels. These DN hydrogels also enhanced bio-mineralization process of hydroxyappatite, confined within the DN hydrogel network.

6.1 Introduction

To address the mechanical weakness of hydrogels used in biomedical applications a plethora of new methodologies are adopted. One important strategy among them is autonomous self-healing hydrogels. Self-healing is an inherent property which enables a hydrogel to intrinsically and automatically heal damages induced by external deformation thereby restoring itself back to normalcy. It occurs without the intervention of any external stimulus and helps to self-mend damage and regain its mechanical properties[1]. Self-healing properties are chemically or compositionally incorporated directly into the polymer backbone or side groups through incorporation of reversible bonds such as dynamic cross-links or reactions[1-2].

The domain of self-healing and self-recovering hydrogels comprises of two major approaches; dynamic covalent reactions[3-4] (chemical cross-linking) and non-covalent interactions (physical cross-linking). For autonomous self-healing hydrogels, the non-covalent reactions are generally preferred, separately or in combination, such as ionic bonding[5], hydrogen-bonding[1], supramolecular interactions[6], hydrophobic bonding[7], and molecular diffusion with chain entanglement[1]. In the case of self-healing hydrogels comprising of two or more polymer networks, presence of reversible non-covalent interactions in all the polymer networks enhance the overall healing efficiency and time of the resultant hydrogel systems. However, healing efficacy and time reduces drastically (< 100%) if only one network possess reversible functional moieties[8].

Self-healing hydrogels find applications in vast domains of research such as robotics, actuators, packaging, drug delivery, tissue engineering, regenerative medicine, 3D printing, implantable bioelectronics, etc[9]. In this work, we have designed a self-healing double network (DN) hydrogel based on alginate for applications in fostering regeneration of mineralized hard-tissues such as cartilages and bones. To enhance the efficacy of self-healing process we have introduced reversible non-covalent interactions in both hydrogel networks of DN hydrogel.

In the first network of alginates, reversible ionic cross-linkers were incorporated and in the second network hydrophobic associations originated from specifically designed poly(hydroxyethyl acrylate – co – stearyl methacrylate) co-polymer were utilized.

Ability of these hydrogels in the natural bio-mineralization process was studied by monitoring their capacity to foster the growth of hydroxyapatite crystals *in-situ*.

6.2 Materials and methods

6.2.1 Materials

Alginate (Alg), sodium chloride (NaCl) and calcium chloride ($CaCl_2$) were procured from Merck, India. Hydroxyethyl acrylate (HEA), stearyl methacrylate (SM), hydroxylmethylpropiophenone (HMPP) and hydroxyapatite (HAP) were purchased from Sigma Aldrich, India. Sodium dodecyl sulphate (SDS) was procured from Loba Chem, India. All the chemicals were of analytical grade and used as received. Distilled water was used for all the reactions unless specified otherwise.

6.2.2 Preparation of hydrogels

Preparation of DN hydrogels consisted of two-step sequential process, where first hydrogel network (from Alg) was prepared initially, followed by the in-situ preparation of the second hydrogel network (from PHEA or PHEA-co-SM). First and second hydrogel networks were also prepared separately and called single network (SN) hydrogels.

6.2.2.1 Preparation of SN hydrogels

Solution of Alg was prepared by dissolving 0.3 gms of Alg in 10 ml of distilled water. 0.015 gms of $CaCl_2$ was dissolved in 2 ml distilled water and added onto Alg solution, stirred for about 15 minutes, poured onto cylindrical teflon moulds (8 mm x 8 mm) and stored at 25 ^{0}C for 12 hours. The resultant hydrogels (as-prepared SN hydrogels) were stored in a closed container until further use. These Alg hydrogels were abbreviated as Alg single network (Alg-SN) hydrogels.

For the preparation of second network, a homogeneous aqueous solution containing 12 wt % HEA, 7 wt % SDS, 4 wt % NaCl, 1.2 wt % SM and 1 µL of photo initiator (HMPP) was poured onto cylindrical teflon moulds (8 mm x 8 mm) and exposed to UV irradiation in a closed chamber for 21 minutes. Hydrogels formed after irradiations were named as PHEA-co-SM SN hydrogels. Another SN hydrogel was also prepared with the same composition but without the SM and the resultant SN hydrogel was abbreviated as PHEA SN hydrogel.

6.2.2.2 Preparation of DN hydrogels

For the preparation of DN hydrogels, as-prepared Alg-SN hydrogels were immersed in 20 ml aqueous solution containing 12 wt % HEA, 7 wt % SDS, 4 wt % NaCl, 1.2 wt % SM and 1 µL of photo initiator (HMPP) and kept in roller mixer for 72 hours (retained the integrity in the roller mixer). The equilibrium swollen hydrogels were irradiated with UV in a closed chamber for 21 minutes. Irradiated hydrogels (as-prepared DN hydrogels) were abbreviated as Alg-PHEA-co-SM double network (Alg-PHEA-co-SM DN) hydrogels.

6.2.3 Uni-axial tensile strength

Universal testing machine (UTM) (Model 5943, Instron, MA, USA) was used to measure the tensile strength of as-prepared SN and DN hydrogels. The hydrogels with 20 mm length, 0.5 mm thickness and 0.8 mm width was clamped in between the lower and upper tensile grip. Upper grip was set at a speed of 3 mm/min to measure the tensile strength of hydrogel during fracture. Stress and strain were recorded and plotted by Bluehill software (Instron, MA, USA). Measurements were repeated thrice, and average values were reported.

6.2.4 Rheological studies on SN and DN hydrogels

6.2.4.1 Strain sweep of Alg SN hydrogel

Rheometer (Model 301, Anton Paar, Austria) equipped with a cone and plate geometry was used to measure the linear visco-elastic regime of Alg SN hydrogel. As-prepared Alg SN hydrogel with 25 mm diameter and 0.8 mm height was placed in the lower plate of the rheometer. Oscillatory shear measurements were performed with constant frequency of 1 rad/s at 25 ^{0}C by varying the strain from 0.1 to 10%. Linear region obtained from the results which is independent of the strain is selected for further rheological measurement. Storage modulus (G') and loss modulus (G") was plotted as a function of strain.

6.2.4.2 Time sweep of Alg SN hydrogel

For time sweep measurement, as-prepared Alg SN hydrogel with 25 mm diameter and 0.8 mm height was placed in the lower plate of the rheometer. Oscillatory shear measurements were performed with constant frequency of 1 rad/s and constant strain of 5 % at 25 ^{0}C for 12 minutes. Storage modulus (G') and loss modulus (G") was plotted as a function of time.

6.2.4.3 Transitions of Alg SN hydrogel

Oscillatory shear experiments as a function of temperature were performed to calculate the transitions of as-prepared Alg SN hydrogels. Hydrogel is loaded onto the rheometer and temperature was ramped from 25 to 75 ^{0}C at the rate of 1 ^{0}C per minute. Frequency and strain was kept constant as 1 rad/sec and 5% respectively. After reaching the temperature at 75 ^{0}C, sample was kept isothermal at 75 ^{0}C for 5 minutes and later cooled back to 25 ^{0}C at the rate of 1 ^{0}C per minute. Storage modulus (G') and loss modulus (G") was plotted as a function of temperature and the cross-over points between G' and G" was noted.

6.2.4.4 Step-strain study of SN and DN hydrogels

Response of hydrogels to higher strain was measured by step-strain measurements where strain was increased beyond the linear visco-elastic limit of the hydrogels and later reduced back to their visco-elastic limit in a cycle at ambient temperature. Similar cycles were repeated with continuous incremental increase in strain values viz; 100, 300, 500, 700, 900 and 1100 % respectively and regular intermittent relaxation times in between the strain cycles. The measurement was repeated with the same program for PHEA-co-SM SN hydrogels, PHEA SN hydrogels and Alg-PHEA-co-SM DN hydrogels at 25 ^{0}C.

6.2.5 Preparation of HAP incorporated SN and DN hydrogels

HAP crystals (100 mg) were dispersed in 10 ml of distilled water by stirring for 2 hours. 0.3 gms of Alg was dissolved in this solution followed by the addition of 0.015 gms of $CaCl_2$, stirred for about 15 minutes, poured onto cylindrical teflon moulds (8 mm x 8 mm) and stored at 25 ^{0}C for 12 hours. A part of the resultant as-prepared Alg SN hydrogels incorporated with HAP were used for the preparation of Alg-PHEA-co-SM DN hydrogel described earlier in **section 6.2.2.2.** Accordingly, HAP incorporated PHEA SN hydrogels and PEHA-co-SM SN hydrogels were prepared by dispersing HAP in the monomer solution used for their preparation as explained in **section 6.2.2.1**

6.2.6 Bio-mineralization of HAP incorporated SN and DN hydrogels

Simulated body fluid (SBF) was prepared as per the protocol reported by Kokubo *et al*[10] HAP incorporated SN and DN hydrogels were punched with the help of a metallic die to form uniform cylinders of 10 mm diameter and 1 mm height.

Cylindrical hydrogels were weighed and placed in individual beakers containing 20 ml SBF, maintained at 37 ^{0}C in a shaking water bath. Weights gained by the cylindrical hydrogel specimens were recorded at specific time intervals and also SBF solutions in the beakers were replenished regularly. Experiment was repeated in triplicate and the weight gained was calculated and plotted as a function of time.

6.2.7 3D imaging HAP and HAP incorporated SN and DN hydrogels

6.2.7.1 3D imaging and size distribution of HAP

HAP was packed inside a plastic vial of 2 ml capacity and was loaded onto micro-computed tomography (micro-CT) (Model Xradia Versa 510, Carl Zeiss X-ray Microscopy, Pleasanton, CA) where 3201 X-ray projections were acquired with 360^{0} rotation at 80 kV X-ray source, with a pixel size of 1.0 microns. Acquired projections were subjected to back projection algorithm to reconstruct a series of virtual cross-sectional 2D images of HAP crystals. 2D images were cropped to a size of 1000 x 1000 x 1000 microns, filtered with non-local means filter and segmented using PoroDict® (Math2Market GmbH, Kaiserslautern, Germany) image processing software to construct a three-dimensional image of HAP crystals to visualize its spatial distribution. Image segmentation processes provide a 3D visualization of HAP crystals with the aid of Otsu global threshold selection method and quantifies its diameter and size distribution.

6.2.7.2 3D imaging a of HAP incorporated hydrogels

Specimens of SN and DN hydrogels incorporated with HAP, before and after bio-mineralization process, were trimmed to 4 mm x 4 mm size and imaged using micro-CT as detailed above in **section 6.2.7.1**. Size distribution of HAP crystals before and after the bio-mineralization process was calculated and plotted.

6.3 Results and discussion

6.3.1 Preparation of Alg SN hydrogels

Alg is an anionic linear polysaccharide derived from brown seaweed and is widely used for various biomedical applications. It contains blocks of $_{L}$-guluronate and $_{D}$-mannuronate and ratio of which depends on the natural source. Biomedical applications of Alg are due to its biocompatibility, low toxicity, relatively low cost and mild gelation by addition of divalent cations[11]. In this work we have cross-linked

Alg using Ca^{2+} ions to prepare hydrogels which is a common approache for the preparation of Alg hydrogels (**Scheme 6.1**). L-guluronate blocks are responsible for the cross-linking process with divalent Ca^{2+} ions to form intermolecular linkages resulting in the formation of a hydrogel network. Affinity of Ca^{2+} ions towards G-block is due to the peculiar structure of G-block which allows high degree of coordination with divalent cations.

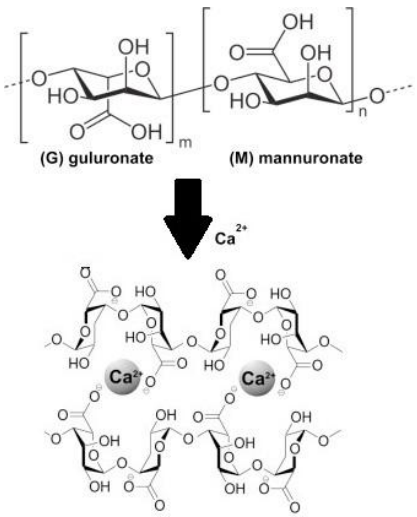

Scheme 6.1: Cross-linking reaction of Alg with divalent Ca^{2+} ions

6.3.2 Preparation of PHEA-co-SM and PHEA SN hydrogels

PHEA-co-SM SN hydrogels were prepared by salt-mediated UV-assisted micellar co-polymerization of HEA and SM (**Scheme 6.2**). Presence of salt increases the size of micelles formed by SDS in water and which in turn can solubilize higher volume of hydrophobic SM in its core[7].

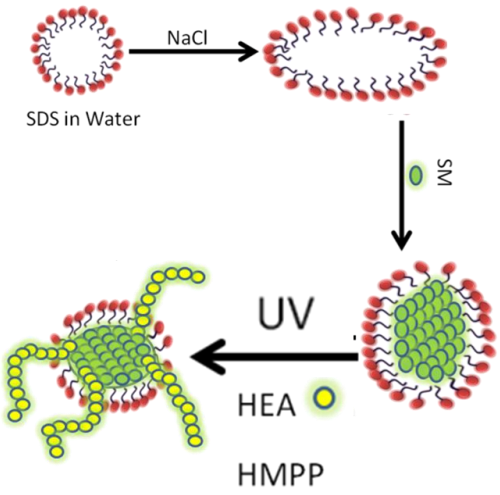

Scheme 6.2: Micellar co-polymerization of HEA and SM mediated by salt

This protocol was reported by Oguz Okay et al[12-13] and helps to design tough as well as stretchable hydrogels by tuning the concentration of hydrophobic monomer and its alkyl chain length. Concentration of the surfactant, SDS is fixed at 7 wt% which is much above the overlap concentration of SDS micelles. Addition of SM reduces the viscosity of SDS-NaCl solution which signifies the accumulation of SM inside the surfactant palisade layer and in the core of the micelles, thereby increasing the curvature of the micelle[7,14]. UV-assisted free radical polymerization of HEA was also performed in the presence of SDS and salt to avoid any possible deviations in the final outcome of PHEA SN hydrogels.

6.3.3 Tensile properties of SN and DN hydrogels

Tensile properties of as-prepared SN and DN hydrogels were measured to study their mechanical strength and stretchability. Stress versus strain plot of SN and DN hydrogels are shown in **fig 6.1**, where DN hydrogels showed a tensile strength of 47 kPa, whereas SN hydrogels prepared from Alg and PHEA-co-SM exhibited 14 and 22 kPa, respectively. DN hydrogels showed two times higher tensile strength than PHEA-co-SM SN hydrogels and three times higher than those of Alg SN hydrogels. Elongation of these hydrogels showed a drastic difference between DN and Alg SN hydrogels. DN hydrogels were able to stretch six times higher than that of Alg SN hydrogels. Moduli of these hydrogels were measured from the slope of their corresponding stress – strain curves.

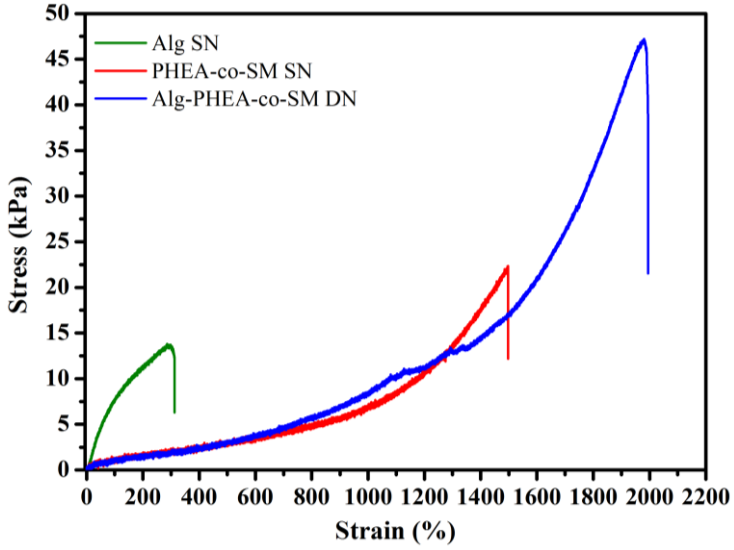

Figure 6.1: Stress vs strain plots of Alg-PHEA-co-SM DN, PHEA-co-SM SN and Alg SN hydrogels

Tensile properties of Alg SN and PHEA-co-SM SN hydrogels matche with the desirable mechanical properties proposed by Gong *et al*[15], which is essential for the preparation of DN hydrogels. Alg SN hydrogel showed a moduli of 7300 Pa whereas PHEA-co-SM SN hydrogel exhibited a moduli of 4170 Pa. This observation indicated that Alg SN hydrogel is hard and brittle, whereas PHEA-co-SM SN hydrogel is stretchable and ductile.

6.3.4 Rheological studies on SN and DN hydrogels

Oscillatory shear measurements provide a quantitative information about the viscoelastic and rheological properties of hydrogels upon deformation under specific stress or strain[16]. Time sweep measurements at constant frequency as well as strain in the linear visco-elastic (LVR) regime of the Alg SN hydrogel are given in **fig 6.2**. As shown in **fig 6.2**, the storage moduli (G') of Alg SN hydrogel is 7300 Pa at 25 ^{0}C. However, oscillatory shear experiments at ambient temperature depict only visco-elastic characteristics of Alg SN hydrogels.

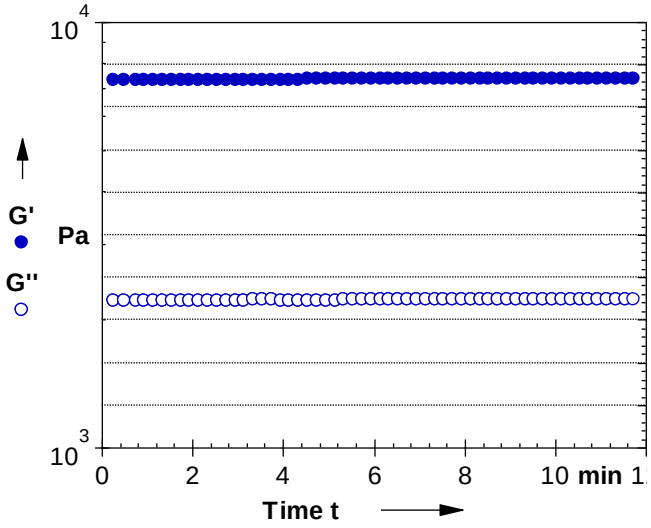

Figure 6.2: Time sweep plot of Alg SN hydrogel at constant frequency and strain

Therefore, to study the temperature induced transitions in Alg SN hydrogels, oscillatory shear experiments as a function of temperature is performed and shown in **fig 6.3**. Ionic cross-link junctions in G-block are sensitive to temperature and are known to exhibit reversible breakage-bondage during heating and cooling cycles respectively[17-18]. Such reversible temperature induced transitions are responsible for

the *gel-to-sol* and *sol-to-gel* transitions in Alg SN hydrogel network cross-linked with ionic moieties.

As seen in **fig 6.3**, Alg SN hydrogel is heated gradually from 25 ^{0}C to 75 ^{0}C and during the process G' reduces gradually which indicates the reduction in the elastic response of the hydrogel network as a function of temperature. Such observation correlates with the breakage of ionic-bonds responsible for the cross-links in G-block and results in the transition from *gel-to-sol*. This transition takes place at 42.8 ^{0}C (Ist transition in **fig 6.3**) and the viscous response dominates further. However, during the initiation of the cooling cycle, elastic response increases gradually resulting in the second transition at 66.5 ^{0}C (IInd transition in **fig 6.3**), from *sol-to-gel*. Such reversible temperature induced transitions are characteristic of ionically cross-linked network and the transition temperature depends various factors such as cross-link density, molecular weight, concentration, heating rate, etc[19-23].

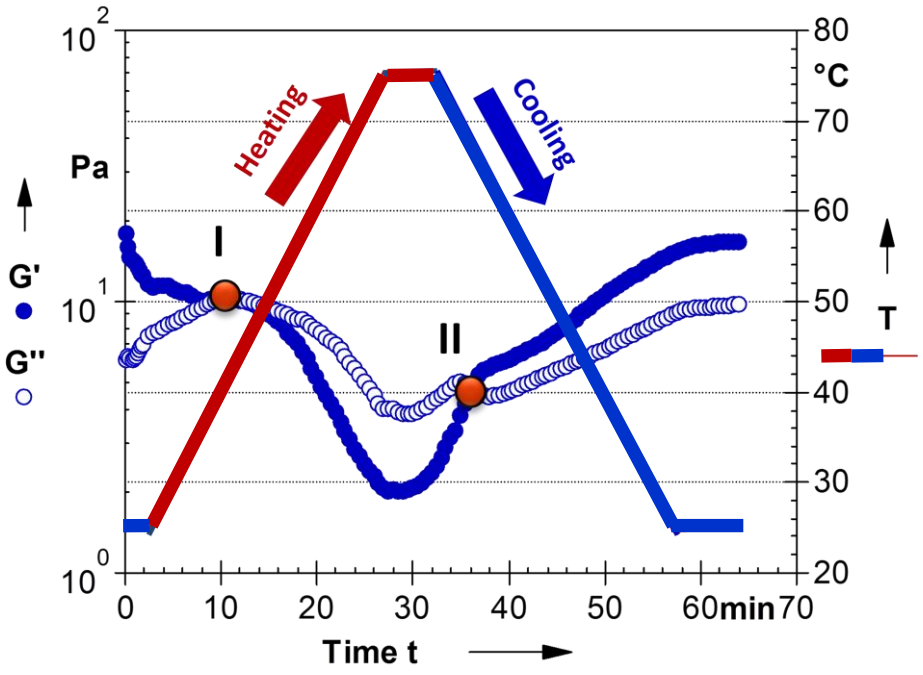

Figure 6.3: Temperature induced transitions (I & II) in Alg SN hydrogel during the heating and cooling process of oscillatory shear experiments

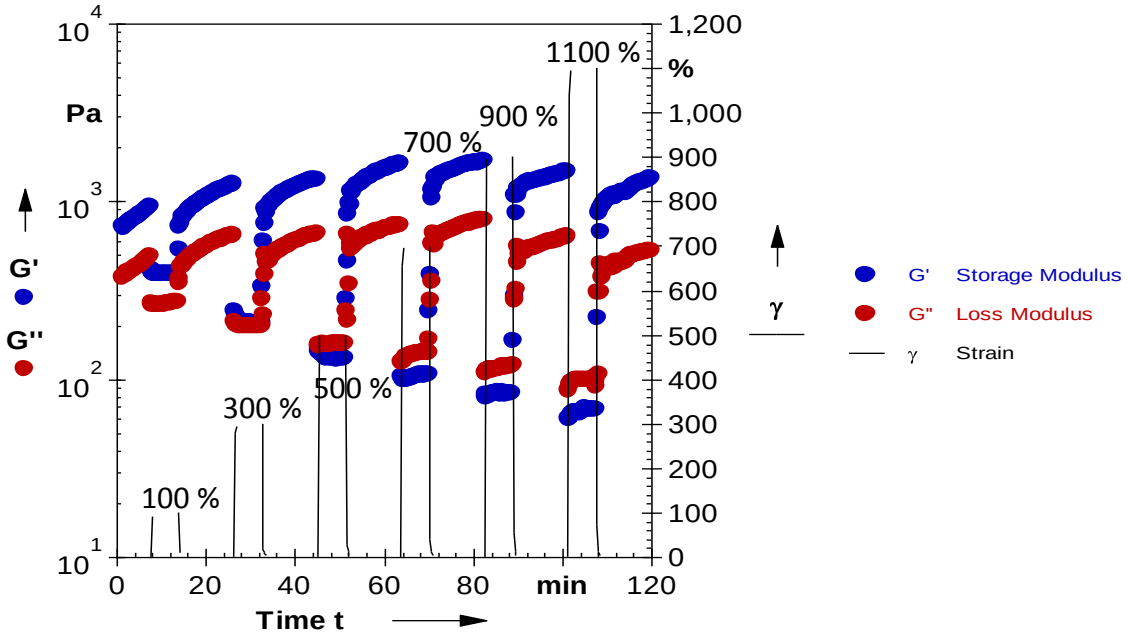

Figure 6.4: Step-strain oscillatory strain amplitude experiments in PHEA-co-SM SN hydrogel

Second network is designed specifically with a co-monomer bearing alkyl chain, to take advantage of non-covalent reversible interactions driven by associative behavior of hydrophobic junctions in the hydrogel network of PHEA-co-SM. To study such behavior step-strain oscillatory strain amplitude experiments were performed[24] where higher strains beyond the LVR regime (strain >> 5%) of the hydrogel network is applied to break the elastic hydrogel network, followed by an immediate relaxation back to LVR regime (strain ≤ 5%), as shown in **fig 6.4**.

As shown in **fig 6.4**, initially oscillatory strain amplitude measurement were performed at 5% strain (strain ≤ LVR ≈ 5%) and frequency of 1 rad/s for 6.25 minutes, where storage moduli (G') dominates the loss modulus (G"), which represents a true elastic hydrogel network. Further, the strain was increased drastically to 100 % (strain >> LVR) at constant frequency (1 rad/s) for 6.25 minutes, where G' and G" decreases immediately. After 6.25 minutes strain was immediately reduced to 5% (≈ LVR) to study the effect of strain on the elastic hydrogel network, thereby completing a cycle. This cycle of strain increment was repeated 5 times furthermore, at a regular time interval of 6.25 minutes, before and after strain increment, where strain was increased consistently in each cycle from 100 to 300, 500, 700, 900 and 1100 % respectively.

It was observed that from the second cycle onwards, in the drastic increment of strain, viscous domain enhances further beyond an elastic domain from one cycle to other. Similarly, elastic domain also enhances further from first cycle to the fifth cycle and then it shows a gradual reduction. These observations point towards the fact that copolymerization of the monomers with alkyl chain (C18) via micellar polymerization introduces dynamic hydrophobic associations between the hydrophobic domains of polymer chains which heals the elastic hydrogel network after deformation induced fracture. Also surfactant micelles act as reversible physical cross-links for self-healing of hydrogels. Thus associations between hydrophobic domains are responsible for the recovery of original modulus almost instantaneously upon reducing the strain to LVR, demonstrating reversible dissociation – association of micellar cross-links.

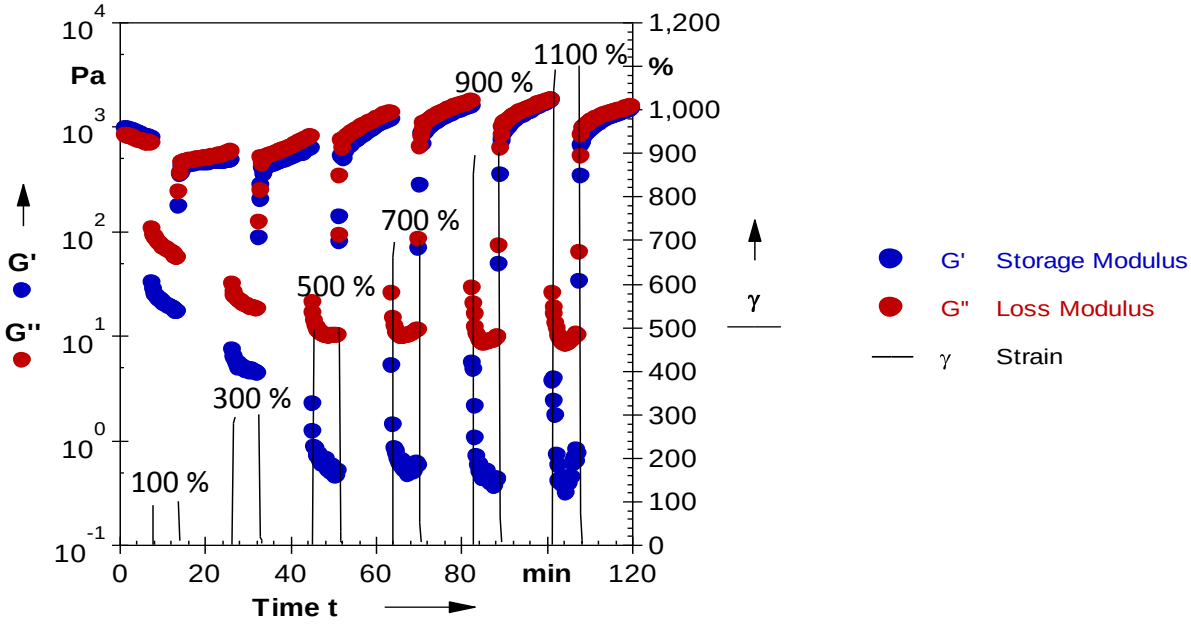

Figure 6.5: Step-strain oscillatory strain amplitude experiments in PHEA SN hydrogel

To verify the role of hydrophobic co-monomer, oscillatory strain amplitude measurements were also performed on SN hydrogel prepared without hydrophobic co-monomer, i.e.; PEHA SN hydrogel, in the presence of surfactant and salt. As shown in **fig 6.5**, results of oscillatory strain amplitude experiments on PHEA SN hydrogels are in contrast with respect to that of PHEA-co-SM SN hydrogels. Right after the completion of the first strain cycle, G" dominates over G' in rest of the strain cycles, which is a clear indication of the breakage of the elastic hydrogel network immediately after the application of 100% strain (strain >> LVR ≈ 5%). During the

rest of the cycles, network structure was not able to recover from the fracture inducted from the first cycle, as indicated by concurrent domination of viscous regime.

Oscillatory stress amplitude experiments underline the role of hydrophobic association among alkyl chains of co-monomer which retains elastic hydrogel network by self-healing mechanism, even after transient network failure induced by higher deformation applied by excessive strain. The role of hydrophobic association in DN hydrogels were further studied by performing oscillatory strain amplitude experiments on Alg-PHEA-co-SM DN hydrogels.

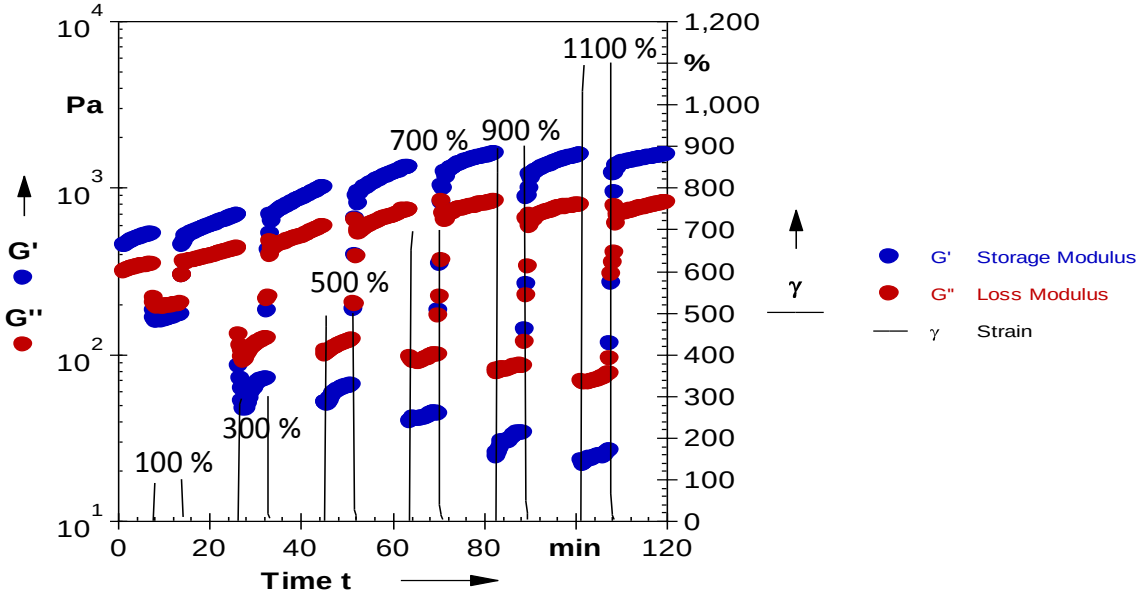

Figure 6.6: Step-strain oscillatory strain amplitude experiments in Alg-PHEA-co-SM DN hydrogel

As shown in **fig 6.6**, in contrast to PHEA-co-SM SN hydrogels, the elastic modulus is dominated by viscous counterpart during the application of 100% strain. However, recovery of the elastic moduli during the relaxation step is similar to that of PHEA-co-SM SN hydrogels. In the case of DN hydrogels, strain induced dissociation and association of ionic cross-links present in the first network also comes into the picture which might have played a key role in the gradual increase of elastic moduli from one cycle to other, in all the six consecutive cycles.

6.3.5 Bio-mineralization studies on SN and DN hydrogels

Bio-mineralization is a study of biologically produced materials such as tooth, shells, etc and the process which leads to the formation of these multi-scale hierarchical

architectures from organic – inorganic composites[25]. Grassmann *et al*[26] has reported the growth of calcite crystallites in gelatin matrix which indicates the biological crystallization process under comparable physiological conditions. Later several reports on bio-mineralization process of hydroxyapatite (HAP)[27], tricalcium phosphate (TCP)[28], calcium phosphates ($CaPO_4$)[29], etc in bio-simulated medium such as hydrogels[30-31], biopolymers[32], etc, throws light into the artificial bio-mineralization methodology[33] which can enhance the growth or formation of mineralized hard tissues such as bone, cartilage, enamel, etc[34]. This methodology has a far reaching potential to develop solutions for regenerative medicine.

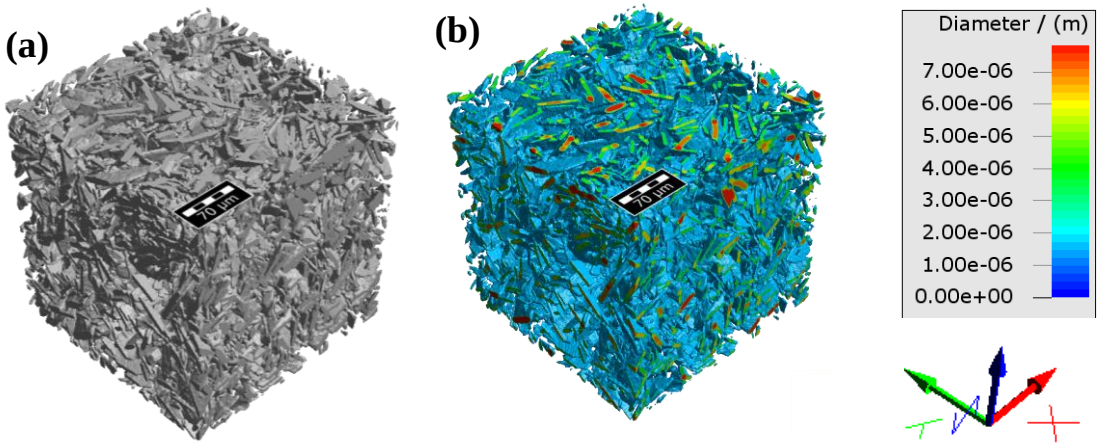

(d) Ion	Con. (mmol/dm^3)
	SBF [10]
Na^+	142.0
K^+	5.0
Mg^{2+}	1.5
Ca^{2+}	2.5
Cl^-	147.8
HCO_3^-	4.2
HPO_4^{2-}	1.0
SO_4^{2-}	0.5

Figure 6.7: (a) Reconstructed 3D image of HAP particles (scale bar is 70 microns), (b) color-coded 3D image of HAP particles with color legend (scale bar is 70 microns), (c) schematic representation of bio-mineralization process in SBF and (d) chemical composition of SBF

To study the efficacy of DN hydrogels in enhancing the bio-mineralization process, HAP has been selected to prepare hydrogel composites from SN (Alg SN, PHEA SN and PHEA-co-SM SN) and DN (Alg-PHEA-co-SM DN) hydrogels. Initially the particle size-distribution of HAP was studied by 3D micro-CT imaging and subsequent image analysis (**Fig 6.7a & 6.7b**). HAP particles possess an average size of 4.5 microns with a size range of 1 to 10 microns. Hydrogel composites embedded with HAP crystals were immersed in simulated body fluid (SBF) (**Fig 6.7d**) at 37 ^{0}C and regular weight gain due to natural bio-mineralization process (**Fig 6.7c**) was noted by gravimetric measurements. The experiments were repeated in triplicate and performed for both SN and DN hydrogels with similar shape and volume.

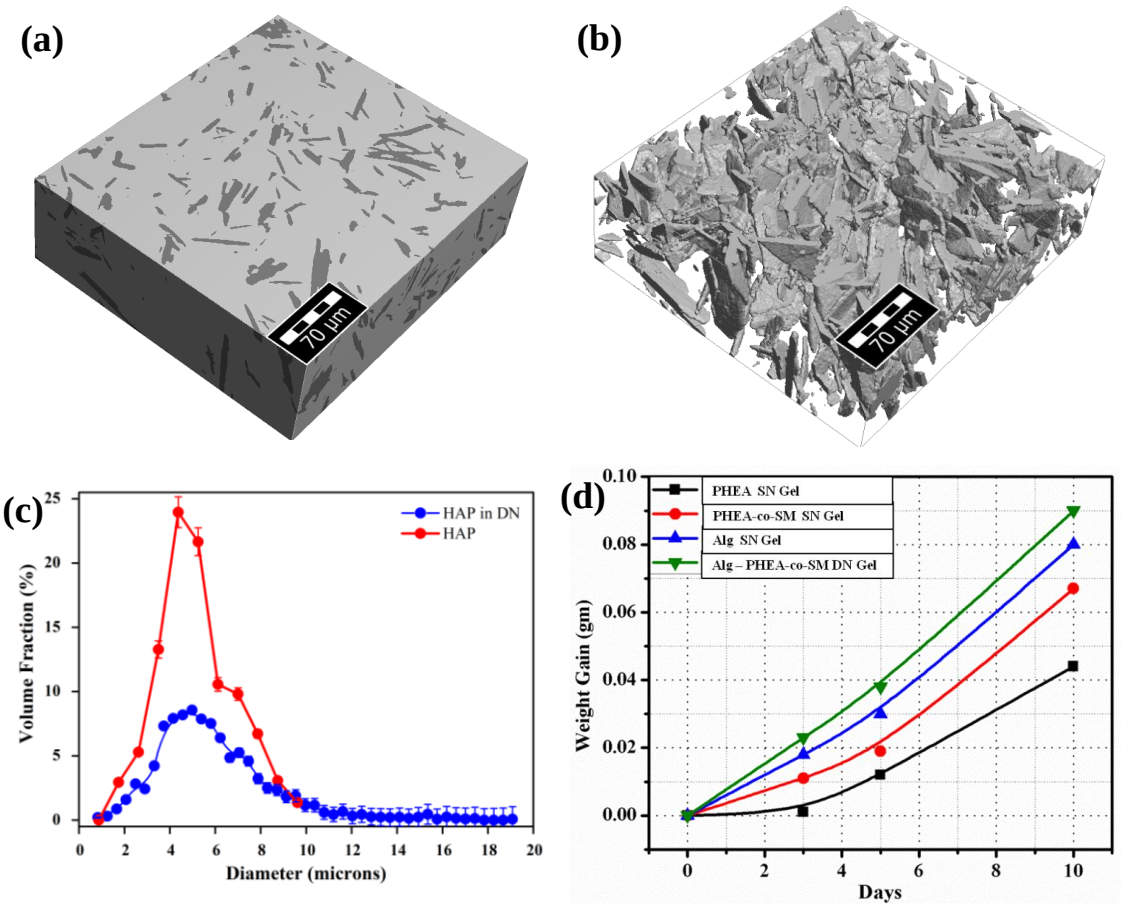

Figure 6.8: (a) Reconstructed 3D image of HAP hydrogel composite (scale bar is 70 microns), (b) 3D image of HAP particles inside the composite (scale bar is 70 microns), (c) size distribution of HAP before and after mineralization, (d) weight gained by HAP hydrogel composites after bio-mineralization

Hydrogel composites embedded with HAP crystals were imaged by micro-CT before and after (**Fig 6.8a & 6.8b**) the bio-mineralization process. Size distribution of HAP was calculated from these images and plotted as a function of volume fraction (**Fig 6.8c**). Histogram of size distribution shows gradual increase in the particle size of HAP after bio-mineralization and reduction in the volume fraction of particles in the lower size range (2 to 8 microns). These observations reveal the crystal growth of HAP during the incubation period in SBF, promoted by the hydrated environment induced by hydrogels. Histogram of weight gained by the HAP crystals during the bio-mineralization process was shown in **fig 6.8d**, where DN hydrogels outplays other SN hydrogels in enhancing the crystal growth, thereby promoting the bio-mineralization process.

Crystal growth inside DN hydrogels may be influenced by the bond dissociation – association process that paves towards micro-structural re-orientation of hydrogel network driven by inter-segmental voids. The results suggests the potential of DN hydrogels for applications in the regeneration of mineralized hard-tissues such as cartilage, bone, enamel, etc.

6.4 Conclusions

Alg based DN hydrogels were prepared by two-step sequential process where Alg SN hydrogels were prepared initially in the first step, followed by salt-mediated micellar co-polymerization of HEA and SM in the second step, resulting in the formation of self-healing DN hydrogels. Tensile properties of DN hydrogels were two to three times higher than that of its SN counterparts and stretchable upto 20 times their initial length before fracture. Alg SN hydrogels showed characteristic temperature transitions driven by the dissociation – association of ionic bonds. PHEA-co-SM SN hydrogels showed self-healing behavior induced by the hydrophobic associations of SM blocks mediated by micelles. DN hydrogels also enhanced the bio-mineralization process by promoting the crystal growth of embedded HAP in the presence of SBF. These results indicate that bio-mineralized Alg DN hydrogel is a promising candidate for a biomimetic hydrogel system that promotes bone tissue repair and regeneration.

6.5 References

(1) Taylor, D. L.; in het Panhuis, M. *Adv Mater* **2016**, *28*, 9060.

(2) Wei, Z.; Yang, J. H.; Zhou, J.; Xu, F.; Zrinyi, M.; Dussault, P. H.; Osada, Y.; Chen, Y. M. *Chemical Society Reviews* **2014**, *43*, 8114.

(3) Barthel, M. J.; Rudolph, T.; Teichler, A.; Paulus, R. M.; Vitz, J.; Hoeppener, S.; Hager, M. D.; Schacher, F. H.; Schubert, U. S. *Adv Funct Mater* **2013**, *23*, 4921.

(4) Oehlenschlaeger, K. K.; Mueller, J. O.; Brandt, J.; Hilf, S.; Lederer, A.; Wilhelm, M.; Graf, R.; Coote, M. L.; Schmidt, F. G.; Barner-Kowollik, C. *Adv Mater* **2014**, n/a.

(5) Bai, T.; Liu, S.; Sun, F.; Sinclair, A.; Zhang, L.; Shao, Q.; Jiang, S. *Biomaterials* **2014**, *35*, 3926.

(6) Herbst, F.; Döhler, D.; Michael, P.; Binder, W. H. *Macromolecular Rapid Communications* **2013**, *34*, 203.

(7) Tuncaboylu, D. C.; Sari, M.; Oppermann, W.; Okay, O. *Macromolecules* **2011**, *44*, 4997.

(8) Wang, W.; Narain, R.; Zeng, H. *Frontiers in Chemistry* **2018**, *6*.

(9) Liu, Y.; Hsu, S.-h. *Frontiers in Chemistry* **2018**, *6*.

(10) Kokubo, T.; Kushitani, H.; Sakka, S.; Kitsugi, T.; Yamamuro, T. *J Biomed Mater Res* **1990**, *24*, 721.

(11) Lee, K. Y.; Mooney, D. J. *Progress in Polymer Science* **2012**, *37*, 106.

(12) Abdurrahmanoglu, S.; Can, V.; Okay, O. *Polymer* **2009**, *50*, 5449.

(13) Gulyuz, U.; Okay, O. *Macromolecules* **2014**, *47*, 6889.

(14) Algi, M. P.; Okay, O. *Eur Polym J* **2014**, *59*, 113.

(15) Gong, J. P.; Katsuyama, Y.; Kurokawa, T.; Osada, Y. *Adv Mater* **2003**, *15*, 1155.

(16) Anseth, K. S.; Bowman, C. N.; Brannon-Peppas, L. *Biomaterials* **1996**, *17*, 1647.

(17) Brassinne, J.; Stevens, A. M.; Van Ruymbeke, E.; Gohy, J.-F.; Fustin, C.-A. *Macromolecules* **2013**.

(18) Draper, E. R.; Eden, E. G. B.; McDonald, T. O.; Adams, D. J. *Nat Chem* **2015**, *7*, 848.

(19) Brun-Graeppi, A. K. A. S.; Richard, C.; Bessodes, M.; Scherman, D.; Narita, T.; Ducouret, G.; Merten, O. W. *Carbohyd Polym* **2010**, *80*, 555.

(20) Lee, Y.; Chung, H. J.; Yeo, S.; Ahn, C.-H.; Lee, H.; Messersmith, P. B.; Park, T. G. *Soft Matter* **2010**, *6*, 977.

(21) Dong, J.; Yin, C.; Zhang, Y.; Zhang, Q. *Journal of Polymer Science Part B: Polymer Physics* **2013**, n/a.

(22) Haraguchi, K.; Taniguchi, S.; Takehisa, T. *Chemphyschem* **2005**, *6*, 238.

(23) Tashiro, K.; Ishino, K.; Ohta, T. *Polymer* **1999**, *40*, 3469.

(24) Can, V.; Kochovski, Z.; Reiter, V.; Severin, N.; Siebenbürger, M.; Kent, B.; Just, J.; Rabe, J. P.; Ballauff, M.; Okay, O. *Macromolecules* **2016**, *49*, 2281.

(25) Estroff, L. A. *Chemical Reviews* **2008**, *108*, 4329.

(26) Grassmann, O.; Müller, G.; Löbmann, P. *Chemistry of Materials* **2002**, *14*, 4530.

(27) Palmer, L. C.; Newcomb, C. J.; Kaltz, S. R.; Spoerke, E. D.; Stupp, S. I. *Chemical Reviews* **2008**, *108*, 4754.

(28) Arias, J. L.; Fernández, M. S. *Chemical Reviews* **2008**, *108*, 4475.

(29) LeGeros, R. Z. *Chemical Reviews* **2008**, *108*, 4742.

(30) Huh, H. W.; Zhao, L.; Kim, S. Y. *Carbohyd Polym* **2015**, *126*, 130.

(31) Douglas, T. E. L. In *Biomineralization and Biomaterials*; Aparicio, C., Ginebra, M.-P., Eds.; Woodhead Publishing: Boston, 2016, p 291.

(32) Boskey, A. L.; Roy, R. *Chemical Reviews* **2008**, *108*, 4716.

(33) Cha, C.; Kim, E.-S.; Kim, I. W.; Kong, H. *Biomaterials* **2011**, *32*, 2695.

(34) Asenath-Smith, E.; Li, H.; Keene, E. C.; Seh, Z. W.; Estroff, L. A. *Adv Funct Mater* **2012**, *22*, 2891.

Summary and Conclusions

Chapter – VII

In the seventh chapter, we have discussed the summary of thesis work.

The objective of the thesis was to undertake design and synthesis of mechanically robust hydrogels from biomimetic resources such as polysaccharides, by employing the DN strategy. Polysaccharides are available in a variety of structures with different properties. Since they contain reactive functional groups, they can be easily modified by various chemical routes. Furthermore, their stability, non-toxicity, and bio-degradability lead their applications in food and pharmaceuticals. For the preparation of biomimetic hydrogels, three polysaccharides were selected, which are carboxymethyl xyloglucan (CMX), carboxymethyl cellulose (CMC) and alginate (Alg).

In the first chapter, various aspects of hydrogels, their characteristics, hydrogels from biomimetic polysaccharides, principles of DN hydrogels, chemical structure, proposed structure model, various methods used for preparation, toughening mechanisms and applications were discussed. Use of the state-of-the-art technique, 3D X-ray micro-CT for studying hydrogels is discussed. In the second chapter the scope and objectives of the thesis were discussed.

In the third chapter, we have reported on the design and synthesis of new microelectrodes, comprising of carbon nano-fiber (CNF) and carboxymethyl xyloglucan (CMX) hydrogel, which enhanced the current density across the interface of artificial prosthesis and human neural system. The chemical structure and molecular weight of purified CMX were studied by NMR spectroscopy and GPC, respectively. Microelectrode was prepared by in-situ cross-linking of CMX inside CNF, with optimized CMX: CNF ratio, resulting in continuous ionic channels confined within the hollow core of CNF. Electron microscopy images of microelectrodes illustrated the formation of CMX hydrogel network inside the CNF hollow core without wrapping its surface. The presence of hydrogel in the CNF was confirmed by SEM and TEM. The electrochemical studies indicated the enhancement in charge density as well as the active surface area of the microelectrodes upon incorporation of CMX hydrogel network. These microelectrodes have great potential as neural interfaces for designing smart prosthetics with voluntary control.

In the fourth chapter, DN hydrogels comprising of CMX as the first network and PHEA as the second network were proposed using a sequential process. CMX was

cross-linked with DVS to form the first network and HEA was photo-polymerized to form the second network. Gelation, swelling behaviour and mechanical properties of these hydrogels were studied. These DN hydrogels exhibited a compressive strength of 3.5 MPa, whereas the first and second network showed compressive strength of 0.02 and 2.3 MPa, respectively. Microgels (MGs) were prepared by the photo-polymerization of SM and HEA using oil-in-water (O/W) method, where concentration of HEA was 5, 10 and 15 mol % as that of SM. Average size and range of these MGs were measured with micro-CT. Release of curcumin in PBS (pH 7.4 and 370C) from these MGs embedded in the DN hydrogels showed release pattern dependent on the concentration of HEA. These drug loaded DN hydrogels showed promise for applications in developing rate pre-programmed release systems for addressing chronic wound healing process.

In the fifth chapter, DN hydrogels consisting of tightly cross linked carboxymethylcellulose (CMC) as the first network and loosely cross linked poly(hydroxyethylacrylate) (PHEA) as a second network were synthesized. The second network also contained a small amount of stearyl methacrylate (SM) as a co-monomer (2, 4 & 6 mol % of HEA) along with hydroxyl ethyl acrylate (HEA). Compressive strength of the CMC-PEHA-DN hydrogel was 280 times more than that of CMC-SN hydrogel and with increase in SM concentration DN hydrogels showed better recovery after deformation. In contrast to hydrophobically modified covalently cross-linked hydrogels, they exhibited more swelling with increase in hydrophobic volume fraction. This observation was due to the presence of surfactant molecules which solvates the hydrophobic polymer fractions in the hydrophilic environment. Stress relaxation measurements showed the ability of DN hydrogels to recover from force of deformation after a prolonged time period. This was possible due to the flexible nature of hydrophobic polymer within the DN structure. Cell viability studies showed the advantage of DN hydrogels over it SN counterparts, where biocompatibility of DN hydrogels was enhanced due to a better response of cells towards hydrogel network structure with faster relaxation rates and also due to the presence of bioactive polysaccharide units in them. DN strategy has put forward a pathway to create a bio-active tough hydrogels using DVS cross-linked CMC network.

In the sixth chapter, we designed and synthesized self-healing DN hydrogels, comprising of alginate as the first network and PHEA-co-SM as the second network. Alginate was cross-linked by divalent Ca2+ ions to form first network and HEA co-polymerized with SM via salt-assisted micelle co-polymerization route to form the second network. Salt-assisted co-polymerization route helped to incorporate 10 Wt. % of SM onto the second network which in turn exhibited self-healing property, driven by the hydrophobic association between the alkyl chains of SM. Elastic modulus and thermo-reversible characteristics of the first network were studied by rheology. Step strain oscillatory rheological measurements and uni-axial tensile measurements were used to study the self-healing characteristics of the second network and the DN hydrogel network. These DN hydrogels also enhanced bio-mineralization process of HAP, confined in the DN hydrogel network.

To conclude, three biomimetic polysaccharides such as CMX, CMC and Alg were utilized to design DN hydrogels with robust mechanical properties and were utilized for various bio-medical applications such as sustained drug delivery system, tissue substitutes and hard-tissue regeneration scaffold. Mechanical properties of these DN hydrogels were at par with that of their synthetic DN counterparts, which were mainly derived from acrylamide based hydrogels, known for their exceptional higher molecular weight and toughness. Therefore, apart from other hydrogel network preparation techniques, DN strategy was proven to be a unique route for designing polysaccharide based hydrogels with exceptional mechanical behaviour. Conventional IPN technique fails to prepare CMX-PHEA or CMC-PHEA based inter-penetrating networks due to the macro-phase separation induced by salts during Michael-addition reaction. Here again DN strategy edges across the IPN technique in the realization of CMX and CMC based DN hydrogels. Also, employing polysaccharides for designing hydrogels opens up a sustainable solution for depleting natural oil resources and are highly recommended for demanding biomedical applications. Self-healing properties of DN hydrogels driven by dynamic non-covalent interactions can further enhance the life expectancy of hydrogel based medical devices and products. Biocompatibilities of polysaccharide based DN hydrogels were higher in comparison with that of SN hydrogels. Such advantage arises from the synergism exerted by the unique DN design offers further scope to study. These hydrogels exhibited great potential in drug delivery, regenerative medicine, implant design etc.

I. List of Publications:

1. Arun Torris and Manohar V. Badiger, *Polysaccharide Hydrogel Incorporated Carbon Nanofiber Microelectrode for Designing Neural Interfaces*, **Journal of Bionic Engineering**, 16 (4), 696 - 710 (2019), DOI: 10.1007/s42235-019-0056-x.

2. Ashok Noothanakanti, Manisha Walunj, **Arun Torris**, Manohar Badiger and Seergazhi Srivatsan, *Self-Assemblies of Nucleolipid Supramolecular Synthons Show Unique Solf-sorting and Co-operative Assembling Process*, **Nanoscale**, 11 (24), 11956 - 11966 (2019), DOI: 10.1039/C9NR01863H.

3. Suvendu Karak, Kaushik Dey, **Arun Torris,** Arjun Halder, Saibal Bera, Fayis K. P. and Rahul Banerjee, *Inducing Disorder in Order: Hierarchically Porous Covalent Organic Framework Nanostructures for Rapid Removal of Persistent Organic Pollutants*, **Journal of the American Chemical Society**, 141 (18), 7572 - 7581 (2019), DOI: 10.1021/jacs.9b02706.

4. Runali Patil, Michael A. Repka, **Arun Torris,** Suresh Bhat and Sharvil Patil, *Mapping Fusogenicity of Ciprofloxacin loaded Liposomes with Bacterial Cells*, **AAPS PharmSciTech**, 20 (5), 180 (2019), DOI: 10.1208/s12249-019-1381-4.

5. Yogesh N. Marathe, **Arun Torris A. T.**, Ramesh C. and Manohar V. Badiger, *Borassus Powder-reinforced Poly(lactic acid) Composites with Improved Crystallization and Mechanical Properties*, **Journal of Applied Polymer Science**, 136, 47440 (2019), DOI: 10.1002/app.47440.

6. Vidyanand Vijayakumar, Meena Ghosh, **Arun Torris A. T.**, Nikhil Chandran M. K., Sanoop B. Nair, Manohar B. Badiger and Sreekumar Kurungot, *Water-in-acid Gel Polymer Electrolyte Realized Through a Phosphoric acid-enriched Polyelectrolyte Matrix Towards Solid-state Supercapacitors*, **ACS Sustainable Chemistry & Engineering**, 6 (10), 12630 - 12640 (2018), DOI: 10.1021/acssuschemeng.8b01175.

7. Mayur Patil, Vishal Patil, Aditya Sapre, Tushar Ambone, **Arun Torris A. T.**, Parshuram Shukla and Kadhiravan Shanmuganathan, *Tuning Controlled Release Behaviour of Starch Granules using Nanofibrillated Cellulose Derived from Waste*

Sugarcane Bagasse, **ACS Sustainable Chemistry & Engineering**, 6 (7), 9208 - 9217 (2018), DOI: 10.1021/acssuschemeng.8b01545.

8. Ashwini Anilrao Deshpande, **Arun Torris A. T.**, Swagata Pahari, Manohar V Badiger, Pattuparambil R Rajamohanan, Prakash P Wadgaonkar, Sudip Roy and Claudio Tonnelli, *Mechanism of the Formation of Microphase Separated Water Clusters in a Water - Mediated Physical Network of Perfluoropolyether Tetraol*, **Soft Matter**, 14, 2339 - 2345 (2018), DOI: 10.1039/C7SM02181J.

9. Sadiya Anjum, Pramod Gaurave, Manohar V. Badiger, **Arun Torris A. T.** Neha Tiwari and Bhuvanesh Gupta, *Design and Development of Trivalent Aluminium Ions Induced Self-healing Polyacrylic Acid Novel Hydrogels*, **Polymer**, 126, 196 - 205 (2017), DOI: 10.1016/j.polymer.2017.08.045.

10. Sachin S. Patil, **Arun Torris** and Prakash P. Wadgaonkar, *Healable Network Polymers Bearing Flexible Poly(lauryl methacrylate) Chains via Thermo-reversible Furan-Maleimide Diels-Alder Reaction*, **Journal of Polymer Sciecne Part A Polymer Chemistry**, 55 (16), 2700 - 2712 (2017), DOI: 10.1002/pola.28677.

11. Vidyanand Vijayakumar, Bihag Anothumakkool, **Arun Torris A. T.**, Sanoop B. Nair, Manohar V. Badiger and Sreekumar Kurungot, *An All-solid-state-supercapacitor Possessing a Non-aqueous Gel Polymer Electrolyte Prepared Using a UV-assisted In situ Polymerization Strategy*, **Journal of Materials Chemistry A**, 5 (8), 8461 - 8476 (2017), DOI:10.1039/C7TA01514C.

12. Anumon V. Divakaran, Lal B. Azad, Sachin S. Surwase, **Arun Torris A. T.** and Manohar V. Badiger,*Mechanically Tunable Curcumin Incorporated Polyurethane Hydrogels as Potential Biomaterials*, **Chemistry of Materials**, 28 (7), 2120 - 2130 (2016), DOI:10.1021/acs.chemmater.5b04964.

13. Bihag Anothumakkool, **Arun Torris A. T.**, Sajna Veeliyath, Vidyanand Vijayakumar, Manohar Virupax Badiger and Sreekumar Kurungot, *High Performance Flexible Solid-state Supercapacitor with Extended Nano Regime Interface Through In situ Polymer Electrolyte Generation*, **ACS Applied Materials and Interfaces**, 8 (2), 1233 - 1241 (2016), DOI:10.1021/acsami.5b09677.

14. Anumon V. Divakaran, **Arun Torris A. T.**, Ashish K. Lele and Manohar V. Badiger, *Porous Poly(ethylene glycol)–polyurethane Hydrogels as Potential Biomaterials*, **Polymer International**, 64 (3), 397 - 404 (2014), DOI:10.1002/pi.4802.

15. Nivika R. Gupta, **Arun Torris A. T.**, Prakash P. Wadgaonkar, Rajamohanan P. R, Guylaine Ducouret, Dominique Hourdet, Costantino Creton and Manohar V. Badiger, *Synthesis and Characterization of PEPO grafted Carboxymethyl Guar and Carboxymethyl Tamarind as New Thermo-associating Polymers*, ***Carbohydrate Polymers***, 117, 331 - 338 (2014), DOI:10.1016/j.carbpol.2014.09.073.

16. Bihag Anothumakkool, **Arun Torris A. T.**, Siddheshwar N. Bhange, Manohar V. Badiger and Sreekumar Kurungot, *Electrodeposited Polyethylenedioxythiophene with Infiltrated Gel Electrolyte Interface: a Close Contest of an All-solid-state Supercapacitor with its Liquid-state Counterpart*, **Nanoscale**, 6, 5944 - 5952 (2014), DOI:10.1039/C4NR00659C.

17. Bihag Anothumakkool, **Arun Torris A. T.**, Siddheshwar N. Bhange, Sreekuttan M. Unni, Manohar V. Badiger and Sreekumar Kurungot, *Design of a High Performance Thin All-Solid-State Supercapacitor Mimicking the Active Interface of Its Liquid-State Counterpart*, **ACS Applied Materials & Interfaces**, 5 (24), 13397 - 13404 (2013), DOI:10.1021/am404320e.

II. List of Patents:

1. Sreekumar Kurungot, Manohar Virupax Badiger, Bihag Anothumakkool, **Arun Torris**, Vidyanand Vijayakumar, *An Electrolyte Composition and a Process for the Preparation Thereof*, **Indian Patent Application Publication**, Publication Date : 10/02/2017, Application No. 2380/DEL/2015, (2017).

2. Sreekumar Kurungot, Manohar Virupax Badiger, Bihag Anothumakkool, **Arun Torris**, *All-solid-state-supercapacitor and a Process for the Fabrication Thereof*, **US Patent**, US 9905371 B2, (2018).

3. Sreekumar Kurungot, Manohar Virupax Badiger, Bihag Anothumakkool, **Arun Torris**, *All-solid-state-supercapacitor and a Process for the Fabrication Thereof*, **PCT Int. Appl.** WO 2014/170912, (2014).

III. List of Conference Proceedings:

1. **Arun Torris**, A.T., Sini, N.K., Lizymol P.P., Kalliyana Krishnan.V., '*Mechanical characterization and morphological evaluation of membrane controlled silicone matrix based drug delivery system*', Proc. National Conference on Medical Materials (NCMM 2007), IIT Madras, India (2007), Page 38.

2. Soumya Columbus, **Arun Torris**, Lissy K. Krishnan and Kalliyana Krishnan. V.,'*Study on the effect of porogen concentration upon the porosity characteristics of polymer scaffolds using micro-computed tomography*', Proc. National Conference on Medical Materials (NCMM 2007), IIT Madras, India (2007), Page 47.

3. **Arun Torris A. T.**, Soumya Columbus, Saaj U. S., Manitha B. Nair and Kalliyana V. Krishnan, *Evaluation of Biomaterials Using Micro-Computerized Tomography*, AIP Conference Proceedings, 1050, 68 (2008); DOI: 10.1063/1.2999995.

4. U. S. Saaj, **A.T. Arun Torris** and V. Kalliyana Krishnan, *Micro Computed Tomography (Micro-CT) and FT- Raman Spectroscopic Studies on Glass Ionomer Cements for Medical Applications*, Proc. International Conference on Advanced Materials (ICAM 2008), India (2008), Page 172.

5. **Arun Torris** and Kalliyana Krishnan. V, *Micro-Computed Tomography: A New Tool for Biomaterial Characterization***,** Proc. 21st Kerala Science Congress, Kollam, Kerala, India (2009), Page 560.

6. Soumya Columbus, **Arun Torris**, Lissy K. Krishnan and V. Kalliyana Krishnan, *Effect of Porogen Size on the Pore Characteristics of Poly (ε-caprolactone)*

Scaffold: A Micro-CT Study, Proc. International Conference on Tissue Engineering & Stem Cell Research Using Nanomaterials (NANOBIO), Kochi, Kerala, India (2009), Page 87.

7. **Arun Torris**, and Manohar V. Badiger, '*Hyaluronic acid – PEG Double Network Hydrogels*', Proc. International Conference on Polymers on the Frontiers of Science and Technology (APA 2013), Punjab University, Chandigarh, India (2013).

8. **Arun Torris**, and Manohar V. Badiger, '*Influence of network architectures on the biomechanical performance of hydrogels*', Proc. International Conference on Polymers: Vision & Innovations (APA 2014), New Delhi, India (2014).

9. **Arun Torris**, and Manohar V. Badiger, '*Polysaccharide derived bio-electrodes for neural interfaces: Carboxymethyl Tamarind*', Proc. Conference on Advancements in Polymer Science and Technology (APA 2015), Saurashtra University, Rajkot, India (2015).

10. **Arun Torris** and Manohar V. Badiger, '*Mechanically Versatile Double Network Hydrogels from Carboxymethyl Xyloglucan and Poly(Hydroxyethyl Methacrylate-co-Trimethylolpropane Allyl Ether)*', Proc. International Conference on Advances in Polymer Science and Technology (APA 2017), New Delhi, India (2017).

11. Sanoop Nair, **Arun Torris** and Manohar Badiger, '*Mechanically Tough Double Network (DN) Hydrogels As Biomaterials*', Proc. of the International Conference on Polymer Science and Technology (MACRO 2017), Trivandrum, India (2017), Page 428.